Cell Migration and Organization

Dissertation

zur Erlangung des Doktorgrades
der Naturwissenschaften

vorgelegt beim Fachbereich Biowissenschaften

der Goethe Universität

in Frankfurt am Main

von

Hasnaa Fatehi
aus Casablanca (Marokko)

Frankfurt am Main 2009
(FB 15)

Vom Fachbereich Biologie der Goethe Universität als Dissertation angenommen.

Dekan: Prof. Dr. Volker Müller
1. Gutachter: Prof. Dr. Jürgen Bereiter-Hahn
2. Gutachter: Prof. Dr. Marcus Bleicher
3. Gutachter: Dr. Michael Meyer-Hermann

What ever you do will be insignificant but it is very important that you do it.

Mahatma Ghandi

Kurzfassung

Zellen sind komplexe biologische Strukturen. Um sie zu verstehen braucht es daher die Kombination mehrerer verschiedener Herangehensweisen. Wir befassen uns hier speziell mit Zellmigration. Obwohl diese im ausgewachsenen Organismus keine so herrausragende Rolle mehr spielt, ist es bekannt das sich einige Zelltypen, unter anderem Lymphozyten, Makrophagen oder Fibroblasten, während einer Immunantwort aktiv durch das Gewebe bewegen. Die Signale, die während einer solchen Immunantwort Informationen zwischen den Zellen übermitteln, sind darüber hinaus essentiell für die selbstregulierende Entwicklung von Geweben und Organen und steuern globale Prozesse in Körper. Funktionsstörungen in diesem Signal-Netzwerk stehen im Zusammenhang mit Leiden, wie zum Beispiel Krebs oder Autoimmun-Erkrankungen wie Diabetes und Hepatitis.

Die hier vorgestellte Arbeit befasst sich mit der Unterscheidung verschiedener Wechselwirkungen auf interzellulärer Ebene anhand der experimentell beobachteten Morphologie eines Zell-Systems. Wir verwenden Computersimulationen als eine bewährte Methode, um von der Morphologie auf die zugrunde liegenden interzelluläre Wechselwirkungen zu schliessen. So konnten Computersimulationen beispielsweise auf der Basis von Migrationsdaten für B-Zellen in Keimzentren, welche mit der Zwei-Photonen-Mikroskopie gewonnen worden waren, aufklären, welche Rolle die Chemotaxis bei der Etablierung der dunklen und hellen Zone in Keimzentren spielt. Dabei stellte sich heraus, daß Chemotaxis - entgegen dem gängigen Migrationsmodell für B-Zellen in Keimzentren - die B-Zell-Migration lediglich zeitlich und räumlich begrenzt bestimmt. Anstatt fortwährend von Chemotaxis getrieben zu sein, bewegen sich B-Zellen auf der Suche nach Überlebenssignalen zumeist per Diffusion (Zufallsbewegung) in den Zonen des Keimzentrum. Wir verwenden in dieser Arbeit ein mathematisches Modell, welches die bedeutenden Rollen von Chemotaxis und Phototaxis in den meist auf Zell-Ebene ablaufenden Aktionen beschreibt und so experimentatorischen Biologen bei deren Unterscheidung helfen kann. Eine wesentliche Frage, die in dieser Arbeit hinsichtlich Zell-Kommunikation und Aggregation diskutiert wird, ist die Distanz, über die diese Prozesse wirken können und ob es, abgesehen von chemischer Diffusion, andere Mechanismen gibt, beispielsweise

Phototaxis, die zu Aggregation führen können. Im vorgestellten Modell können Zellen Signale empfangen und aussenden; diese integriert, werden um Informationen über ihre Umgebung zu sammeln und dementsprechend zu reagieren. Eine gut untersuchte Art zellulärer Kommunikation arbeitet über die Freisetzung von Chemokinen und Diffusion. Auch Licht kann einen großen Einfluss auf das Verhalten der Zellen haben, speziell bei Aggregations-Prozessen. Die folgende Arbeit will vor allem ein Modell vorstellen, welches dazu beitragen kann, experimentatorischen Biologen dabei zu helfen, die Unterschiede in den Auswirkungen von Chemotaxis und Phototaxis zu erkennen, sowie die Mechanismen aufzuzeigen, die der zellulären Aggregation zu Grunde liegen.

Unser Modell ist ein Ansatz Chemotaxis und Phototaxis zu simulieren. Die Ergebnisse unserer Simulationen zeigen, daß Zellaggregation ein Prozess ist, der komplizierter ist als es zunächst erscheinen mag. So kann zum Beispiel das Herauslösen von Zellen aus einem bestehendem Aggregat den überraschenden Effekt haben, den Grad der Aggregation schlußendlich zu erhöhen. Dagegen erschwert vermehrte diffusion der Zellen den Aggregationsprozess. Bei bestimmten Werte der Herauslösungsrate werden sich Zellen, die von kleineren Aggregaten abgelöst werden, bei größeren Aggregaten ansiedeln, da diese stärkere Signale aussenden. Eine Beobachtung der Zellbewegungen in der Simulation zeigt, daß Aggregate aufgrund solcher Diffusions- und Umordnungsprozesse um ihren Schwerpunkt oszillieren. Zellen, die sich innerhalb eines Aggregates aufgrund von Diffusion bewegen, kehren in Abhängigkeit von den Anziehungskräften zu der stabilsten Position zurück. Außerdem sind sich die durch Chemotaxis und Phototaxis verursachten Aggregationsmuster sehr ähnlich und können nicht mit bloß Auge unterschieden werden. Bei gleicher Zell-Zell Interaktionsreichweite R kann es jedoch zu sehr unterschiedlichen Aggregations-Muster kommen, wie unsere Simulationen zeigen. Während R die Signal-Reichweite zwischen zwei Zellen ist, sind die Aggregationsmuster durch die effektive Reichweite R_{eff} charakterisiert. Die effektive Reichweite berücksichtigt kollektive Effekte von Aggregaten und hängt von dem zugrundliegenden Signalprozess ab. Die effektiven Kommunikationsdistanzen innerhalb derer Zellen sich wahrnehmen sind die Schlüsselparameter, um zwischen Chemotaxis und Phototaxis zu unterscheiden. Es konnte gezeigt werden, daß der Bereich der R-Werte bei denen Chemotaxis und Phototaxis unterschieden werden kann experimentell relevant ist. Zum Beispiel wurde bei blutbildenden CD34+ Zellen eine Kummunikationsreichweite von ca. 14 Zelldurchmessern beobachtet. Dieser Umstand kann genutzt werden, um einen unbekannten Signalprozess

aus geschätzten Signal Schwellwerten und Signalstärken zu ermitteln. Eine experimentelle Bestimmung von R aus Zwei-Zell-Experimenten und R_{eff} aus der Analyse von Aggregationsmustern ist dann ausreichend, um zwischen Chemotaxis und Phototaxis zu unterscheiden. Die Ergebnisse der Dissertation stellen das erste Modell dieser Vorgänge dar und zielen darauf ab, chemotaktisches und phototaktisches Verhalten auf einen phenomenologischen Niveau zu vergleichen. Für weitergehende Analysen müssen die spezifischen Genotypen der Zellen berücksichtigt werden. Heute fehlt es noch an experimentellen Daten, die für die eine theoretische biologische Modellierung notwendig sind. Daher betonen wir die Unterschiede zwischen diesen beiden Mechanismen, die es erlauben zwischen Prozessen der Aggregation im Experiment zu unterscheiden. Außerdem kann unser Modell die Untersuchung weiterer Parameter vereinfachen, die bei der Analyse von großen Systemen mit hohen Zelldichten und erschiedenen Wechselwirkungen notwendig sind.

Zusammenfassung

Das funktionelle Immunsystem kann zwischen *selbst* und *fremd* unterscheiden. Das Immunsystem besteht aus zwei verschiedenen Strukturen, die kontinuierlich fremde Entitäten unterdrücken oder diese unter Kontrolle halten, indem ihre Ausbreitung oder ihre Vermehrung verhindert wird. Das angeborene Immunsystem ist die erste Verteidigungslinie gegen fremde, potentiell gefährliche Entitäten (z.B. Bakterien, Pilze, Viren u.s.w.). Es verfügt über mehr oder weniger festgelegte Reaktionen gegen bestimmte Klassen von Erregern. Des Weiteren hat das adaptive Immunsystem in Wirbeltieren die Fähigkeit bereits bekannte Erreger zu erkennen und zu speichern, um den Körper besser gegen zukünftige Angriffe zu schützen. Es ist adaptiv, da spezifische Antikörper für jedes Antigen produziert werden, mittels somatischer Mutation. Dieser Prozess findet in den Keimzentren der Lymphknoten statt. Das Immunsystem ist über den gesamten Körper verteilt. Lymphknoten sind Teil des Lymphsystems und sind zentrale Organe, die die Immunität des Körpers sicherstellen. Sie bestehen aus verschiedenen Zelltypen, die für das adaptive Immunsystem wichtig sind. Lymphknoten spielen die Rolle von Organen, in welchen fremde Antigene von Lymphozyten analysiert werden. In speziellen Regionen der Lymphknoten, den sogenannten Keimzentren, findet die Vermehrung, Mutation und Selektion der Lymphozyten statt. Diese Keimzentren sind in zwei Bereiche, die dunkle und helle Zone, unterteilt. Es wurde postuliert, dass die Affinitätsreifung von Antikörpern einen starken und häufigen Austausch von Zellen zwischen diesen Zonen bedingt. Daher spielen die weitreichende Migration und die kurzreichweitige Interaktion durch lokale chemische Signale und Kontakte zwischen Zellen, eine zentrale Rolle für die Immunantwort.

Die Anwendung der Zwei-Photonen-Mikroskopie hat wertvolle neue Informationen über die Bewegungmuster von B- und T-Zellen in den Keimzentren enthüllt. Da diese eine Echtzeit-Beobachtung von einigen der vielen Mechanismen die nach der Immunisierung stattfinden erlauben, wurden viele neue Erkenntnisse gewonnen und gängige Hypothesen korrigiert. Für das Verständnis der Mechanismen ist, die vor der Immunisierung (Einführung des Antigens) ablaufen, sowie für die Veränderungen des zellulären

Verhaltens nach der Immunisierung, ist eine gründliche Untersuchung der Keimzentren von nöten. Daher ist die Analyse und Interpretation von Zelltrajektorien und der chemische Interaktionen, die die Vorgänge in den Keimzentren beeinflussen, von großer Wichtigkeit.

Zellen sind komplexe biologische Strukturen. Um sie zu verstehen, braucht es daher die Kombination mehrerer verschiedener Herangehensweisen. Wir befassen uns hier speziell mit Zellmigration. Obwohl diese im ausgewachsenen Organismus keine so herrausragende Rolle mehr spielt, ist es bekannt, dass sich einige Zelltypen, unter anderem Lymphozyten, Makrophagen oder Fibroblasten, während einer Immunantwort aktiv durch das Gewebe bewegen. Die Signale, die während einer solchen Immunantwort Informationen zwischen den Zellen übermitteln, sind darüber hinaus essentiell für die selbstregulierende Entwicklung von Geweben und Organen und steuern globale Prozesse in Körper. Funktionsstörungen in diesem Signal-Netzwerk stehen im Zusammenhang mit Leiden, wie zum Beispiel Krebs oder Autoimmun-Erkrankungen wie Diabetes und Hepatitis.

Chemische Kommunikation beinhaltet die Regulierung der Synthese von Signal-Molekülen in der Sender-Zelle zur Anpassung der Konzentration an eine gewünschten Reizschwelle. Die Diffusion der Moleküle in Richtung der Empfänger-Zelle, sowie die Bindung derselben an passende Rezeptoren verursacht Veränderungen in der Empfänger-Zelle hin zu zum Beispiel migratorischem oder aggregierendem Verhalten. Es ist bekannt, dass einzelne Zellen, wie Bakterien, bei ihrer Nahrungssuche auf eine Kombination von Taxis (Richtungs-Signal) und Kinesis (Geschwindigkeits-Signal) setzen. Immunzellen scheinen eine ähnliche Methode zu verwenden, um Zelltrümmer oder Bakterien zu finden. Unter Chemotaxis versteht man den Prozess, bei dem die Zelle eine gerichtete Bewegung ausführt, indem sie dem Gradienten eines Chemo-Attraktantes folgt. Über die Zellmembran verteilte Rezeptoren, welche sensitiv für spezielle Chemo-Attraktanten sind, messen den Gradienten dieser Moleküle über die räumliche Ausdehnung der Zelle und können so dessen Richtung bestimmen. Wird ein solcher Gradient detektiert, bildet die bislang unpolarisierte Zelle Fortsätze aus, so genannte *Pseudo*– oder *Uropodien*. Eine solche polarisierte Zelle besitzt nun eine führende und eine folgende Seite mit unterschiedlichen Empfindlichkeiten für das Attraktant. Verändert sich im Folgenden die Richtung des Gradienten, so bleibt die Aufteilung der Zelle bestehen, das heißt sie bewegen sich in einer Kurve hin zu ihrem neuen Ziel.

Phototaxis ist die gerichtete Bewegung einer Zelle entlang eines Licht-Gradienten. Lange Zeit ging man davon aus, dass Phototaxis keinen relevanten Prozess für Eukaryoten darstellt. Chemotaxis konnte so grundsätzlich von einer erhöhten Aufmerksamkeit und dem Fokus wissentschaftlicher Experimente profitieren. Nichtsdestotrotz gab es in den letzten Jahren immer mehr Untersuchungen, die sich mit der Bedeutung von Phototaxis bezüglich zellulärer Interaktionen befasst haben. Hinweise auf die Existenz licht-basierter Kommunikations-Prozesse und licht-geleiteter Bewegungen in Bakterien werden in der folgenden Arbeit genauso diskutiert wie neueste Ergebnisse zum Einfluss dieser Prozesse auf das Überleben von Bakterien bei Futtermangel. Auch wenn es bisher keine klaren Beweise für einen Einfluss von Licht-Signalen auf Aggregation und Migration von Zellen in Keimzentrum gibt, so deuten einige Ergebnisse doch darauf hin, dass Phototaxis für die Erhöhung der Ansteckungskraft von Bakterien und deren Aggregation eine Rolle spielt. Desweiteren wurden auch durch licht-abhängige Kommunikation ausgelöste Veränderungen im Verhalten von Neurophilen beobachtet.

Die Beobachtung von Zell-Migration und -Aggregation in einem bidimensionalen Substrat mit Hilfe eines Mikroskopes, kann der Komplexität der Prozesse, die zu diesem scheinbar simplen Phänomen führen, nicht gerecht werden. Daher ist es unerlässlich mathematische Hilfsmittel zu entwickeln, um Hypothesen zu testen, Daten zu analysieren, verschiedene Zell-Funktionen zu interpretieren und bereits existierende Modelle zu verbessern. Die Systeme, die wir analysieren wollen, besitzen immer größere Komplexität hinsichtlich ihrer gegenseitigen Abhängigkeiten. Zudem sind herkömmliche Modellierungs-Ansätze an ihrem Design-Limit angekommen. Heutzutage werden Systeme *bottom-up* statt *top-down* konstruiert. Agenten-basierte Modelle stellen ein flexibles und intuitives Framework bereit, um alle verschiedenen Arten der Komplexität von biologischen Systemen abzubilden. Die Struktur des Systems kann durch globale Anpassungen des Systems, aber auch durch individuelle Veränderungen der Organisation der Agenten spezifiziert werden. Agenten sind identifizierbare, lokalisierte, zielgerichtete und flexible Berechnungs-Einheiten. Sie sind diskret und besitzen klar definierte Attribute un Verhaltensweisen. Außerdem können Agenten nach ihrer Funktion und ihrem Verhalten separiert werden, um der kontext– und zeitabhängigen Natur biologischer Funktionen Rechnung zu tragen. Sie gewährleisten so maximale Kontrolle über alle System-Eigenschaften.

Die hier vorgestellte Arbeit befasst sich mit der Unterscheidung verschiedener Wechselwirkungen auf interzellulärer Ebene anhand der experimentell beobachteten Morphologie eines Zell-Systems. Wir verwenden Computersimulationen als eine bewährte Methode, um von der Morphologie auf die zugrunde liegenden interzelluläre Wechselwirkungen zu schliessen. So konnten Computersimulationen beispielsweise auf der Basis von Migrationsdaten für B-Zellen in Keimzentren, welche mit der Zwei-Photonen-Mikroskopie gewonnen worden waren, aufklären, welche Rolle die Chemotaxis bei der Etablierung der dunklen und hellen Zone in Keimzentren spielt. Dabei stellte sich heraus, dass Chemotaxis - entgegen dem gängigen Migrationsmodell für B-Zellen in Keimzentren - die B-Zell-Migration lediglich zeitlich und räumlich begrenzt bestimmt. Anstatt fortwährend von Chemotaxis getrieben zu sein, bewegen sich B-Zellen auf der Suche nach Überlebenssignalen zumeist per Diffusion (Zufallsbewegung) in den Zonen des Keimzentrum. Wir verwenden in dieser Arbeit ein mathematisches Modell, welches die bedeutenden Rollen von Chemotaxis und Phototaxis in den meist auf Zell-Ebene ablaufenden Aktionen beschreibt und so experimentatorischen Biologen bei deren Unterscheidung helfen kann. Eine wesentliche Frage, die in dieser Arbeit hinsichtlich Zell-Kommunikation und Aggregation diskutiert wird, ist die Distanz, über die diese Prozesse wirken können und ob es, abgesehen von chemischer Diffusion, andere Mechanismen gibt, beispielsweise Phototaxis, die zu Aggregation führen können. Im vorgestellten Modell können Zellen Signale empfangen und aussenden; diese werden integriert, um Informationen über ihre Umgebung zu sammeln und dementsprechend zu reagieren. Eine gut untersuchte Art zellulärer Kommunikation arbeitet über die Freisetzung von Chemokinen und Diffusion. Auch Licht kann einen großen Einfluss auf das Verhalten der Zellen haben, speziell bei Aggregations-Prozessen. Die folgende Arbeit will vor allem ein Modell vorstellen, welches dazu beitragen kann, experimentatorischen Biologen dabei zu helfen, die Unterschiede in den Auswirkungen von Chemotaxis und Phototaxis zu erkennen, sowie die Mechanismen aufzuzeigen, die der zellulären Aggregation zu Grunde liegen.

Wir untersuchen räumliche zelluläre Aggregationen von Zellen mit dem Ziel Unterschiede der emergierenden Muster und deren Abhängigkeit von Chemotaxis und Phototaxis zu verstehen. Dazu benutzen wir ein Agenten-basiertes Modell, das Zellen als Knoten auf einem Gitter darstellt. Diese Zellen sind Einheiten, die Signale empfangen und emittieren. Alle empfangenen Signale werden innerhalb eines vorgegebenen Bereichs integriert und dienen als Entscheidungsgrundlage ob eine Zelle sich bewegt, abhängig von

vorgegebenen Schwellwerten. Agenten-basierte Modelle sind relativ einfach zu implementieren und sehr gut geeignet, um Systeme zu untersuchen, in welchen Musterbildung eine wichtige Rolle spielt. Allerdings ist, wie bei vielen theoretischen biologischen Modellen, die Festlegung der Systemeigenschaften eine Herausforderung, da experimentelle Daten für die Modellparameter bisweilen fehlen. Die mathematische Beschreibung der Signale, die zur Simulation des beschriebenen Systems benutzt wurde, sind der Literatur entnommen. Das erste Signal beschreibt die Diffusion der Chemokine in dem zellulären Medium und das zweite Lichtdiffusion innerhalb eines Volumens. Um Gitterartefakte durch die deterministischen Eigenschaften der gerichteten Bewegung zu vermeiden, wurde ein Diffusionsprozess der Zellen implementiert, zusätzlich zu der Zufallsbewegung der Zellen wenn kein Stimulus vorliegt. Unter Zuhilfenahme der zitierten Methoden wurde ein Modell entwickelt und der eigeführte Parameterraum mit verschiedenen Simulationen erforscht, zum Beispiel die Reichweite der Anziehung, der Schwellwert für die Signalverarbeitung, die Stärke der Diffusion u.s.w.

Unser Modell ist ein Ansatz Chemotaxis und Phototaxis zu simulieren. Die Ergebnisse unserer Simulationen zeigen, dass Zellaggregation ein Prozess ist, der komplizierter ist als es zunächst erscheinen mag. So kann zum Beispiel das Herauslösen von Zellen aus einem bestehendem Aggregat den überraschenden Effekt haben, den Grad der Aggregation schlußendlich zu erhöhen. Dagegen erschwert vermehrte Diffusion der Zellen den Aggregationsprozess. Bei bestimmten Werten der Herauslösungsrate werden sich Zellen, die von kleineren Aggregaten abgelöst werden, bei größeren Aggregaten ansiedeln, da diese stärkere Signale aussenden. Eine Beobachtung der Zellbewegungen in der Simulation zeigt, dass Aggregate aufgrund solcher Diffusions- und Umordnungsprozesse um ihren Schwerpunkt oszillieren. Zellen, die sich innerhalb eines Aggregates aufgrund von Diffusion bewegen, kehren in Abhängigkeit von den Anziehungskräften zu der stabilsten Position zurück. Außerdem sind sich die durch Chemotaxis und Phototaxis verursachten Aggregationsmuster sehr ähnlich und können nicht mit bloßem Auge unterschieden werden. Bei gleicher Zell-Zell Interaktionsreichweite R kann es jedoch zu sehr unterschiedlichen Aggregations-Mustern kommen, wie unsere Simulationen zeigen. Während R die Signal-Reichweite zwischen zwei Zellen ist, sind die Aggregation-Muster durch die effektive Reichweite R_{eff} charakterisiert. Die effektive Reichweite berücksichtigt kollektive Effekte von Aggregaten und hängt von dem zugrundliegenden Signalprozess ab. Die effektiven Kommunikationsdistanzen innerhalb derer Zellen sich wahrnehmen sind

die Schlüsselparameter, um zwischen Chemotaxis und Phototaxis zu unterscheiden. Es konnte gezeigt werden, dass der Bereich der R-Werte, bei denen Chemotaxis und Phototaxis unterschieden werden kann experimentell relevant ist. Zum Beispiel wurde bei blutbildenden CD34+ Zellen eine Kummunikationsreichweite von ca. 14 Zelldurchmessern beobachtet. Dieser Umstand kann genutzt werden, um einen unbekannten Signalprozess aus geschätzten Signal-Schwellwerten und Signalstärken zu ermitteln. Eine experimentelle Bestimmung von R aus Zwei-Zell-Experimenten und R_{eff} aus der Analyse von Aggregationsmustern ist dann ausreichend, um zwischen Chemotaxis und Phototaxis zu unterscheiden. Die Ergebnisse der Dissertation stellen das erste Modell dieser Vorgänge dar und zielen darauf ab, chemotaktisches und phototaktisches Verhalten auf einen phenomenologischen Niveau zu vergleichen. Für weitergehende Analysen müssen die spezifischen Genotypen der Zellen berücksichtigt werden. Heute fehlt es noch an experimentellen Daten, die für die eine theoretische biologische Modellierung notwendig sind. Daher betonen wir die Unterschiede zwischen diesen beiden Mechanismen, die es Erlauben zwischen Prozessen der Aggregation im Experiment zu unterscheiden. Außerdem kann unser Modell die Untersuchung weiterer Parameter vereinfachen, die bei der Analyse von großen Systemen mit hohen Zelldichten und erschiedenen Wechselwirkungen notwendig sind.

Abstract

Information sent to and received by cells is essential for a homeostatic development of tissues and organs. These same signals are responsible for the good functioning of lymphatic organs and therefore govern the immune response. Dysfunctioning of the signaling networks is related to pathological situations, among which one can find cancer and auto-immune diseases.

Intercellular communication involves the synthesis and the adjustment of signals by the secreting/emitting cell in order to reach the needed threshold. Diffusion of the signal to the target cell in addition to its interpretation lead to functional changes like cell migration and aggregation. Individual cells such as bacteria find food or increase their virulence through taxis (directional stimulus) and/or kinesis (speed stimulus). Immune cells appear to use the same processes to find bacteria and cellular debris, as well as to perform the cellular dance observed in germinal centers. This behavior is a result of an up or down regulation of specific signals that suggest to B and T-cells the paths to follow. Furthermore, cell segregation in the white pulp of the spleen, was also shown to be a result of a tight adjustment of T-cell kinesis. Restriction to cellular tracks and other experimentally provided measurements does not ensure a full comprehension of the observed cellular behavior. Thus, the study of patterns opens new gates to our understanding of the immune system.

With the help of the agent-based modeling technique, cellular migration and aggregation are investigated in response to various cell-cell interactions. This work aims to explore different mechanisms that lead to cellular migration and aggregation, by defining the emergent properties of interest and that will help distinguish between interactions, starting by a simple look at the emergent patterns, followed by an analysis of their size, their degree of aggregation and the effective communication distances. Finally, the results obtained from the *in silico* experiments provided a guideline to differentiate between many cell-cell interactions under specific circumstances. Chemotaxis and phototaxis with and without diffusive cellular motion were shown to be distinguishable through an analysis of the emerging aggregation profiles.

Contents

Contents 1

1 Introduction and Motivation

1.1 Introduction and Motivation

As an essential entity for life, cells are complex biological structures, and their comprehension requires a combination of several approaches. Cells continuously perform actions to maintain homeostasis, among these actions migration and aggregation are widely observed throughout a lifetime. At the adult stage, cells like lymphocytes, macrophages and fibroblasts perform very precise moves and intercellular contacts to insure the best immune response.

Observing cell migration and aggregation on a bidimensional substratum with a microscope does not allow to imagine the extraordinary complexity of all processes that lead to this seemingly simple phenomenon. Therefore, it becomes essential to develop mathematical tools to test hypotheses, analyze data, interpret different cell functions and upgrade already existing models. Recently, the intravital two-photon microscopy provided great insights on cell tracks before and after immunization in the germinal center. The analysis of tracks shows typical properties of a random walk. Yet, mathematical modeling, based on the study of germinal center patterns combined with cell tracks, lead to a better understanding of the ongoing processes in the GC. By going beyond the simple experimental data analysis and making use of the typical germinal center patterns, Figge et al [Figge 08] showed that cells in GCs do not only perform a random walk but also follow gradients of chemokines accurately adjusted to direct the movement of cells from one zone to the other.

Moreover, in the spleen and under non-inflammatory conditions, T-cells are surrounded by a shell of B-cells. Mathematical modeling [Beyer 09] shows this cell segregation to be the result of an increased chemokinesis of T-cells. If T-cell chemokinesis is reduced the shell pattern is inverted and in the case of an equal chemokinesis of T and B-cells, the observed cell segregation disappears.

In our model, cells are able to emit and receive signals that are integrated to collect information concerning their environment and react with respect to this. One common way of cellular communication is through chemokine release and diffusion. Likewise, light can also play a role in affecting cellular behavior and response, particularly, in aggregate formation. The main motivation of the following work, is to propose a model that helps distinguishing between different signals, with different scaling behaviors and the random walk.

1.2   The Immune System

A functional immune system, is capable of the self/non-self discrimination of entities in the body. Effectively, two distinguished structures enter the immune system composition, and look continuously after suppressing foreign entities from our body, or keeping them under control, by preventing their proliferation and/or propagation. The innate system, is the first line of defense used to fight against non-self potentially dangerous entities (*i.e*, bacteria, fungus, viruses etc...). It ensures more or less predetermined reactions to certain classes of pathogens. More substantial, in vertebrates the adaptive system provides the ability to recognize and memorize formerly encountered pathogens for a better protection from future invasions. It is adaptive, because of the production of specific antibodies for each antigen, called somatic hypermutation, occurring in germinal centers within lymph nodes.

The immune system is the most diffuse cellular system in the body (Fig. 1-1). Accordingly, long-range migration of cells and short-range interactions by local chemical signaling and by cell-cell contacts are critical for the control of an immune response. Cellular homing and migration within lymphoid organs, antigen recognition, cell signaling and activation represent only a tiny part of the avalanche of processes taking place after immunization. However, these events were not directly observed in vivo until only recently with the help of two-photon microscopy that shed light on many processes, allowing sometimes the correction of commonly believed mechanisms.
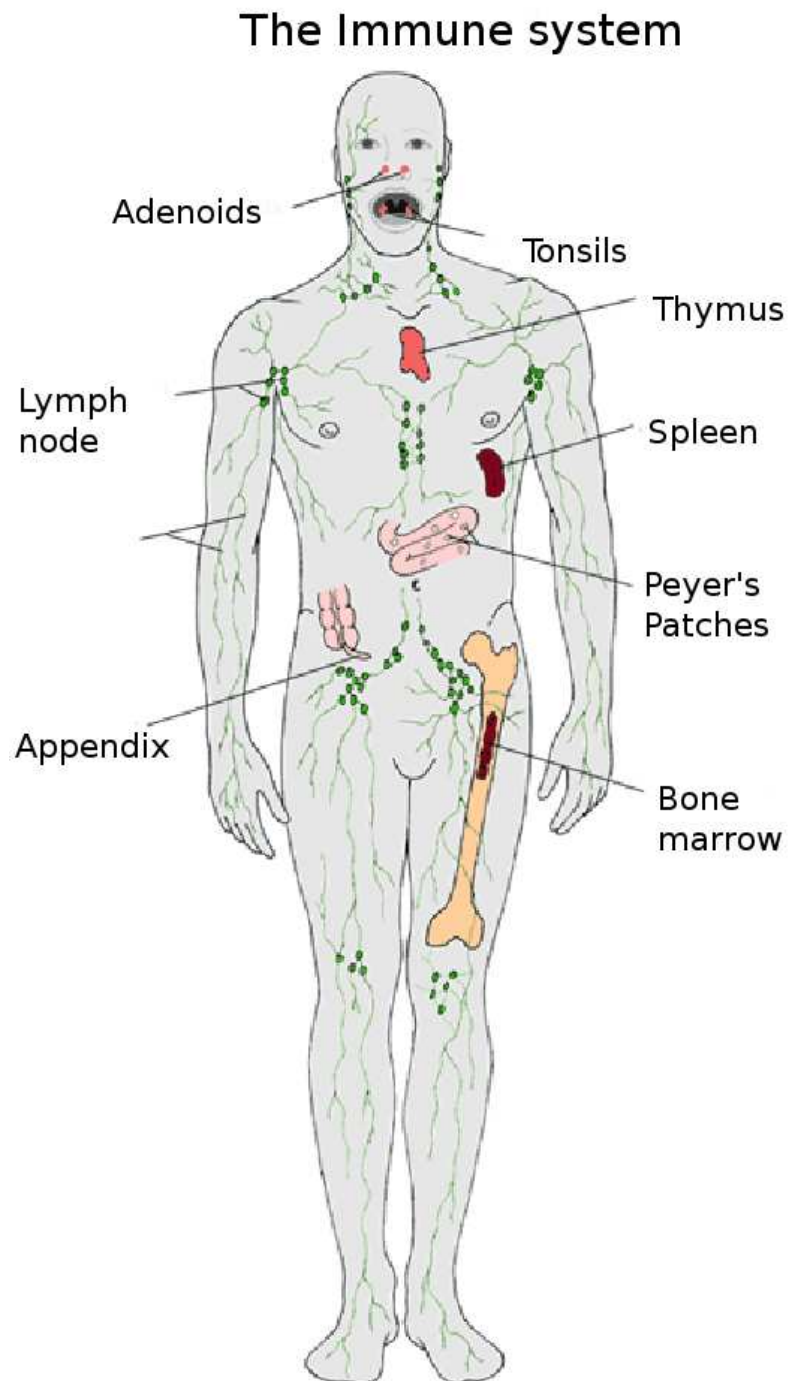
Figure 1-1: *Representation of the human immune system, including primary lymphoid organs (Thymus and Bone marrow) and secondary lymphoid organs, like lymph nodes or Peyer's Patches.*[1]

1.3   The germinal center

Lymph nodes (Fig.1-1) form a part of the lymphatic system and are essential organs for immunity. Distributed over many regions of the body, lymph nodes contain several types of cells and are necessary for the adaptive immune response. Lymph nodes play the role of key organs where foreign antigens are presented to lymphocytes. Special areas of the lymph nodes are dedicated to lymphocytes proliferation, mutation and selection, and are known as germinal centers (GCs).

Germinal centers are usually divided in two distinguished zones, the dark and the light zone (DZ and LZ). Thus, affinity maturation of antibodies has been posited to require frequent and intense trafficking between both zones. The recent use of two-photon microscopy revealed precious information on the migration patterns of B-cells and T-cells in the GCs. Understanding the ongoing mechanisms before immunization (introduction of the antigen) and the changes in cellular behavior after immunization requires a thorough exploration of GCs and the subsequent changes to immunization. Thus, the analysis and interpretation of cell tracks, patterns and interactions that orchestrate cellular migration and aggregation are of major importance.

1.4   Aim of this study

One of the crucial questions raised regarding cell migration and aggregation, is the distance cells sense each other, and whether there are other signaling mechanisms besides chemical diffusion that lead to aggregation. This work investigates the cellular aggregation and tries to understand the differences between the emergent patterns and their dependence on different signals for example chemotaxis and phototaxis. The analysis of the average attraction distance between cells, named effective communication distance, is considered as an important emergent property of the system. The shape of aggregates, their size and therefore the average distance between them under different signals are the major focus of the presented work.

In addition, the model includes random motion of cells accounting for cellular movement in absence of signals and for unrepresented mechanisms. The importance of cellular adhesion in aggregate formation is also investigated via a parameter regulating cell detachment from aggregates during their diffusion. This work focuses on the differences

between patterns that emerge as a consequence of different signaling pathways, and the information held in these patterns to distinguish between different cellular interactions.

1.5   Methods used and developed in this work

Within an agent-based modeling frame, cells are assimilated to nodes on a lattice and modeled as emitting and receiving entities, that integrate all signals within a certain pre-defined range and make decisions to move or not in dependence of a pre-imposed threshold. ABMs (Agent-Based Models) are very suitable for studying systems where pattern emergence is of importance. The signal expressions used to simulate our system were taken from literature. The first signal represents the diffusion of chemokines in the cellular medium, and the second represents light diffusion within a volume. To overcome lattice artefacts induced by the deterministic nature of directed movements, a diffusion process of cells was implemented to mimic the cellular behavior in the absence of signal-induced stimuli.

1.6   Results

With the help of the above cited method, a model was developed and different simulations were run to explore the introduced parameter space, like the maximal communication distance, the threshold, the detachment, the probability of diffusing and the probability of responding to signals etc... Our model leads to a consistent description of cellular migration and aggregation. An important result is the coming up of two distinguished regimes, where for the same implemented one-cell/one-cell interaction distance, the emergent structures hold clearly discernible information. The simulations display as well the role of diffusive motion and adhesion in pattern formation or dissolution and can help predict the subjacent phenomenon that rules a particular aggregation. To summarize, the model helped defining the importance of directed motion and simple random walk in aggregate formation, and their influence on the emerging average effective communication distance and therefore the observed patterns.

---

[1] http://www.uabhealth.org.

2 Cell migration and interaction

Cellular migration and interaction are major processes continuously performed to keep our body functioning in a homeostatic manner. Tissues and cells need to interact and exchange information concerning their environment. Beyond simple sharing of information, the main purpose of intercellular communication, is to give directives to other cells for them to perform actions like mitosis, apoptosis, cellular division or migration to new sites as shown in the case of mould formation in Figure 2-1, always with a view to restore equilibrium in the concerned system.

We focus in this chapter on two main signaling pathways used by cells to migrate from one point to another. In Section 2.1 we introduce the importance of cellular random walk as a basic adopted behavior in absence of signals. The mechanism of chemical signaling between cells is discussed in Section 2.2, where examples of typical cellular interaction ranges are provided for different cells. Finally, in Section 2.3, light communication between cells is introduced as a promising new signaling pathway that is regaining the attention of biologists.

2.1 Random walk: Cells migrating like drunk

In the absence of stimuli, cells perform a random walk characterized by their irregular motion in random directions, where the next direction of migration can be as unpredictable as is the next step of a drunkard.

This phenomenon was first observed with the aid of a microscope in the motion of pollen grains in liquid by the English botanist Robert Brown (1773-1858). Later, Albert Einstein (1905) explained that the random walk observed by Brown was the result of an uncountable number of thermally driven collisions of water molecules. This explanation provided a link to the macroscopic (physical) process of molecular diffusion based on Fick's phenomenological law [Deutsch 04].

A more general definition of diffusion is given later by Okubo in 1980 [Okubo 80], who stated that the collective behavior of many particles is a diffusive phenomenon. This

is to say that "the microscopic irregular motion of each particle gives rise to a regularity of motion of the total particle group (macroscopic regularity)" [Okubo 80].

Cells perform random walks with a directional persistence time, *i.e.* cells persistently migrate in the same direction for a characteristic time before a new migration direction is randomly chosen. However, the random walk of cells may be biased in the presence of stimuli giving rise to the combined random and directed migration of cells.

2.2   Chemotaxis: Cells adhering to chemoattractants

Chemotaxis is the directed motion of cells following a spatial gradient distribution of chemoattractants [Iglesias 02, Devreotes 03]. Receptors distributed over the cell membrane are sensitive to specific chemoattractants and cells are capable of measuring the spatial distribution of the chemoattractant across their surface.

In the presence of a gradient, which is to say, a difference in the chemoattractant concentrations, the unpolarized cells respond by creating extensions of their cytoskeleton called uropods or pseudopods. After this, cells become polarized and develop a leading and a trailing edge, where both edges present distinct sensitivities for the chemoattractant. Yet, the polarized cell maintains the same leading edge when turning in the direction of changing gradients of the chemoattractant distribution. The chemotactic response of a cell involves different levels. While the receptor expression is directly related to the genetic level, the process of receptor internalization is relevant for the spatial re-distribution of receptors on the cell surface [Moser 04].

The sensitivity of cells to the chemoattractant concentration generally obeys a bell-shaped curve. As a matter of fact, chemotaxis is only initiated for concentrations above a threshold value,*e.g.* 10 nM for lymphocytes [Kim 98, Tomhave 94, Yoshida 98, Willimann 98]. At high chemoattractant concentrations cells may become desensitized and stop further reactions to the chemoattractant, which is for example the case for neutrophils [Tomhave 94].

In the presence of multiple chemoattractants, cells seem to compute a vector sum of the incoming gradient signals to determine the integrated response in terms of the migration direction [Foxman 99]. Interestingly, if multiple signals are provided in sequential order, the current migration direction is dominated by the most recent chemoattractant, even if it is presented in lower concentrations [Foxman 99]. One explanation for this

behavior could be the desensitization of receptors [Bardi 01]. However, experiments conducted with neutrophils involving different signaling pathways but introducing different chemoattractants suggest a sort of hierarchy of chemoattractants [Heit 02]. The hierarchical levels are referred to as *target* and *intermediary* chemoattractants. If different gradient signals from the same hierarchical level are provided, cells respond by computing the vector sum. However, chemoattractants from the target level are always preferred over the intermediary level. Yet, blocking of intermediary chemoattractants by target chemoattractants can be incomplete [Tomhave 94]. Curiously, the presence of an intermediary chemoattractant can enhance chemotaxis to a target chemoattractant allowing the cell to respond to lower concentrations than with the target chemoattractant alone [Tomhave 94].

Cells were seen to sense the presence of other cells at typical distances depending on their genotype. For example, endothelial cells from bovine pulmonary arteries appeared to sense each other at a distance of 40 µm [Lee 94]. Hematopoietic progenitor cells are aware of each other at distances below 100 µm [Möbest 02]. Francis et al. state that hematopoietic progenitors ($CD34^+$ cells) communicate without direct contact and the communication distances are in the order of 100 µm [Francis 97]. Taken together, direct measurements suggest that the effective range of the gradients sensing is 80-140 µm beyond the corresponding target zone [Okada 05].

2.3   Phototaxis: Cells drawn to the light

The movement of organisms in response to a light source is referred to as phototaxis. This important photo-biological process involves reception of light and translation of photonic information. Phototaxis is referred to as positive if the cell movement is in the direction of light and as negative in the opposite case.

In simple organisms such as bacteria, a gradient of light intensity, *i.e.* difference in light intensities, is interpreted and translated to a directed movement or to a change in the frequency of the random turnings [Hoff 94]. In higher animals, these functional steps become distinct with specific organs such as eyes, neurons and muscles, each with higher complexity in their mechanisms.

The light source is not always external. Emission of light radiation by cells in the visible range of the electromagnetic spectrum has been described by many researchers

for a variety of organs. Using photomultipliers, emission of radiation has been readily detected from liver, heart, lung, nerve and muscle cells [VanWijk 88]. Photon emission of leukocytes has also been measured [Trush 78] and a direct relation between photon emission and the process of phagocytosis has been suggested. Various emission bands in the range of 400-700 nm were measured in animal cells [VanWijk 88].

The bio-photons are believed to carry information that can be used by cells for long-range interactions and communication to regulate functions such as biochemical activity, cellular growth, differentiation [Popp 02] and phototaxis [Popp 88]. Recently a new study on bacterial pathogens revealed that light regulates several developmental and behavioral responses like swimming, flagella beatings and rotation [Häder 91]. It can be concluded that bacteria are provided with sophisticated mechanisms that sense changes in environmental parameters such as light and nutrients. Under certain conditions, such changes initiate the motion of an individual bacterium or of an entire colony, like under starvation conditions as shown in Figure 2-1. In this case, bacteria proceed in a collective move to increase resource availability [Levy 08]. An individual bacterium is indeed less likely to move toward light. The observed dynamics of mould formation (see Figure 2-1) appears to be a complex function of cell density, surface properties and genotype [Levy 08]. Burriesci and Bhaya [Burriesci 08] showed additional details about the motility of Cyanobacterium cells under phototaxis. Cyanobacterium were observed to have a delayed motion, where it will take them a typical time after irradiation to initiate a motion towards the light source. Such motion is observed in regions with a high density of bacteria. In areas of low density, bacteria tend to be immobile or move slower, and only move faster for higher densities leading to finger formation. In this study, experiments also showed that the cells leave a chemical trace behind providing a preferred pathway to follower cells.

Aggregation under infra-red light of 3T3 cells was related to nuclei being able to emit and receive light irradiation that induces the cell migration [Albrecht-Buehler 05]. This gives rise to cellular aggregation with aggregates forming at characteristic distances well above several cell diameters. This finding suggests the possibility of long-range cellular communication via light. Already in 2002, Popp et al. were able to track back the emission of bio-photons to the nuclei's DNA [Popp 02].

Effects of light irradiation on chemical interactions have also been observed in bacteria, where the blue-light activated histidine kinase lead to an increase in viru-
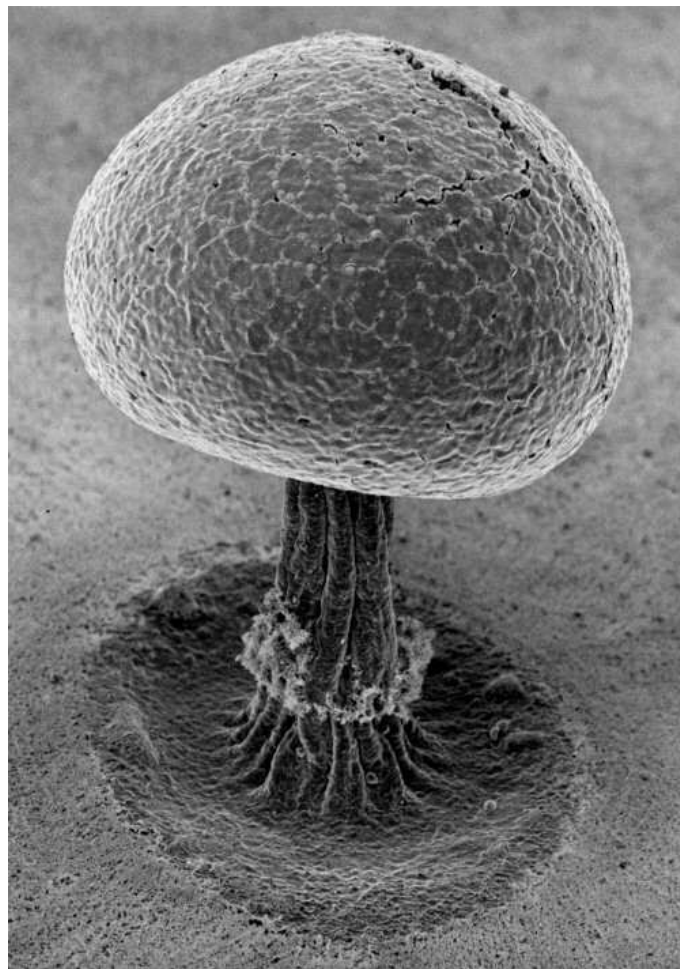
Figure 2-1: *Scanning electron micrograph showing self-organization of cells into a slime mould under starvation conditions.*[1]

lence [Swartz 07]. Swartz et al. [Swartz 07] identify a functional role for a new type of light sensors in bacteria light-Oxygen-Voltage (LOV) histine kinase. Light increased the enzymatic activity of this kinase, which remarkably increased the virulence of bacteria. Deletion of the gene encoding LOV kinase from the Brucella abolished the light-mediated virulence response, reducing bacterial proliferation in light-exposed macrophage cells to the level observed in the dark [Swartz 07]. Besides, in the multicellular Dictyostelium Discoideum slug, cells organize themselves through cell-cell communication to coordinate their movement and were able to sense and react to external signals like light and temperature [Miura 00]. The Dictyostelium Discoideum cAMP secreted waves were also shown to change in presence of light irradiation. However, the precise role of cAMP, which is one of the most known pathways of inter-cellular communication, is still to be determined in the context of phototaxis [Miura 00].

---

[1] www.fungalcell.org.

3   Modeling interacting cell systems

The systems that need to be analyzed are becoming more and more complex in terms of their inter-dependencies. In addition, the old modeling techniques are approaching their design limits. Nowadays, systems are built from the ground-up, in contrast to the top-down modeling approach.

Theoretical models are developed in order to mimic biological systems and to identify the underlying processes between constituents using computer simulations. The art of mathematical modeling is to choose an adequate modeling approach. This process starts by specifying the questions to be answered and continues by identifying all variables and connections between them that are relevant for answering these questions. Each modeling approach has its assets and drawbacks. As a rule of thumb, computationally cheap methods often only give a very rough representation of reality and, therefore, they often only provide answers to questions of a very general kind. Questions with regard to specific system properties typically require detailed calculations involving sophisticated computational methods. Ideally, different modeling approaches can be combined where answers to questions obtained at a certain level of resolution serve as input for modeling at a level of higher resolution. The simplest model perspective is the macroscopic approach which assumes that the cellular system under consideration is homogeneously mixing over its entire spatial extent. This implies that all constituents are present in sufficiently large amounts such that concentration of cell types rather than individual cells can be considered. If this condition is met, the system dynamics may be well described in terms of ordinary differential equations that yield continuous and deterministic results.

However, stochastic effects take over where cell numbers are locally small, and the dynamic formation of cellular aggregates out of single cells requires a spatio-temporal modeling approach. This is achievable within the agent-based modeling frame, where each individual cell is treated as an agent that migrates and interacts with other agents according to specific rules that are motivated by the underlying biological processes.

3.1   The agent-based model approach

Agent-based models (ABMs) offer a flexible and intuitive framework for coping with many types of complexity that are encountered in biological systems. The structure of the system can be specified both by placing constraints on the system as a whole and by specifying the organization of agents individually. Agents are identifiable, situated, goal directed and flexible computational entities. They are discrete and defined in terms of both their attributes and their behavior. Furthermore, agent instances can be separated from their function and behavior which addresses the context- and time-dependent nature of biological functions. This ensures a maximal degree of control over all system properties.

A biological entity can be represented as participating in multiple pathways and processes at different times or in different environments. Both system and entity behavior can be dependent on a unique history because agents have unique identities. The actions of agents can be scheduled to take place synchronously (*i.e.*, every agent performs actions at each discrete time step) or asynchronously (*i.e.*, agent actions are scheduled with reference to a clock or to the actions of other agents).

Furthermore, actions follow discrete-event cues or a sequential schedule of interactions and are not simultaneously performed at a constant time-step. The behavior of agents can vary from completely reactive –this is to say that agents only perform actions when triggered to do so by some external stimulus, *e.g.* actions of another agent– to goal-directed through seeking for a particular goal.

Besides, due to the richer behavioral representations afforded by ABMs, they acquire several advantages from their computer-simulation heritage. Because an ABM is a dynamical system, the model can incorporate positive and negative feedbacks, such that the behavior of an agent has an influence on the subsequent behavior of other agents. Interactions in ABMs can be dynamically changed as the simulation runs, because they are defined at the agent level.

Figure 3-1 shows the position of agent-based models on a physical space representation versus the internal state representation with a comparison to other modeling techniques. Ordinary differential equations enable a continuous description of space and time, discretization of the state with a continuous description of space leads to state based models and the increase of spatial resolution while keeping low state description

can be treated within partial differential equations (PDEs). Finally, ABMs come as a discrete high-resolution description of both state and space. ABMs are applicable to many situations, for instance when the agent diversity has an effect on the evolution of the system. Thus, agent simulation can be used to study how patterns and organizations emerge and to discover how system-level structures form when they are not apparent from the behavior of individual agents. Agents can act according to base-level rules with regard to their characteristic behavior, as well as according to high-level rules that induce changes of the base-level rules in the course of time. In this way ABMs capture phenomena of adaptivity in biological systems.

In general, ABMs are used in different applied sciences where the complexity of systems hampers the drawing of conclusions or the setting of hypotheses in a straight-forward manner. Finally, this realistic modeling approach is of great help when experiments are too expensive or simply not feasible. Moreover, the predictive power of ABMs can help reducing the number of animal experiments by making concrete proposals for new relevant experiments.

A unique aspect of ABMs compared with other computational strategies is the inclusion of agents whose behaviors are directed by logical rules. The rules are a collection of clear, concise statements, often represented as 'If-Then-Else' relationships in the algorithm. The heterogeneity in agent behavior can be incorporated by drawing parameters of a utility function from a statistical distribution, or by using alternative decision making approaches for different agent types. ABMs can be deterministic, probabilistic, or a combination of the two, with the possibility to tune stochasticity.

Building a model requires a clear definition of the system and the questions to be answered. Subsequently, agents must be identified and in addition to the theory that defines their behavior, the interactions between the same agents have to be designed too. However, it is difficult to locate key model parameters, including rate constants, in published literature. In these cases, parameters need to be estimated, and the model has to be validated, either with experiments or compared to other models. Moreover, a realistic computational time for running the simulations should also be considered while designing the model.

Fortunately, ABMs have found applications in solving practical problems and advancing research agendas. In the following Section 3.2, we will refer to a few standard mathematical models in biology.
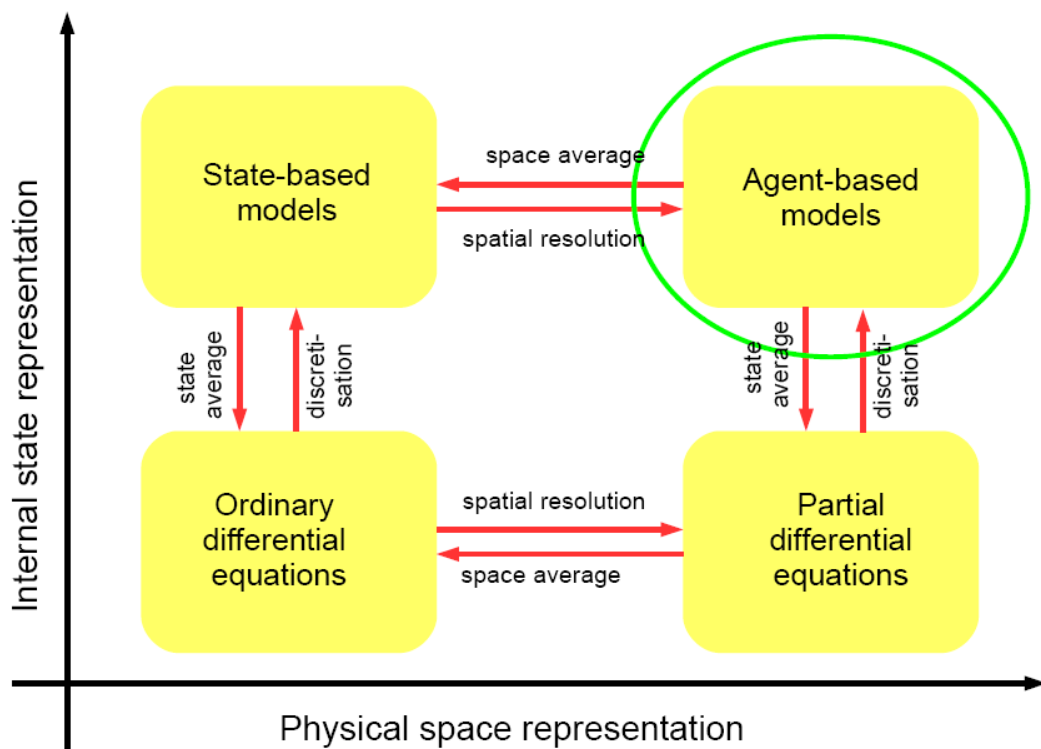
Figure 3-1: *Methods used to model biological systems*

3.2 Agent-based models in biology

In biology, three classes of models can be distinguished. The first instance in which model observations have been validated or refined by experiments, a second instance in which models have generated novel hypotheses that still need to be verified by future experimental efforts, and a third instance in which the development of new models in the future would improve the understanding of biological processes. Usually, the set of all the components and the interactions between them gives rise to the general behavior of the system under observation.

The immune system is capable of self-organizing and adapting to various environmental perturbations or external stimuli, while being able to discriminate between self and foreign antigens as much as to develop memory. ABMs constitute a very adequate modeling structure for the representation of the immune system. They can help answering many questions concerning the effect of agent diversity on the evolution of the system, predict possible dominance of a precise agent, or the evolution to a stable mix of agent types. Recently, two-photon microscopy shed light on new cellular interactions and dynamics. Typically, the formation of germinal centers or the cellular migration between the dark and the light zones, profited from new data but also from predictions and explanations provided by ABMs applied to this specific matter.

3.2.1 Continuum approach: The seminal Keller-Segel model

The simplest description of a cell population, which produces a chemical signal and responds to it by performing a chemotaxic move is the Keller-Segel model originally developed in the context of investigating slime mould formation.

Keller and Segel were the first to formulate a model that describes the formation of the chemotactic bands of traveling bacteria observed by Adler in 1966. The model is written in a nondimensionalized form with the cell density and the chemical concentration both depending on time and position. The first equation 3.1 describes the chemotactic reaction of cells, and the second equation 3.2 is a quasistationary approximation of a reaction-diffusion equation for the chemical concentration. In this model, it was assumed that bacteria did not reproduce during the time scale of interest and responded to a single

substrate of attractant which did not diffuse.

$$\frac{\partial b}{\partial t} = \nabla \left(\mu(s) \nabla b \right) - \nabla \left(\chi(s) b \nabla s \right) + g(b, s) - h(b, s), \qquad (3.1)$$

$$\frac{\partial s}{\partial t} = D \nabla^2 s - f(b, s) x, \qquad (3.2)$$

where $b = b(x, t)$ is the density of bacteria population, $s = s(x, t)$ is the attractant concentration at spatial position x and time t, $\mu(s)$ is the bacterial diffusion coefficient, $\chi(s)$ the chemotactic coefficient, $g(b, s)$ and $h(b, s)$ are for growth and death respectively, $f(b, s)$ is a function describing attractant degradation and D is the diffusion coefficient of the attractant.

The solution showed that the initial bacterial density does not greatly affect the results. Unfortunately, this rudimentary description did not lead to the experimentally observed patterns. Because the Keller-Segel model did not successfully reproduce all of the experimental observations, other models were derived from the Keller-Segel's first formulation, either by accounting or not for bacteria's reproduction or death-growth ratio, or including and excluding diffusion of bacteria. Varying the parameters and boundary conditions allowed several new observations. For example, In 1973 Segel and Jackson noted that constant rates of diffusion and chemotaxis were only valid in the case of a population of identical organisms and individual response to chemoattractants would result in a variance in the overall population response. Nossal and Weiss, by reformulating the boundary conditions in 1973, showed that the bacterial density curve increased at a rate proportional to the square root of time. A lack of bacterial growth did not prevent the formation of the typically traveling bacteria bands, but cells were lost to diffusion, resulting in a decrease in band speed leading to a broadening of the bacterial profile.

More complex but more biologically realistic models were developed after the Keller-Segel's description [Monk 89] of chemotaxis. However, fully continuous modeling techniques were not suitable for studying systems with many cell types and different interactions. ABMs come as the method of choice, for them being highly adaptable to different systems. Still, some models called Hybrid models continue to use a discrete description of the system in combination with reaction-diffusion equations often inspired from Keller-Segel's model.

3.2.2 Discrete Modeling of immunological systems

The first mathematical models for spatial patterning were based on a continuum description of the chemoattractant diffusion. Dallon and Othmer (1997) [Dallon 97] developed for the first time a model where cells were considered as discrete entities with a continuous description of the chemoattractant concentration. Many models have been now developed following this philosophy or with a full discretization of space and time among which we can find models of the immunological system. A few examples are reviewed here.

Cancer models Tumors are typically characterized by an unbalanced rate of cellular death and production. Besides, cancerous cells develop various techniques that avoid encounters with lymphocytes. In fact, they are able to trick immune mechanisms that aim to destroy malignant or foreign entities. Understanding the evasive behavior of these cells is of major importance, and the control of the production-death rates will facilitate the control of tumor evolution and spreading in the body.

In 1991, Chowdhury et al. [Chowdhury 91] presented an ABM for characterizing interactions between tumor and immune cells. The model was constituted of several independent agents, accounting for different cell types like B-cells, T-helper cells, T-killer cells, T-suppressor cells and tumor cells with and without antigen [Chavali 08]. Using different concentrations of cell-types. The results were presented as a loss of steady-state fixed points consisting of high or low concentrations of cell-types corresponding to cancerous or non-cancerous states.

Years later, Mallet et al. [Mallet 06] presented a hybrid ABM-partial differential equation model of moderate complexity to describe the interactions between a growing tumor next to a nutrient source and the immune system of the host organism [Chavali 08]. Natural killer cells, cytotoxic T lymphocytes and tumor cells constitute the implemented agents that evolved within the surrounding of diffusing nutrients modeled with PDEs and solved for concentrations of nutrient species. The PDEs solutions were reinjected into the ABM to evaluate cell activities, such as motility and division. The model allows both temporal and two-dimensional spatial evolution of the system under investigation and is comprised of biological cell metabolism rules.

Germinal center   Newly generated data performed with two-photon imaging as published by three experimental groups [Depoil 05, Allen 07b, Schwickert 07], provided more details concerning the movement of lymphocytes in GCs during the affinity maturation. A three-dimensional reconstitution of B-cell tracks, relying on speed and turning angle distributions obtained by two-photon imaging, was used for implementation in a model imagined by Figge et al. [Figge 08] using a statistical and a functional approach to simulate cell migration during affinity maturation in the GCs. The results suggest that B-cells in GCs perform a random walk with a directional persistence time and transient sensitivity to chemokines.

Immunological synapse formation   T-cell activation requires interaction of T-cell antigen receptors with proteins of the major histo-compatibility complex (antigen). This interaction takes place in a specialized cell-cell junction referred to as an immunological synapse. To investigate the formation of geometrically repatterned immune synapses observed in vitro, cells were left to evolve on a lattice with artificially imposed barriers [Figge 06, Figge 09]. Starting with randomly distributed TCR-pMHC (receptor) and LFA-1-ICAM-1 (ligand) complexes on the lattice, a set of rules and different pre-imposed probabilities to perform actions, representing attractive and repulsive forces between ligands and receptors, Figge et al. [Figge 06, Figge 09] successfully reproduced the initial experimental data.

Lymph node   In this model, sixty-four virtual viruses were generated by an assortment of speed of growth, infectivity level and lethal load [Kohler 00]. The aim of this model was to explore a wide range of virus-host relations, and to offer realistic predictions to help vaccine development against specific diseases. Several parameters were injected in this model aiming to reproduce experimental observations, such as positive and negative selection in the thymus, antibody dynamics and response to different antigens.

The results of in silico experiments were able to predict the success rates of certain combinations of viral parameters and the immune response to them. Furthemore, this model enabled the determination of a list of viruses that are more or less sensitive to the humoral or cellular responses. This was achieved by the exploration of all included parameters and their inter-dependencies.

Lymphocyte shape dynamics   A theoretical sub-cellular model for B and T-cell motility in the GC was developed by Meyer-Hermann et al. [Meyer-Hermann 05a]. The movement and deformation of cells were correlated to each other using a subunit system. Cell movement is considered to be composed of the movement of cell membrane subunits evolving on a lattice as agents.

The ratio of cell's long-axis/short-axis describing the cell's elongation, presumably induced by its motility, was in agreement with the experimental data. The results revealed that the rearrangement of subunits with respect to a virtually shifted barycenter of the cell (active movement) and a rearrangement of the subunits with respect to the actual barycenter (reshaping force) [Meyer-Hermann 05a] are sufficient to describe lymphocyte motility as a random walk with a persistence time of about 2 minutes.

Discrete Modeling of phototaxis   Agent-based models of the phototactic behavior of bacteria are still very rare. Recently, Levy et al. [Levy 08] presented a model where the excitation of each individual bacterium was assumed to vary depending on the excitation of the neighboring bacteria. Individual cells were less likely to move toward light, in contrast to groups of cells that were more likely to move. The observed dynamics appeared to be a complex function of cell density, surface and genotype. The ABM takes into account the excitation of each bacterium, in addition to a surface memory effect. The assumption of the existence of an excitation mechanism is of critical importance. In fact, this property is what distinguishes the model from other chemotactic models [Levy 08]. An excitation threshold below which cells will move only according to the surface memory or to the imposed diffusion process. Note that the bacterial population is considered in this model to be of fixed size and the external light source was always present.

The chart flow in Figure 3-2 describes the logical rules implemented in this ABM, that lead to the emergence of different patterns observed in vitro, including fingering depending on different initial conditions.

3.2.3   On discrete Random Walk

Isotropic random walk   The motion of agents on a spatial lattice can be either directed or random, dependent or independent on each other, active or passive with regard to signals. The random walk is a stochastic displacement where single agents make ran-
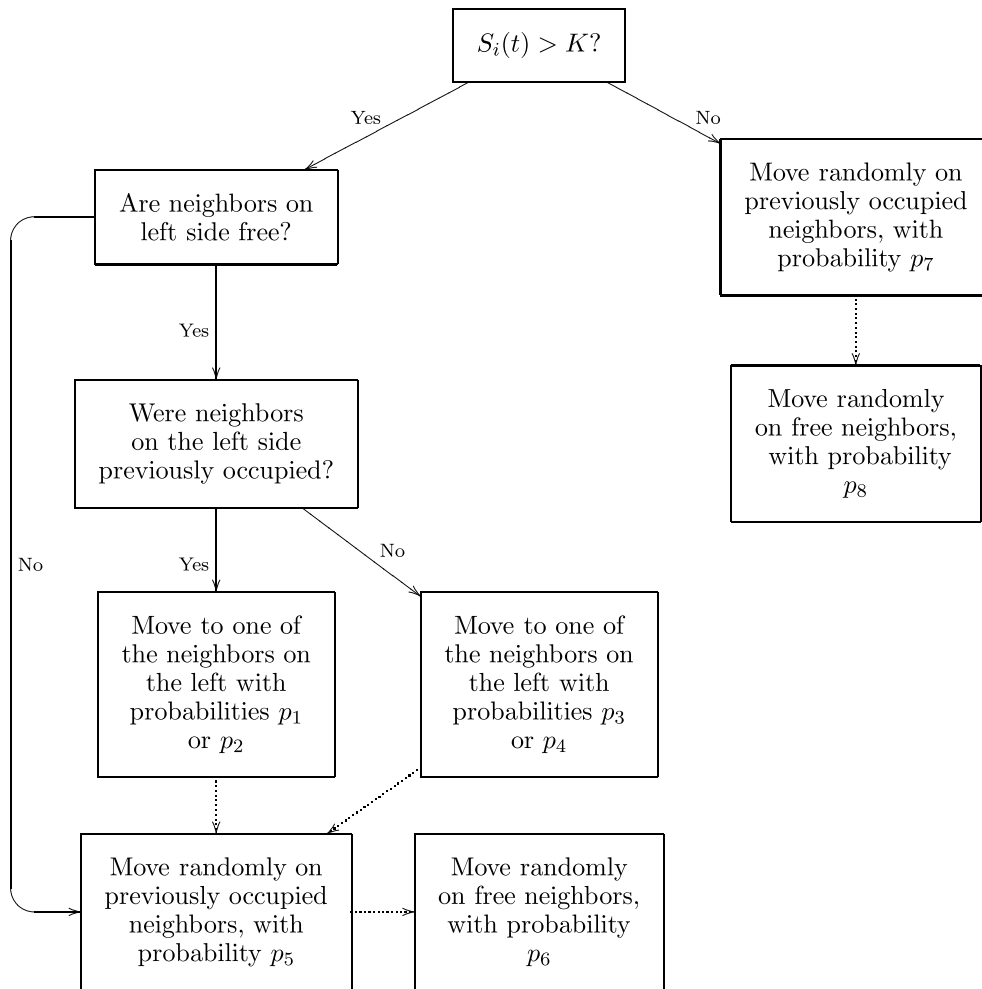
Figure 3-2: *Rules of motion for the cellular automaton model. The dotted lines are traversed only if the cell did not move in any of the previous steps. After applying these rules of motion to every cell in the colony, the excitation is updated based on the excitation of the new neighboring cells [Levy 08].*

dom steps in each time step.

Random walk is described by choosing a new random direction at each time t and moving a step in that direction, the spatial steps are always of equal length in any direction and successive moves are independent of each other. Since the particles should not have any preferential direction, an equal probability is taken for jumps in all the directions. In this case the random walk is called isotropic or unbiased. The implementation of random walks in ABMs is pretty easy and the interaction with the neighborhood defines the range of possible moves and the sequential procedure allows some particles to move more than others.

Persistent random walk   Animal and cell movements are often characterized by some directional correlation called persistence. Most of the commonly used random walk models assume that the direction of travel during step i of a random "walker" is independent of the direction taken at step $i-1$. However, the movements of many entities including animals, exhibit persistence, *i.e.* the direction of travel during step i is clearly dependent on the direction traveled in step $i-1$. Furthermore, it was also observed, that environmental variation can lead to changes in the persistence of movement and that with a suitable model it is possible to relate the dynamics of cellular distributions to environmentally induced changes in this persistence.

Persistent random walks involve a correlation between successive step orientations. Each newly taken step, has a higher probability of pointing to the same direction as the previously taken step, called local directional bias [Benhamou 06]. This probability is reduced with time leading to a uniformly distributed orientation on a long run. Imposing a certain probability to move in a preferred general direction, is also possible and is named global directional bias [Benhamou 06].

Turning angle   Typical random walk models allow only a restricted number of turning angles at each step. More complete models integrate a continuous choice of the new direction for the next step. In a two dimensional system, the walker is allowed to move in any direction θ on the unit circle [Uttieri 07]. Circular distributions can be used to pick random angles for either the direction of movement or the turning angle at each step of a two-dimensional random walk.

4 Intravital microscopy of cell migration and interaction

Since a few years, the migration and interaction of cells are extensively explored by non-invasive intravital microscopy techniques [Cahalan 08]. This technique presents the advantage of following cells in real time and within their natural cellular environment.

A large body of data has been generated in this way, including four-dimensional records of cell tracks, *i.e.* the time-dependent position of single cells in three spatial dimensions, as well as cellular contact times of interactions. The working principle of imaging by multi-photon microscopy is summarized in Section 4.1 and an overview of dynamical cell properties that can be explored by this experimental technique is presented in Section 4.2.

Mathematical methods are required to analyze the experimental data in order to extract meaningful conclusions and to initiate new insights and experiments. Recent results from applying intravital microscopy within the field of immunology are reviewed in Section 4.3.

4.1 Intravital microscopy: Working principle

Optical multi-photon microscopy is the method of choice for *in vivo* imaging of single-cell dynamics and cellular interactions. Similar to conventional methods that employ fluorescence techniques, like wide-field and confocal microscopy, multi-photon microscopy is based on light excitations of fluorophores that absorb and re-emit light at different wavelengths. Single-photon excitations typically require photon wavelengths in the order of 400 nm. This wavelength corresponds to high photon energies that give rise to phototoxicity and strong scattering in biological tissue (see Figure 4-1).

Multi-photon microscopy is based on the light excitation by two or more photons occurring simultaneously. Thus, using a two-photon microscope, a fluorophore is simultaneously excited by two photons. Figure 4-2 shows a comparison of two-photon

fluorescence and single-photon fluorescence. Each of the two photons contributes one half of the energy required to induce fluorescence, such that low-energetic photons with long wavelengths in the order of 800 nm can be used. This strongly decreases the absorption and scattering of light in biological tissue, as schematically shown in Figure 4-1. Moreover, infrared photons have negligible impact on the biological sample with regard to phototoxicity and photobleaching, such that imaging up to millimeter-depths can be realized without inducing significant damage to the biological sample. This is the main advantage of intravital multi-photon microscopy.

The required photon density at the focal spot of the microscope objective is generated by a pulsed laser, which is adjusted in such a way that two factors are balanced: On the one hand, the density has to be sufficiently high in order to induce multi-photon excitations, on the other hand it has to be kept sufficiently small in order not to damage the biological sample. These requirements on the photon density for the induction of multi-photon fluorescence is only met within the confined volume of the focal spot (see Figure 4-2), since the fluorescence power decays with $1/z^2$, where z denotes the axial distance away from the focal focus as shown in Figure 4-3. As a consequence, the resulting images are free of out-of-focus fluorescence (see Figures 4-2 and 4-3) and therefore provide higher image contrast as compared to single-photon techniques.

As with conventional microscopes, the multi-photon microscope allows to generate image sequences, which is achieved by scanning the focal spot across the sample. The data are typically analyzed by advanced tracking software that can identify individual cells and follow their history, *i.e.* the migration path and the interaction events, in the three-dimensional stacks of image sequences. The high spatial and temporal resolution makes laser scanning multi-photon microscopy being the state-of-the-art technique for intravital cell imaging in biological tissue.

4.2   Exploring Dynamic Cell Properties

Multi-photon imaging yields data on the position and on the geometric shape at each time point of the measurement and for each cell within the three-dimensional focal spot.

We consider an image sequence that consists of $N+1$ single measurements, recorded with the time step Δt. The position of the ith cell, $(x_i(n), y_i(n), z_i(n))$, and its geometric shape are observed at time points $t_n = n\Delta t$ with $n = 0, 1, 2, \ldots, N$. The

geometric shape of the ith cell may be quantified by the shape index $s_i(n)$ and captures time-dependent changes of the cell geometry. It is convenient to combine the data on the cell track and cell shape in the lists

$$\mathcal{T}_i \equiv \begin{pmatrix} x_i(0) & x_i(1) & x_i(2) & \ldots & x_i(N) \\ y_i(0) & y_i(1) & y_i(2) & \ldots & y_i(N) \\ z_i(0) & z_i(1) & z_i(2) & \ldots & z_i(N) \end{pmatrix} \tag{4.1}$$

and

$$\mathcal{S}_i \equiv \begin{pmatrix} s_i(0) & s_i(1) & s_i(2) & \ldots & s_i(N) \end{pmatrix} \tag{4.2}$$

for each cell $i = 1, 2, \ldots, I$, respectively.

The shape index may be defined in various ways. For example, the cell geometry can be viewed as an ellipsoid with equatorial radii a, b, and c. Performing a two-dimensional projection, the ellipsoid may be approximated by an oblate ($a = b > c$) or a prolate ($a = b < c$) spheroid. In this case the shape index can be defined as the ratio of the long to the short axis and is a function of time (see Figure 4-4). As a consequence, $s_i(n) \geq 1$, where $s_i(n) = 1$ indicates a spherical and $s_i(n) > 1$ indicates an elongated cell shape.

The cell track lists $\mathcal{T}_i$ serve as the basis for calculating characteristic quantities of the cell migration. Viewing these lists as $3 \times N$ matrices, the nth column contains the position vector of the ith cell at time t_n:

$$\vec{\mathcal{R}}_i(n) \equiv \begin{pmatrix} x_i(n) \\ y_i(n) \\ z_i(n) \end{pmatrix}. \tag{4.3}$$

Typically, observables of interest are presented as the average over all monitored cells. The average of observable O_i is obtained by summation of the corresponding quantity for each cell i and dividing by their total number I:

$$\langle O_i \rangle \equiv \sum_{i=1}^{I} O_i. \tag{4.4}$$

However, it should be noted that the number of cells may be a function of time, $I = I(n)$.

This is due to practical reasons, since cells may exit the focal spot at longer times and cannot be imaged and tracked anymore. The fewer remaining cells may give rise to standard deviations of the averaged observables that are increasing with the measurement time.

We now turn to examples of observables that serve to characterize the migration behavior of cells. The time-dependent displacement vector of a cell,

$$\vec{r}_i(n) \equiv \vec{\mathcal{R}}_i(n) - \vec{\mathcal{R}}_i(0) \,, \tag{4.5}$$

is measured relative to its starting point and is used in the calculation of the mean cell velocity

$$\langle \vec{v}_{i,m}(n) \rangle \equiv \frac{\langle \vec{r}_i(n) \rangle - \langle \vec{r}_i(n-m) \rangle}{m\Delta t} \tag{4.6}$$

at times $t_n = n\Delta t$ with $n \geq m$. It is important to note that $\vec{v}_{i,m}(n)$ may depend on the choice of the time interval $m\Delta t$. Therefore, the interpretation of a cell's speed, $v_{i,m}(n) = |\vec{v}_{i,m}(n)|$, may lead to wrong conclusions: For small time intervals $m\Delta t$, the cell speed may be overestimated due to the jitter motion of otherwise stationary cells. On the other hand, if the cells perform random walk migration, the actual cell speed may be underestimated for too long time intervals $m\Delta t$.

As has been explained before, random walk migration refers to cells that do not move unidirectionally but randomly change their migration direction. Such random changes may occur at each time step of the measurement, or only after a number of time steps have elapsed. In the latter case, a directional persistence time exists and corresponds to the time interval Δt_p during which cells migrate in the same direction before randomly turning into another direction.

Analyzing the time-dependence of the measured mean displacement, $\langle |\vec{r}_i(n)| \rangle$, reveals characteristic differences between unidirectional migration and random walk migration. If cells perform unidirectional migration, *e.g.* by following chemokine gradients, their mean cell velocity is a constant and

$$\langle |\vec{r}_i(n)| \rangle = \langle |\vec{v}_{i,n}(n)| \rangle \, t_n \,. \tag{4.7}$$

In other words, $\langle |\vec{r}_i(n)| \rangle$ equals exactly the mean path length $\langle l_i(n) \rangle$. The latter is defined by:

$$\langle l_i(n) \rangle \equiv \frac{1}{n} \sum_{n'=1}^{n} \langle |\vec{r}_i(n') - \vec{r}_i(n'-1)| \rangle . \tag{4.8}$$

such that

$$\frac{\langle |\vec{r}_i(n)| \rangle}{\langle l_i(n) \rangle} = 1 \tag{4.9}$$

for unidirectional migration.

In contrast, for cells performing random walk migration, the mean path length becomes significantly larger than the mean displacement,

$$\frac{\langle |\vec{r}_i(n)| \rangle}{\langle l_i(n) \rangle} \ll 1 , \tag{4.10}$$

at times $t_n \gg \Delta t$. This is a consequence of the fact that the cells randomly change their migration direction and eventually re-approach their starting point, as can be seen in Figure 4-5. The difference between unidirectional migration and random walk migration is depicted in Figure 4-6. In the latter case, the mean displacement does not scale linearly with time but with the square-root of time,

$$\langle |\vec{r}_i(n)| \rangle = \sqrt{2dM}\sqrt{t_n} . \tag{4.11}$$

Here, the proportionality constant depends on the system's spatial dimension d and the motility coefficient M. The mean displacement for different migration behaviors is schematically shown in Figure 4-7. Note that random walk migration with a directional persistence time is a combination of unidirectional migration on small time scales and random walk migration on large time scales. The time scale is set by the directional persistence time: At times $t_n < \Delta t_p$, $\langle |\vec{r}_i(n)| \rangle$ scales linear with time and assumes scaling with the square-root of time for $t_n > \Delta t_p$.

Taken together, multi-photon imaging provides a firm data basis to characterize the migration behavior, shape dynamics, and cellular interaction times of cells in intact biological tissue. A summary of accessible motility parameters is presented in Table 4.3.3. The main strength of multi-photon microscopy is the ability to maintain resolution and contrast within scattering tissue, which allows direct visualization of cells in their natural

environment and in response to systematic manipulations [Helmchen 05].

4.3   Analysis of multi-photon data in immunology

Optical microscopy employing fluorescence techniques has proven to be highly suited for imaging in immunology, permitting both labeling of specific cells, organelles, or proteins and functional reading of biological events [Petty 07] The accurate and ingenious choreography of cell motility and cell-cell interactions in a variety of in vivo settings has been revealed at imaging depths up to one millimeter into living tissue [Cahalan 08]. Quantitative information on the cell motility, shape dynamics and contact durations for cellular interactions can be derived from these data by mathematical analysis that shape our interpretation of these data. In this section we consider various examples of mathematical analysis of two-photon microscopy data including lymphocyte migration, interaction and shape dynamics.

It should be stressed that mathematical analysis is not just a descriptive approach. Rather, it constitutes a predictive consistency check of working hypotheses underlying the interpretation of experimental data. An example of this process will be described in Chapter 5 on B-cell migration in germinal centers.

A mandatory prerequisite for realistic models of lymphocyte migration and interactions is a firm experimental data basis. New system features are discovered by including more detailed aspects of cell dynamics into the mathematical models. This is becoming more feasible in recent years due to continuously growing computer resources. At the same time experimental techniques are developing fast and highly accurate data are generated, such that the real challenge for modelers and experimentalists is to keep pace in working hand in hand. The highest benefit can be expected from symbiotic effects of theory and experiment.

4.3.1   T-cell migration in lymphoid tissue

Various studies have concentrated on imaging individual T-cells within lymphoid organs [Mempel 04, Miller 02, Miller 03, Miller 04]. In general, the experimentally derived mean displacement curves as a function of the square-root of time show the characteristics of random walk migration with a directional persistence time.

A mathematical analysis was performed within a statistical cell track model approach with the aim to estimate values of parameters underlying T-cell migration [Beauchemin 07]. We briefly outline the general procedure of this mathematical analysis that involves the reconstruction of experimentally observed cell tracks in order to identify underlying migration mechanisms.

Cells are treated as independently migrating point particles that have a speed and a polarity vector. Cell tracks are re-constructed by calculating the position vector $\vec{r}_i(n+1)$ of the ith cell at time $t_{n+1} = (n+1)\Delta t$ from its position $\vec{r}_i(n)$ and its velocity $\vec{v}_i(n)$ at time t_n:

$$\vec{r}_i(n+1) = \vec{r}_i(n) + \Delta t \vec{v}_i(n) \,. \tag{4.12}$$

Thus, the new cell position is calculated by updating the velocity,

$$\vec{v}_i(n) = v_i(n)\vec{e}_i(n) \,, \tag{4.13}$$

at each time step Δt of the measurement. The velocity is represented in terms of the cell speed $v_i(n)$ and the cell polarity vector $\vec{e}_i(n)$, which in spherical coordinates is given by

$$\vec{e}_i(n) = \begin{pmatrix} \sin(\vartheta_n)\cos(\varphi_n) \\ \sin(\vartheta_n)\sin(\varphi_n) \\ \cos(\vartheta_n) \end{pmatrix} \,, \tag{4.14}$$

with $\vartheta_n \in [0, \pi[$ and $\varphi_n \in [0, 2\pi[$ denoting the spherical angles.

Depending on the available data basis, one has to specify the procedure according to which Eq. (4.12) is updated. In Ref. [Beauchemin 07], the three-dimensional T-cell tracks were projected on a two-dimensional plane by neglecting the z-component of the polarity vector Eq. (4.14). The new polarity vector reads

$$\vec{e}_i(n) = \begin{pmatrix} \sin(\vartheta_n)\cos(\varphi_n) \\ \sin(\vartheta_n)\sin(\varphi_n) \\ 0 \end{pmatrix} \tag{4.15}$$

and does not have anymore the property of being a unit vector. The re-construction of cell tracks was then performed according to Eqs. (4.12) and (4.13). In doing so, the cell

speed was set to a constant value,

$$v_i(n) = v, \tag{4.16}$$

for all cells.

Figure 4-8 gives an idea how the reconstituted two-dimensional tracks may look like. The square root time plotted against the mean displacement of the cells is clearly indicative of a random walk. Furthermore, the time step Δt was decomposed into two time intervals: (i) the persistence time Δt_p during which cells migrate with constant speed, and (ii) the re-polarization time Δt_r during which cells do not move but are thought to reposition their lamellipods and uropod. After having paused, T-cells randomly pick a new direction of migration. This was realized by choosing new angles ϑ_n and φ_n from uniform distributions [Beauchemin 07].

The set of parameters contains three quantities: $\{v, \Delta t_p, \Delta t_r\}$. Re-constructing a number of 10^6 individual cell tracks in a randomized fashion, the parameters were explored in the range $v = [5, 50]$ μm/min, $\Delta t_p = [0.5, 20]$ min, and $\Delta t_r = [0, 3.5]$ min. Then, the optimal values were determined from a fitting procedure to the experimental data. Combining the T-cell tracks of different experimental data sets [Mempel 04, Miller 02, Miller 03, Miller 04], the optimal values of the parameters are $\{v = 18.8$ μm/min, $\Delta t_p = 2$ min, $\Delta t_r = 0.5$ min$\}$. It can be concluded from this analysis that T-cells perform random walk migration with a persistence time of 2 minutes and the time for re-polarization is 30 seconds. Interestingly, neglecting the re-polarization time, $\Delta t_r = 0$ min, the optimal values changed into $\{v = 16.6$ μm/min, $\Delta t_p = 2$ min$\}$. Thus, the T-cell speed attains a somewhat smaller value, however, the persistence time remains unchanged.

It has been concluded from this analysis that the re-polarization time does not play a central role in improving the agreement with the experimental data.

4.3.2   T-cell interaction with dendritic cells

Applying the agent-based model approach, which we introduced in Chapter 3, the interaction of T-cells with dendritic cells can be studied and compared to data obtained from two-photon imaging of lymph nodes of mice [Beltman 07b, Beltman 07a]. In particular, a Potts model has been used where cells are represented by several connected points in a three-dimensional lattice. The considered cell types include T-cells, dendritic cells and static fibroblastic reticular cells forming the reticular network in lymph nodes. In the model, surface and volume energies are assigned to cells that are in contact with other cells and changes in the cellular configuration are determined by a minimization procedure of an energy functional.

The energy functional is given in terms of a Hamiltonian that has the general form:

$$
\begin{aligned}
H \;=\; & \sum_{ijk} \sum_{i'j'j'} J\left[\vec{\tau}(\sigma_{ijk}), \vec{\tau}(\sigma_{i'j'j'})\right] \left(1 - \delta_{\sigma_{ijk},\sigma_{i'j'j'}}\right) + \\
& + \sum_{\vec{\sigma}} \left[\lambda_v (v_{\vec{\sigma}} - V_{\vec{\sigma}})^2 + \lambda_p (p_{\vec{\sigma}} - P_{\vec{\sigma}})^2\right] \; .
\end{aligned}
\tag{4.17}
$$

The first term represents the surface energy J, which depends on the interacting cell types $\vec{\tau}(\vec{\sigma})$. Here, $\vec{\sigma}$ denotes the identification number of the cells on the lattice. The sum accounts for all lattice points $\{ijk\}$ and neighboring lattice points $\{i'j'j'\}$, where the Kronecker delta excludes all surface energy self-terms. The volume energy is determined by λ_v. It is a measure for the cell inelasticity and drives the actual cell volume $v_{\vec{\sigma}}$ to a pre-defined target cell volume $V_{\vec{\sigma}}$. For dendritic cells the relatively large surface to volume area is imposed by the λ_p-term in the Hamiltonian. The actual dendritic cell surface is given by $p_{\vec{\sigma}}$ and the target surface is given by $P_{\vec{\sigma}}$.

The details on the time evolution of the system for motile T-cells can be found in Ref. [Beltman 07b] together with the chosen model parameters. The procedure involves random changes in the cellular configuration that give rise to the energy difference ΔH between the two configurations. A Metropolis Monte Carlo algorithm is used to decide whether or not the new cellular configuration is accepted.

In agreement with the experimental data, the model predicts that T-cells perform random walk migration with a directional persistence time in the order of two minutes [Miller 03]. The model suggests that the migration behavior is a consequence of

T-cells having a preferred direction of motion that is adjusted by the reticular network and dendritic cells in the nearby environment. It has been proposed that T-cells migrating preferentially along the fibres of the reticular network could give rise to small, dynamic streams of T-cells through the lymph node.

With regard to the interaction between T-cells and dendritic cells, the simulations revealed that T-cells are able to scan 100 different dendritic cells per hour. This result is of interest for estimating the efficiency of negative selection in the thymic medulla and it is concluded that maturing T-cells scan about 3.4×10^4 different dendritic cells in 14 days [Beltman 07b]. It should be noted, however, that the contact duration and the scanning estimate depend on the imposed densities of the different cell types. Moreover, this estimate involves many brief contacts that last around one minute and also counts the simultaneous interaction between one T-cell and multiple dendritic cells.

The three distinct phases of T-cell stimulation have also been investigated within the cellular Potts model [Beltman 07a]. In a first phase, T-cells are rapidly migrating trough the lymph node and undergo brief encounters with dendritic cells. Then, in a second phase that starts several hours after T-cells are first exposed to their cognate antigen, T-cells are clustered around dendritic cells for more than 30 minutes. Finally, in a third phase, T-cells are again rapidly migrating and proliferating in response to antigen stimulation. The simulations based on two-photon imaging suggest that, in order to enter the second phase of T-cell stimulation, stop signals have to be provided by dendritic cells. Most probably, these signals are integrated by the T-cells during the first phase and initiate the transition to the second phase.

4.3.3 Cell shape dynamics of migrating T and B-cells

Two-photon microscopy data reveal that cell motility and cell shape are closely interlinked with each other [Miller 02]. Therefore, to analyze these data, cells cannot be treated as point particles but have to be modeled in a spatially resolved fashion. Different model approaches that can describe the shape dynamics of migrating cells [Beltman 07b, Beltman 07a, Meyer-Hermann 05b] exist. In general, an agent-based model is used with a sufficiently high lattice resolution in order to represent each cell by a collection of subunits. In addition, updating rules have to be implemented in the agent-based model to mimic realistic shape deformations of migrating cells.

Following Ref. [Meyer-Hermann 05b], cells are represented by the cell volume, the cell polarity and a list of connected cell subunits that constitute the cell shape on the lattice. Two main contributions of cell dynamics have been identified:

(i) Rearrangement of subunits with respect to the virtually shifted cellular barycenter (active movement). In reality, the direction of active movement is a complex interplay of the cytoskeleton organization and intra-cellular signaling pathways. In the model, the normalized polarization vector determines the direction of the active movement and is assumed to change randomly with a probability that is associated with the persistence time.

(ii) Rearrangement of the subunits with respect to the actual barycenter (reshaping forces). This ingredient of the cell motility model concerns the cell shape stability, since during the procedure of active cell movement the details of forces that reshape the cell towards a sphere are ignored. Within a phenomenological approximation, all reshaping forces are included in a single force, which is an overall elastic force that drives the subunits of an elongated cell back to the current barycenter and promotes a spherical shape.

The two ingredients active movement and reshaping forces turned out to be sufficient in order to describe the lymphocyte motility data obtained from two-photon imaging [Miller 02]. For example, the shape index was calculated from the data obtained for T-cell and B-cell migration in lymph nodes of mice. Projecting the cell volume on a two-dimensional plane and approximating the area by an ellipse, the shape index $s_i(n)$ of the ith cell can be calculated as the ratio of the long to the short axis. Thus, at each time step t_n, $s_i(n) > 1$ corresponds to an elongated cell shape that becomes circular for $s_i(n) = 1$.

The measurement of $I = 46$ T-cells and B-cells reveals that the average shape index is around 2.3 for T-cells and 1.6 for B-cells. Thus, the cellular elongation is about a factor 1.5 larger for T-cells compared to B-cells and this result is in agreement with the observations by two-photon microscopy [Miller 02]. It may be speculated that this points to cardinal differences in the cytoskeleton dynamics of migrating T and B-cells [Meyer-Hermann 05b]. Nevertheless, in the simulations both cell types dynamically round up and take a symmetric shape during the process of re-polarization. The shape index is a direct consequence of the reshaping forces that cells experience while they are continuing to migrate.
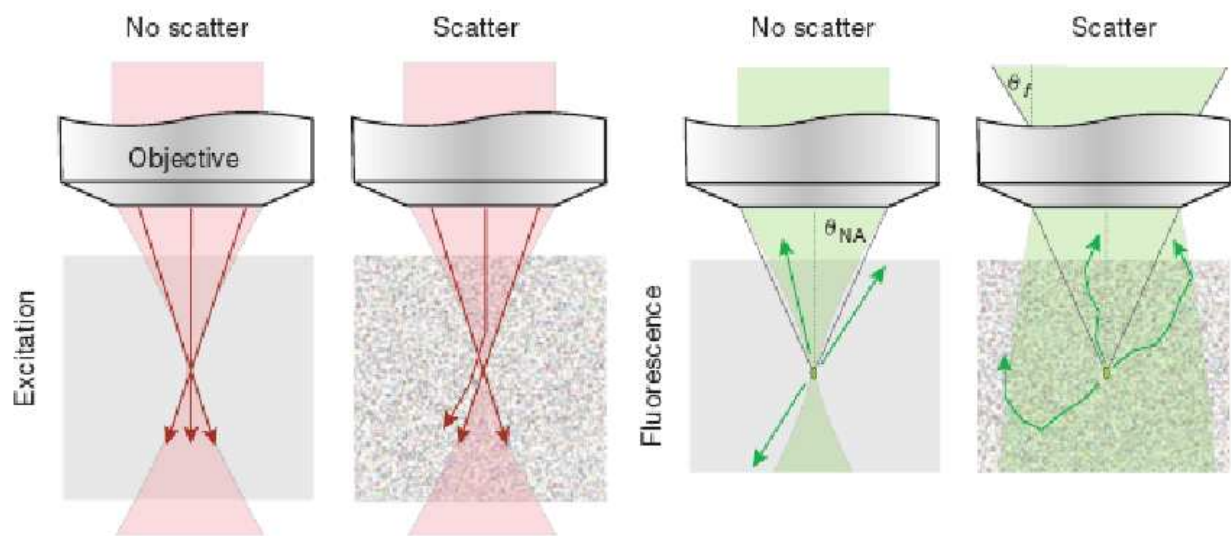
Figure 4-1: *Signal generation and fluorescence collection in clear tissue (no scatter) and in scattering tissue (scatter). In clear tissue all excitation light reaches the focus, but in scattering tissue, scattering (even by a small angle) causes light rays to miss the focus and be lost to signal generation. This leads to a roughly exponential decrease in excitation with depth. In clear tissue only fluorescence light rays initially emitted into the collection cone, determined by the objective's NA, can be detected, but in scattering tissue fluorescence light is (multiply) scattered and may even 'turn around'. Fluorescence light apparently originates from a large field of view but a larger fraction than in the nonscattering case is actually within the angular acceptance range θ_f of the objective [Helmchen 05].*

Parameter	Description (Unit)
Instantaneous velocity	Velocity calculated as displacement/time during a single time step ($\mu m/min$).
Mean velocity	Mean velocity of a cell over several time steps (usually the entire imaging period)($\mu m/min$).
Contact time	Time for which a cell is in contact with a defined cell or structure (sec:min).
Shape index	Measure of cell polarization (long axis/short axis)
Path length	Cumulative distance traveled by a cell over a given time (μm).
Displacement	Straight-line distance of a cell from its starting point after any given time (μm).
Molitily coefficient	$M = displacement^2/4t$ (for 2-D measurements) or $M = displacement^2/6t$ (for 3-D measurements); analogous to the diffusion coefficient for Brownian motion ($\mu^2 m/min$).
Chemotactic index	Displacement/path length for a given time interval (a measure of cell directionality).
Turning angle	The angle through which a cell deviates between successive time steps (degrees).
Persistence time (length)	Time (length) for which a cell continues moving in a straight line before making appreciable turn (min(μm)).

Table 4-1: *A list of parameters utilized to characterize cell motility and migration after extraction and interpretation of data provided by two-photon imaging [Cahalan 08].*

[1]Boston University, Biomicroscopy Lab.
[2]The Parker Lab, Dept. of Neurobiology and behavior, Uni. of California, Irvine.
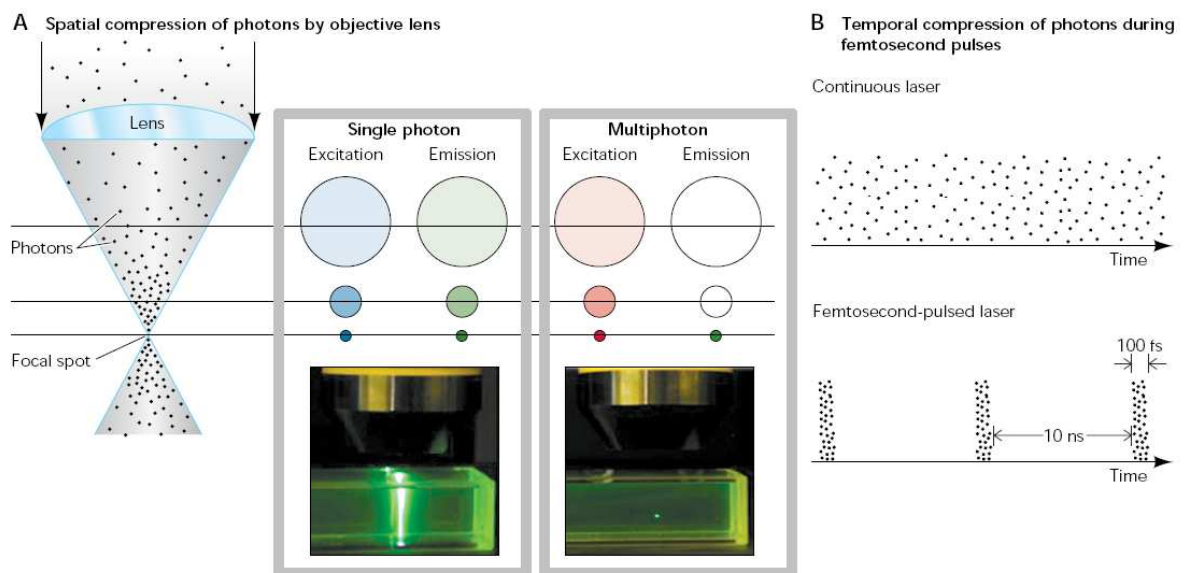
Figure 4-2: *A cuvette of fluorescent dye excited by single-photon excitation (right line) and multiphoton excitation (localized spot of fluorescence at left) illustrating that two-photon excitation is confined to the focus of the excitation beam.*[1]
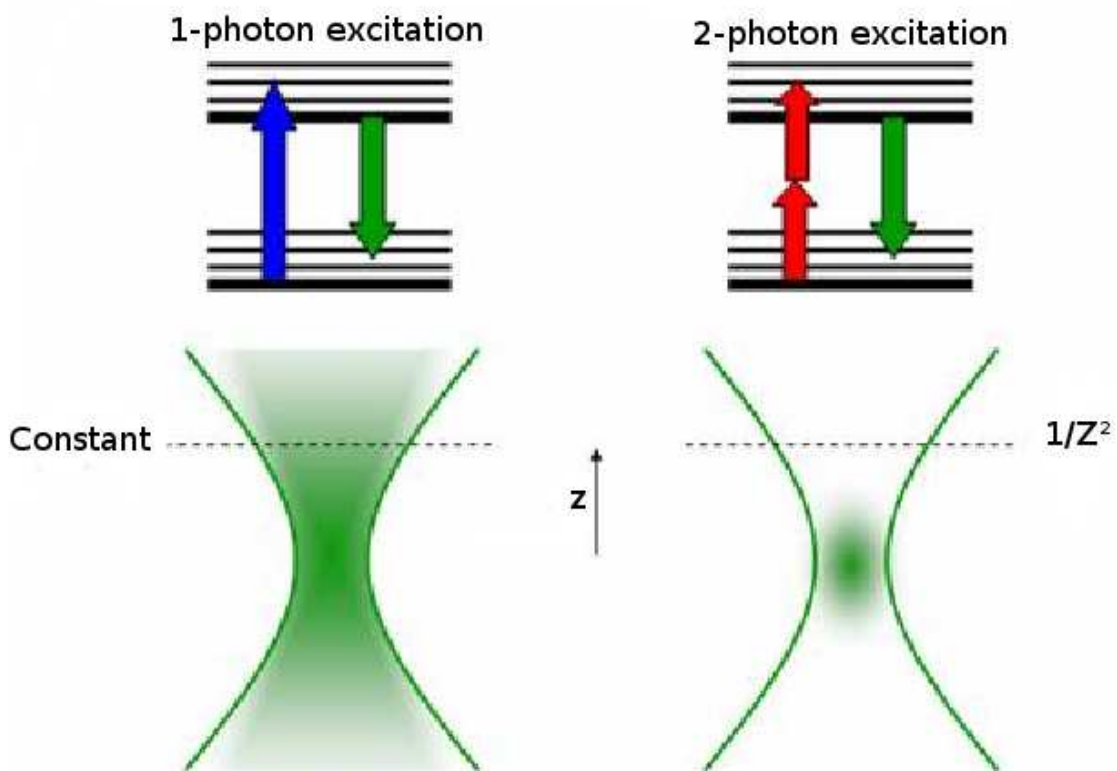
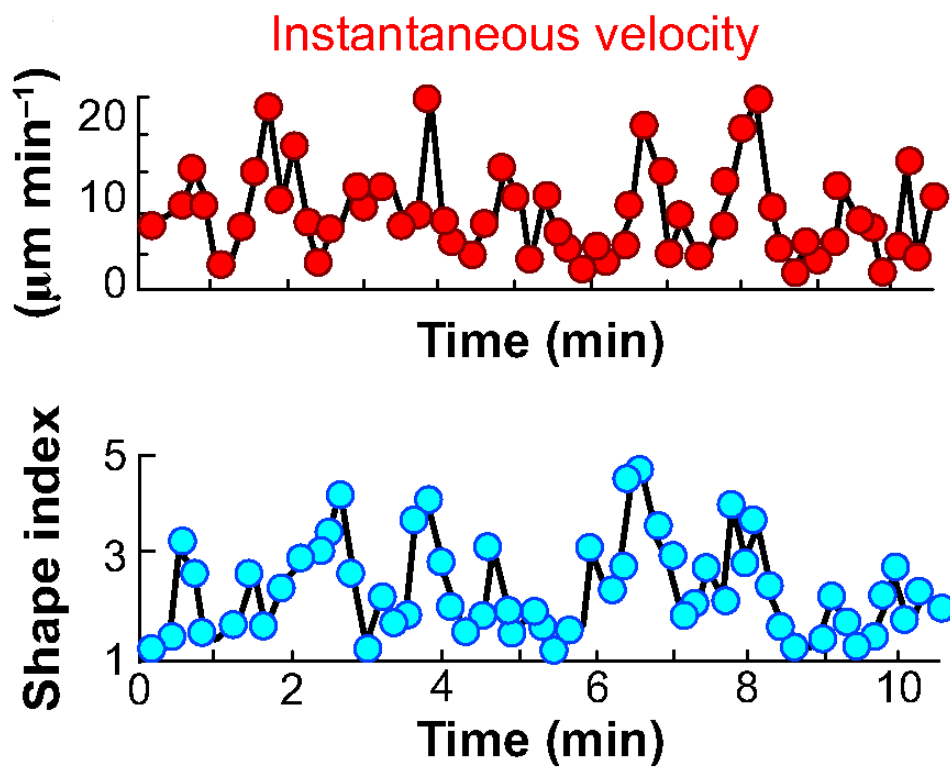**Figure 4-3:** *Working principle of one and two-photon microscopy, z denotes the axial distance away from the focus.*[2]

Figure 4-4: *The instantaneous velocity of T-cells fluctuates in a characteristic manner versus time accompanied by changes in shape index (long-axis/short-axis) as the cell elongates while moving faster [Cahalan 08].*
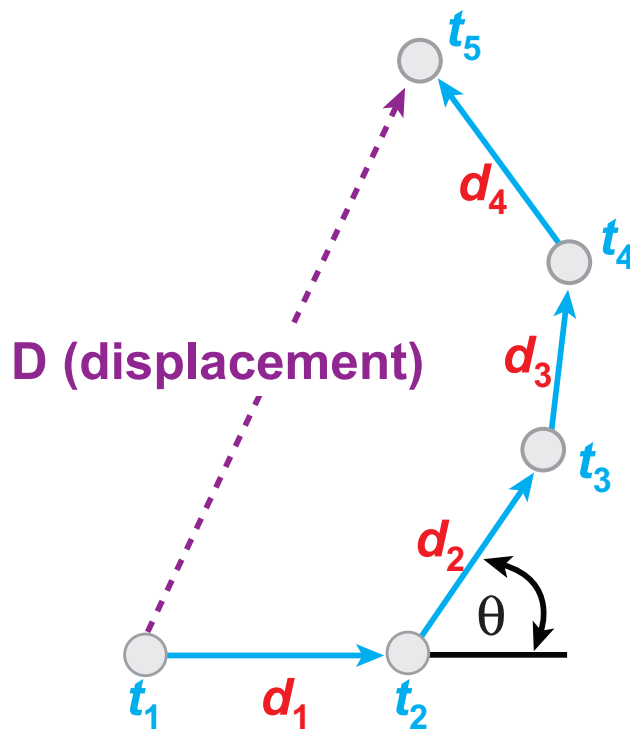
Figure 4-5: *Schematic showing a cell track at five successive time points, t1, t2, etc. Instantaneous velocities are calculated from the net distance d traveled during each time interval δt, and the turn angle θ is the angle through which the cell turns between time steps. The displacement D is the straight-line distance of the cell from its origin at any given time. Path length is given by the sum of d1, d2, d3, etc. Persistence time (or length) is the time for which a cell continues to move without turning appreciably, as is illustrated for time points t2t4 [Cahalan 08].*
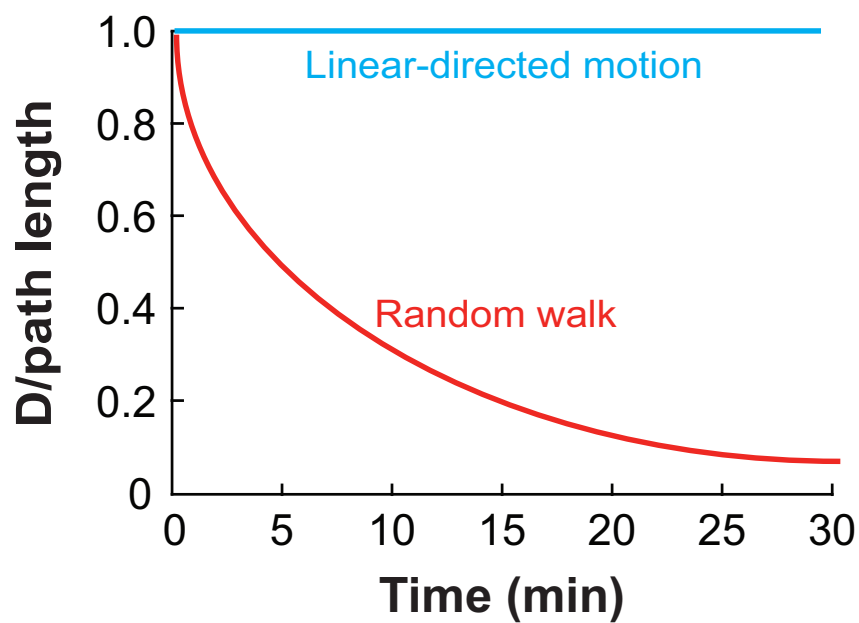
Figure 4-6: *Chemotactic index defined as path length/displacement from origin constant with a value of unity for linear-directed motion and decreases progressively with time for cells following a random walk [Cahalan 08].*
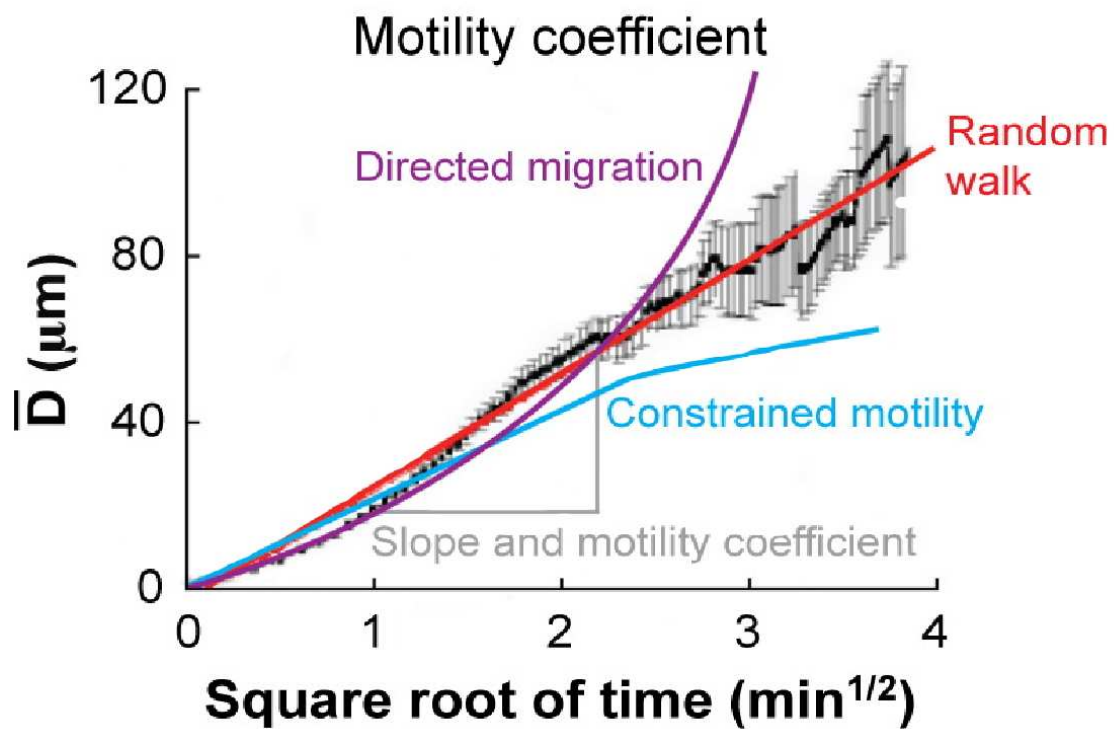
Figure 4-7: *Mean displacement from origin of multiple cells is expected to follow a straight line when plotted as a function of square-root of time, if the motility follows a random walk [Cahalan 08].*
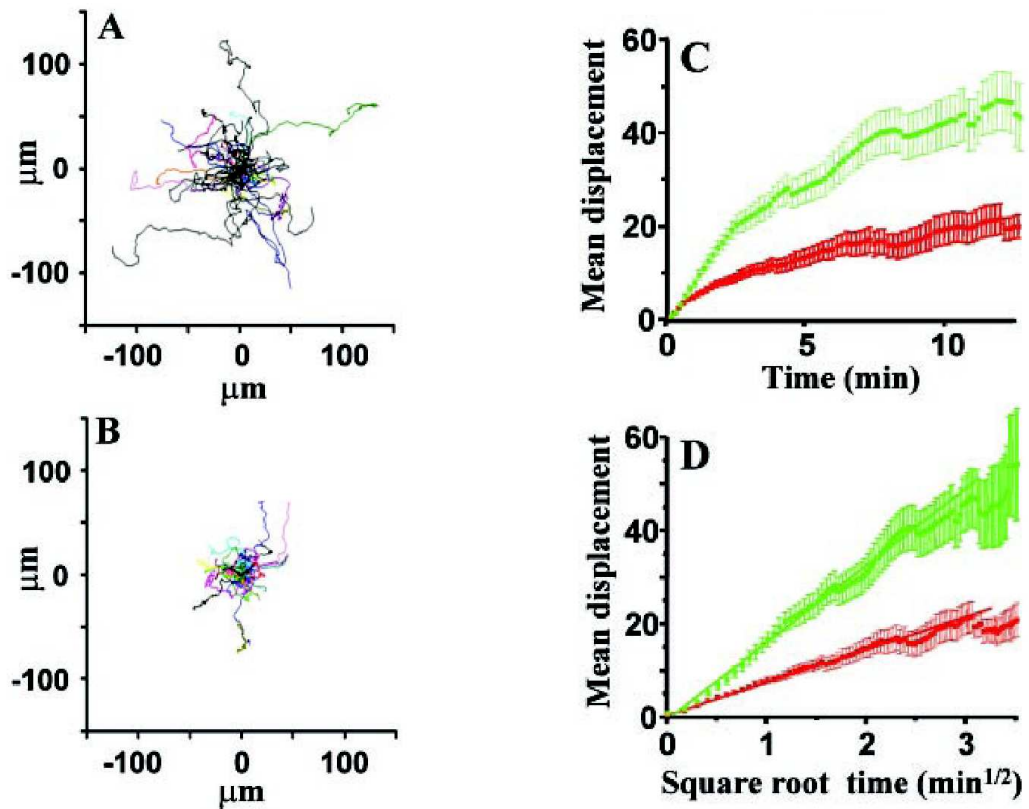
Figure 4-8: *T and B-cells move within the lymph node by a random walk. (A) Super-imposed tracks of 43 T-cells in the diffuse cortex, normalized to their starting coordinates. (B) Corresponding tracks of 41 B-cells in a primary follicle. (C) Mean displacement plot for T (green) and B (red) cells from (A) and (B). (D) The data from (C), replotted as a function of the square root of time. Points fall on straight lines, consistent with random movement, and the slope of each line represents the motility coefficient M, given by $M = x^2/4t$, where x is the mean distance from origin at time t [Miller 02].*

5 Cell migration in the Germinal Center

Germinal centers (GCs) are located in the lymph nodes (see Figures 1-1 and 5-1), and represent the major sites for high-affinity maturation. The initiation of an immune response leads to the activation of B-cells specific to a foreign antigen and the formation of GCs. Within GC reactions, B-cells mutate their antibody coding region and by this generate memory and plasma cells that produce antibodies with a high-affinity to a specific antigen. GCs reappear after subsequent encounters with the same antigen by activation of the memory B-cells that have been generated in the primary response. Figure 5-2 shows an in vitro image of a transversal cut of a GC.

Germinal centers characteristically arise during the first days following immunization by exposure to an antigen and last for about three weeks. GCs produce memory B-cells that continue to proliferate in follicles during the months following T-cell dependent anti-body responses [MacLennan 94].

In this chapter, we will first introduce the morphology of germinal centers in Section 5.1. Then elucidate, in Sections 5.1.1 and 5.1.2 the role two-photon imaging plays in understanding T and B-cell dynamics inside GCs. In Section 5.2, we will discuss the changes occurring in cellular behavior after immunization.

5.1 Introduction to Germinal Centers

The light and dark zones Germinal centers are divided into two compartments, the dark and the light zone. In the light zone, lymphoid cells are smaller and less closely distributed in comparison to the dark zone where GC B-cells are closely arranged. Both in the light and the dark zone, B-cells are separated by the FDC (follicular dendritic cell) network [Allen 07a] which is more extensive in the light zone. FDCs that constitute this network have the capacity to take up antigen and hold it on their surface for periods of more than one year [Allen 07a]. It has been suggested by Lui et al. and Wang et al. [Lui 91, Wang 05], that in the beginning of an immune response the dark zone is inexistent, and as the GC develops the GC B-cells will move from the FDC network to
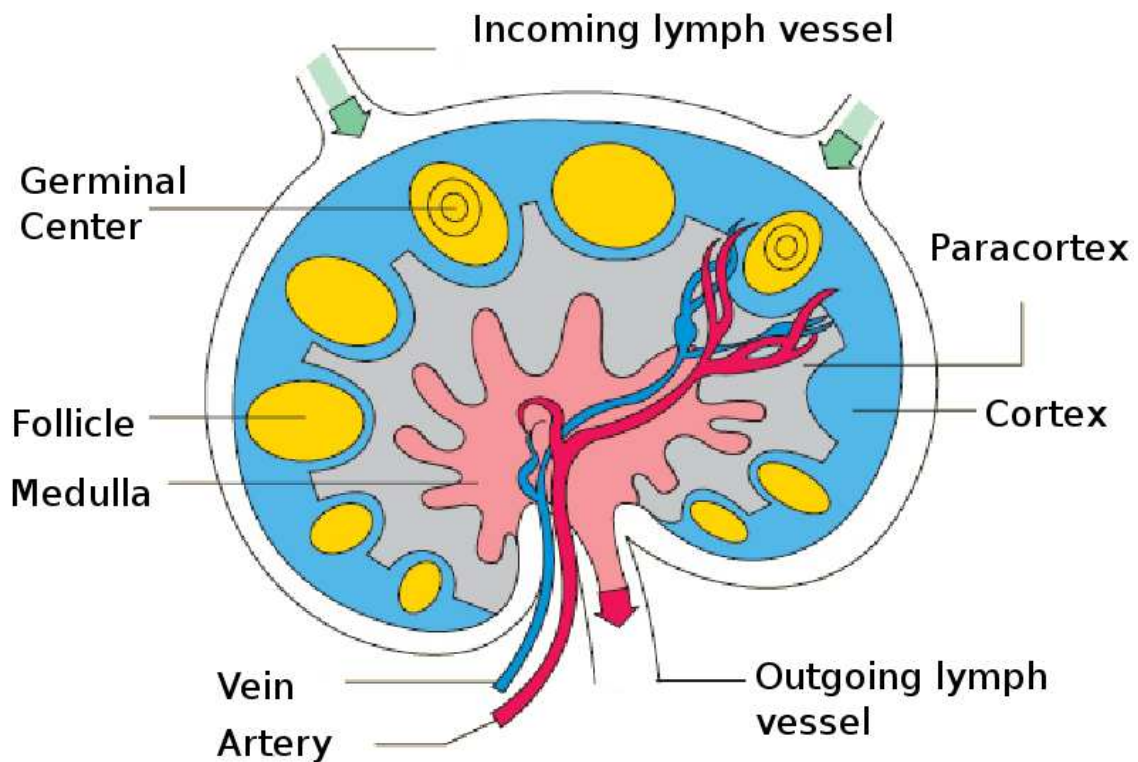
Figure 5-1: *Sketch of the typical anatomy of lymph nodes. In yellow, is the germinal centers with their usual spherical shape, positioned inside follicles and close to afferent/efferent veins.*[1]
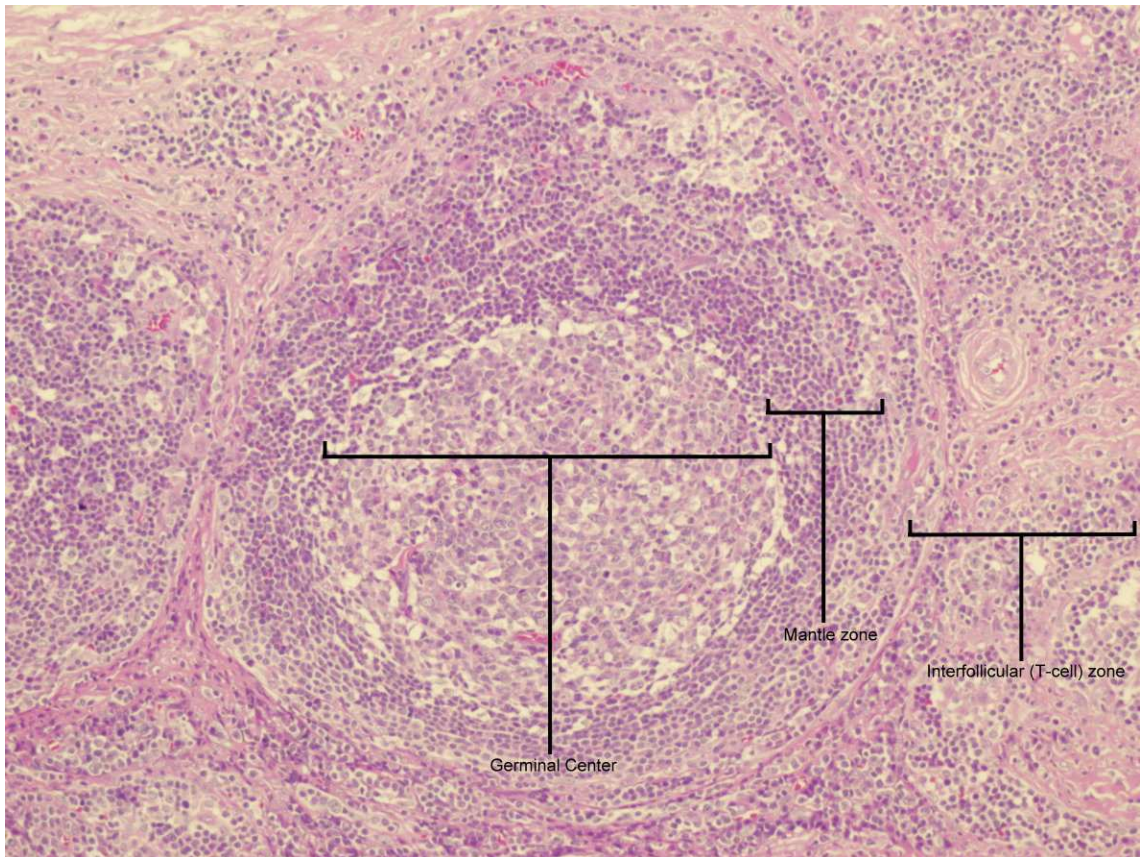
Figure 5-2: *In vitro picture of a germinal center surrounded by the mantle zone and the T-cell zone.*[2]

establish the dark zone. The orientation of the light zone in GCs, often next to afferent vessels coming from different organs, suggests the existence of antigen transport into the follicles. In 1994, MacLennan et al. [MacLennan 94] presented a model for GC functioning. GC B-cells were defined as centroblasts in the dark zone, and as centrocytes in the light zone. Centroblasts were mitotically active and have no immunoglobulin (Ig) on their surface undergoing rapid proliferation, hypermutation and exiting the cell cycle, after what they re-express surface Ig, decrease their size, and move to the light zone as anti-body expressing centrocytes that will compete for antigen/immune-complex binding, suggesting that centroblasts in the dark zone are continuously giving rise to centrocytes.

Affinity maturation   can be summarized as the process of somatic hypermutations, proliferation and selection of B-cells happening in GCs. During the first week following the administration of antigen (immunization), naïve B-cells are recruited in the boundary of follicles facing the T-zone. B-cells that receive T-cell help get activated, return into the follicle and become the founder cells for a GC reaction. Somatic hypermutation of B-cells occurs in GCs. Different somatic mutations are observed in GCs but are not the same in all cells. Most of these mutations affect the antibody affinity adversely, so that cells would be unlikely selected to become memory or antibody producing plasma cells. Many cells that were picked up and genetically analyzed from the same GCs, were stemming from the same clone which suggests that the resulting B-cells in a GC reaction are of oligoclonal origin. Moreover, some short-lived plasma cells from the primary extra-follicular tissues did not show signs of hypermutations, which suggests the absence of affinity maturation process outside GCs. However, more recent results exhibit evidence for mutation events outside B-cell follicles [Shlomchik 03].

While the general principles of a GC reaction and many molecular mechanisms have been identified, many important aspects of affinity maturation in GCs are still not understood. For example, the selection mechanisms that give rise to positive or negative selection events are not understood while these are of major importance for the control of GC reactions in the context of medical applications or vaccination. Recently, a process of affinity dependent selection in GCs by T-cells was predicted [Meyer-Hermann 06] and increasing evidence was found by intravital multi-photon imaging [Allen 07a].

5.1.1   T-cells in Germinal Centers

T-cells develop in the thymus where they reach their maturation. T-cells belong to the lymphocytes group and are distinguishable from other lymphocytes like B-cells by the presence of TCRs (T-Cell Receptors) displayed on their surface (see Figure 5-3). They are differentiated in several subsets, like T-Helper cells, cytotoxic cells and regulatory cells. The GC response has a strong dependence on T-cell signals such that GCs forming with T-independent antigens and without T-cell help collapse shortly after compartmentalization into dark and light zones. Figure 5-4 shows in detail the role of different T-cell subtypes in the immune response after activation by an antigen. Most of T-cells in the body belong to one of two subsets, distinguishable by the presence on their surface of one or the other of two glycoproteins designated as CD4 and CD8. $CD8^+$ T-cells bind epitopes that are part of class I MHC (Histo-compatibility Complex) molecules, and $CD4^+$ bind epitopes that are class II MHC molecules (see Figure 5-3). $CD4^+$ helper T-cells are of major importance for GCs onset.

T-cell motility   T-cells are highly motile entities constituting between 5-20% of the GC cells with a higher density in the light zone but have been also observed within the dark zone. Recent studies using two-photon imaging, showed that the CCR7 chemokine has a substantive role in promoting T-cell motility in the lymph node. As a matter of fact, CCR7-/- T-cells show a 20%-30% reduction in T-cell velocities [Huang 07, Worbs 07, Asperti-Boursin 07, Okada 07]. CCL19 and CCL21 are both ligands for CCR7, and both enhance motility of T-cells when bound to substrates in vitro [Stachowiak 06, Woolf 07]. In mice lacking CCL19 and CCL21, velocities of wild-type T-cells are inhibited to a similar extent as in CCR7-deficient T-cells [Worbs 07, Asperti-Boursin 07, Okada 07]. The motility of wild-type T-cells in mice recovers to normal after an injection of CCL19 [Worbs 07]. Together, these results indicate that CCR7 plays an important role in enhancing T-cell motility within the lymph node (see Figure 5-1), with residual motility of cells perhaps reflecting chemokinesis mediated by another chemokine. Self-recognition mediated by contact with MHC class II is vital for T-cell survival and proliferation in vivo [Delon 02]. Cells injected into MHC class II-deficient recipients become progressively immotile and disabled in their in vivo proliferative response to antigen.
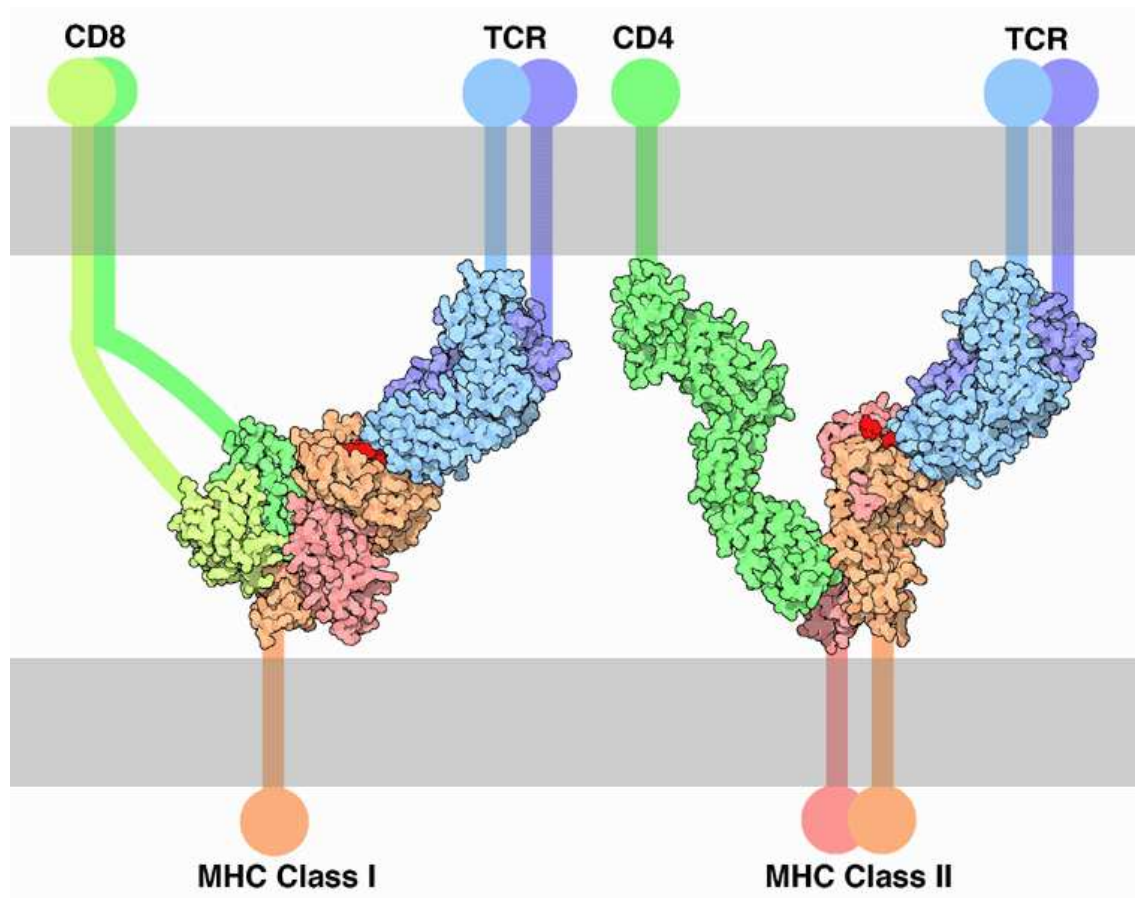
Figure 5-3: *Differences between CD8 and CD4 T-cells in binding MHC I and MHC II respectively. MHC class I, which is found on the surface of most of our cells, interacts with T-cell receptors and CD8 on cell-killing T-cells. MHC class II interacts with T-cell receptors and CD4 on other T-cells that stimulate the immune system.*[3]
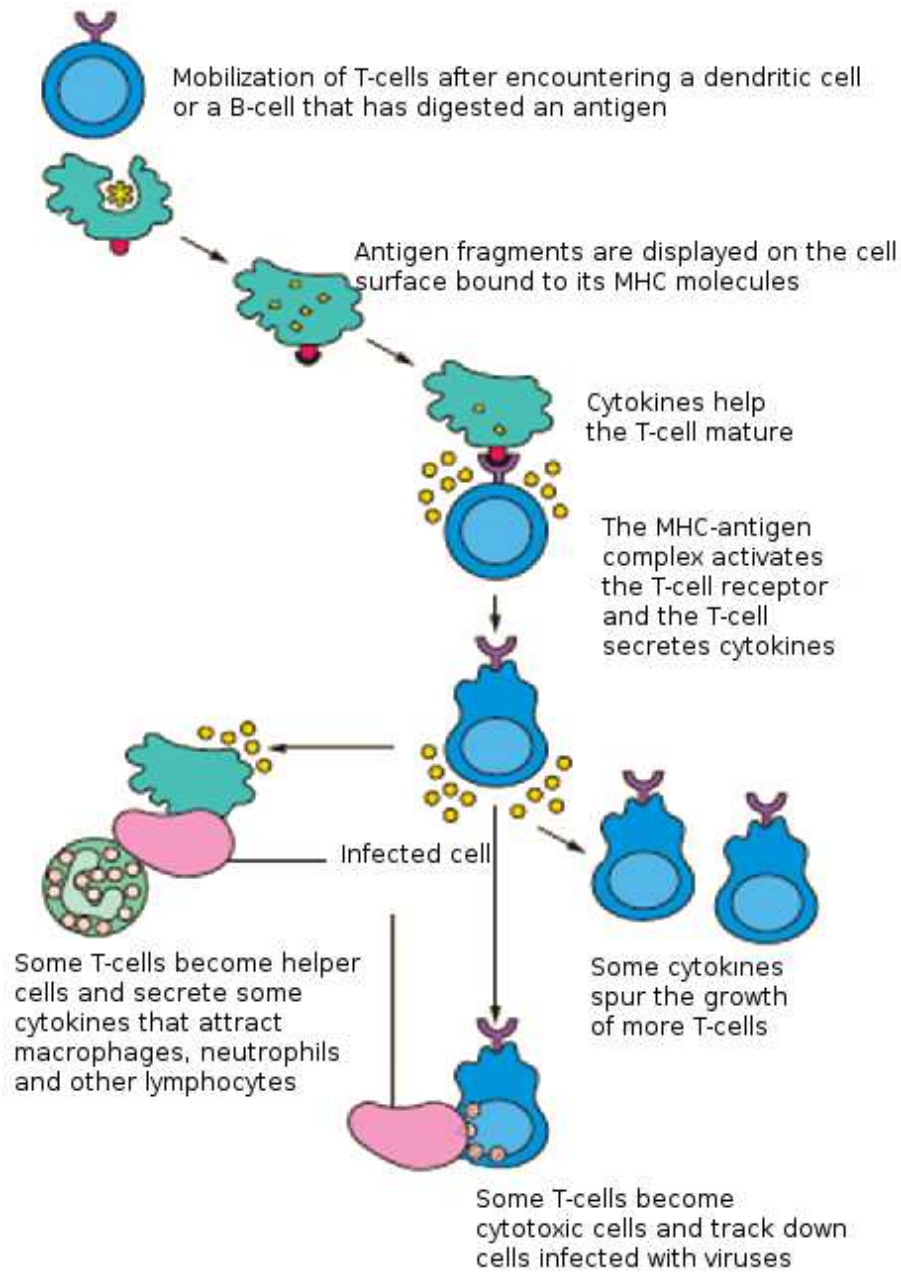
Figure 5-4: *Role played by the activated T-cells following an immunization [NIH 03].*

5.1.2   B-cells in Germinal Centers

B-cells are the basis of a humoral immune response, as opposed to the cell-mediated immune response governed by T-cells. B-cells can differentiate to antibody producing plasma cells. The produced antibodies are directed against specific antigens (see Figure 5-5). B-cells also perform the role of antigen presenting cells (APCs) or develop into memory B-cells after activation by an antigen intrusion. Note that B stands for bone marrow where they are produced and matured.

Quickly after immunization B-cells move to the secondary lymphoid organs where they proliferate within the FDC network. However, naïve B-cells have little capacity if at all to respond to antigen localized on FDCs (see Figure 5-6), indicating that the cells that colonize GCs have been activated first at the follicular border to the T zones of secondary lymphoid organs. After activation, B-cells migrate either to extra-follicular sites of antibody production where they differentiate into short-lived plasma cells or enter primary follicles and seed a GC reaction in response to antigen held on the FDC network. On the long term of an immune response, one can observe the disappearance of short-lived plasma cells present in the extra-follicular foci, and the increase in number of memory B-cells. Long-lived plasma cells secrete for several weeks anti-bodies and exhibit high affinity maturation measurements together with memory B-cells. This supports the hypothesis of a selection process happening in the GCs. Memory B-cells can also be found in small quantities even after the GCs are no longer present and for the following months of the established T-dependent responses. This gives rise to plasma cells that live longer and new memory B-cells without forming new GCs or undergoing further rounds of somatic hypermutation. GC B-cells express high amounts of MHC II (Histo-compatibility complex). The antigen is endocytosed into MHC class II processing compartments, faster than the naïve B-cells, suggesting that GC B-cells have their own way of processing and presenting pathways for the antigen (see Figure 5-6).

Most of GC B-cells die in the GC, and are digested by the TBMs (Tingible Body Macrophages) present in both light and dark zones. In addition, to undergoing negative selection because of inadequate BCR engagement, cells can die because of mutations that disactivate the BCRs expression, or because of the accumulation of too many mutations leading to a DNA-damage checkpoint. Cells also might die to keep the homeostasis of GCs, like size control, and limit the spreading of rapidly dividing cells. After dying,
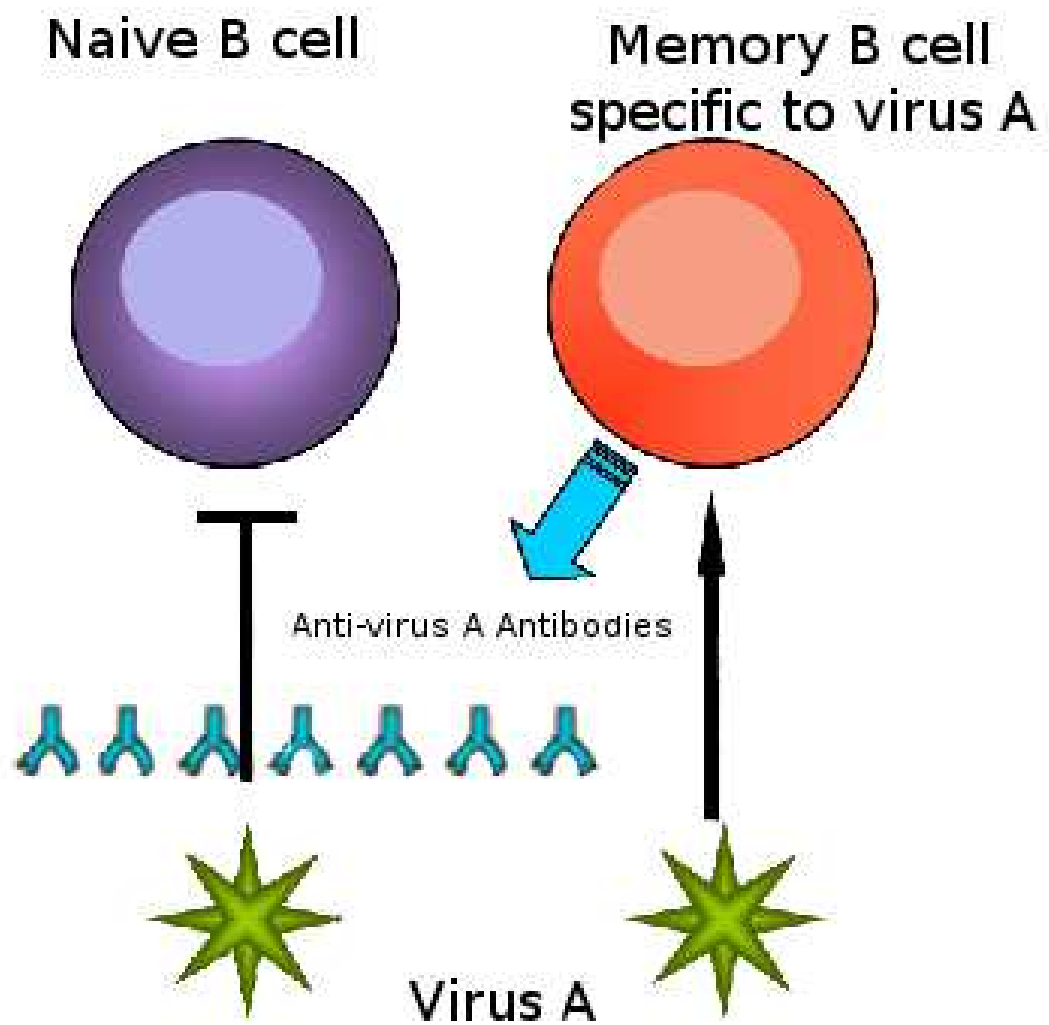
Figure 5-5: *Differences between naïve and memory B-cell. The latter being able to quickly differentiate to plasma cells that produce antigen specific antibodies.*

A B-cell is triggered after the antigen encounter

The B-cell engulfs the antigen and digests it

The antigen fragments bound to its unique MHC molecules

Arrival of a mature T cell

Cytokines secreted by the T-cell help B-cell to multiply into antibody producing plasma cells

Released into the blood, antibodies lock onto matching antigens. The antigen-antibody complexes are then cleared by the complement cascade or by the liver and spleen
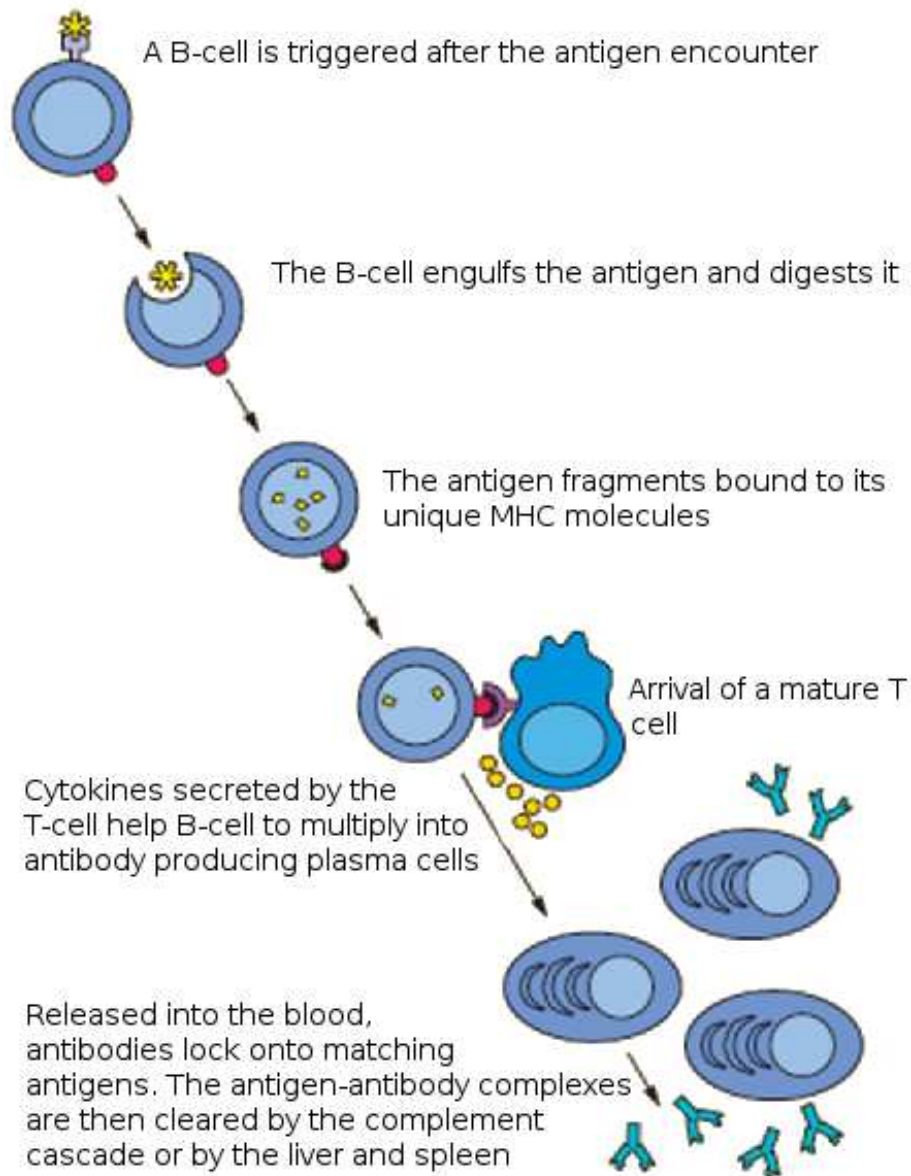
Figure 5-6: *Role played by the activated B-cells following an immunization [NIH 03].*

GC B-cells fragment into small blebs (vesicles), picked up by macrophages and/or GC T-cells. The absence of nuclear breakdown outside macrophages, is probably to prevent auto-immune reactions [Miller 02].

Tracking of cells showed that most B-cell/T-cell contacts are of short time (less than 5 mins). GC B-cells were seen to compete for cognate interaction with the T-cell help and are 5-20 times more abundant than the T-cells in the GCs. Competition for T-cell help might achieve selection against high-affinity clones that react with self antigens because of the internalization of a mixture of foreign and self antigens and as a result dilute the amount of foreign peptide-MHC complexes that are displayed compared to nonreactive high affinity clones. Autoreactive clones might be selectively recognized and controlled or eliminated by regulatory T-cells.

B-cell division in Germinal Centers   Flow cytometry cell-cycle analysis, showed cells in the S phase in both zones, in addition to cells in the G2 and M phases, in both light and dark zones. However, more cells in G2 and M phases were observed in the dark zone (see Figure 5-7). Unfortunately, the flow-cytometry analysis does not provide information for the differentiation of both zones, the only indicator is CXCR4 high or low expression by cells. High expression pointing to a positioning in the dark zone of GC B-cells. To find out whether GC B-cells are dividing in both dark and light zone, a thymidine analog pulse that labels cells in the S phase, was together used with flow cytometry for tracking cells with a higher CXCR4 expression. Cells were observed to move from the dark zone to the light zone to perform the M phase (see Figure 5-7), than come back to the dark zone and leave again to the light zone [Allen 07a], before completing a second division round. However, it is not clear whether the clones left the GC or underwent apoptosis. The frequency in one zone, decreased as the frequency in the other zone increased. These observations do not exclude that some of the GC B-cells never leave one zone or another, or stay for longer. The cell cycles of different GC B-cells were seen to be asynchronous, varying between 7 to more than 12 hours. Cells seemed waiting for a signal from BCRs or helper T-cells in order to re-enter the S phase, which would increase their efficiency in the case GCs have different distributions of antigens.
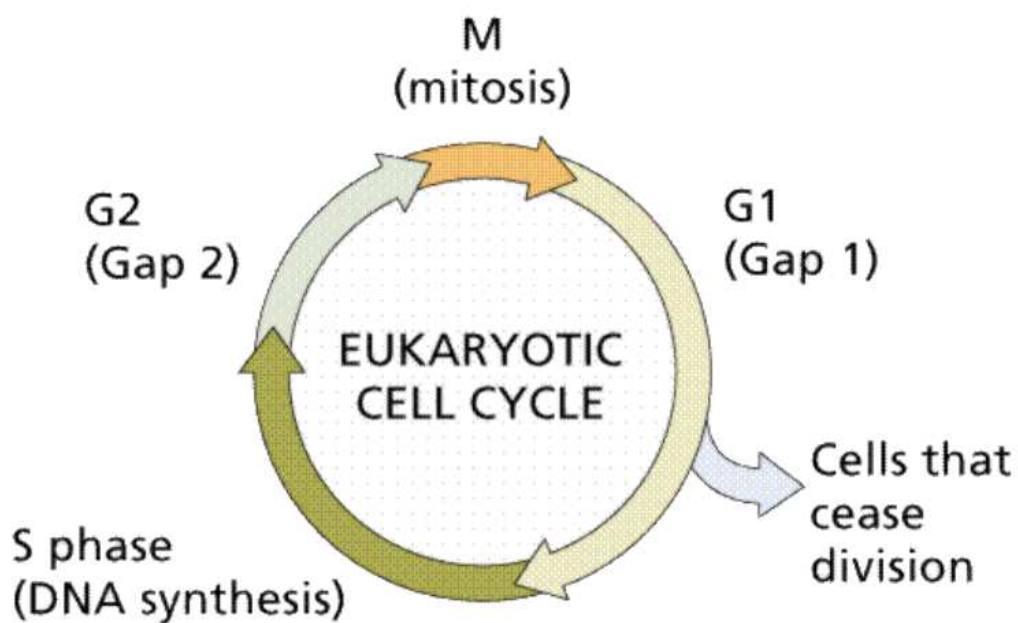
Figure 5-7: *Sketch of the cell cycle showing all relevant phases in a cell's life. The resting phase* G_0 *being purposely omitted.* G_1 *and* G_2 *designate phases where the cell synthesizes enzymes and proteins, needed either for the S phase or the M phase.*[4]

Difference between centroblasts and centrocytes   It is commonly believed that B-cells, do differentiate into centrocytes and centroblasts each of them occupies a different zone. Centrocytes occupy the light zone and are non proliferative cells and centroblasts are larger cells that proliferate very fast and undergo somatic hypermutation leading to centrocytes in the light zone. However, recent observations of centroblasts and centrocytes shows that they have similar morphologies, motility profile, and cycles in both zones. What is then the difference between both zones? Is the surface Ig expressed in centrocytes and assumed lacking in centroblasts enough to differentiate between them? In fact, many studies showed that the light zone contains bigger amounts of surface Ig suggesting that centrocytes present in the light zone are the surface Ig carriers. However, new experiments using in vivo two-photon microscopy suggest that GC B-cells express continuously a reduced amount of surface Ig, lower than the naïve B-cells. This set aside the idea of an eventual Ig surface difference between centroblasts and centrocytes. A difference in gene expression between GC B-cells and naïve B-cells was observed, but no difference between centroblasts and centrocytes was recorded. These two cell types seem in fact much more similar than previously thought. In addition, CD77 was thought to be widely expressed in centroblasts but showed a broad staining in all GC B-cells too. Therefore, CD77 is not sufficient in order to distinguish between centroblasts and centrocytes. Presently, all conducted studies using flow cytometry and two-photon imaging refute a crucial difference between centroblasts and centrocytes, concerning surface Ig expression and only point out a difference in the expression of some plasma cell-specific genes.

B-cell motility   B-cells are highly polarized while crawling, sometimes to an extreme of being four to five times longer than they are wide, and they move in a stop-and go manner, with pauses between bursts, and reach peak velocities up to 20 m/min for B cells [Cahalan 08]. Several hours after entering the G1 phase of the cell cycle, CXCR4 is downmodulated on some of the cells. These cells are then no longer retained by SDF-1 in the dark zone and can migrate to the light zone in response to CXCL13. During this period, the cells most likely have substantially turned over their low amounts of surface Ig, replacing the original BCRs with newly mutated versions. Within the light zone, the GC B-cells rapidly move about the FDC network where they can pick up antigen, receiving prosurvival BCR signals while also internalizing, processing, and presenting the

antigen as peptides on MHC class II molecules [Allen 07a].

5.1.3   FDCs in Germinal Centers

Follicular dendritic cells are probably of stromal origin and form a part of the immune apparatus in lymphoid follicles. FDCs main function is processing antigen material and presenting it on their surface on FC-receptors to other cells for examination and up-take. Follicles develop in humans during the second trimester of fetal development and FDCs appear within few days following the formation of B-cell clusters necessary for the existence of FDCs in follicles. The surface of FDCs is covered with diverse chemokines and carry surface-bound CXCL13, a chemokine ligand of CXCR5 expressed by B-cells. Similarly, FDCs also secrete the chemokines CCL19, CCL21, and CXCL12 and stain most strongly for surface-bound CCL21 in the paracortex [Bajenoff 06, Asperti-Boursin 07]. The antigen is presented in the shape of ICs (Immune complexes) highly ordered molecules called also Iccosomes [Cyster 00, Kosco-Vilbois 03, Aydar 03]. When the FDC network becomes filled with B-cells, an identified differentiation signal is delivered inducing them to move to one pole of the FDC network and form the dark zone of the GC [Wang 05, Lui 91]. Antigen trapping on FDCs is not a passive process. It involves active transport of immune complexes to the surface of FDCs. This process takes several hours and is delayed until the onset of antibody production in primary antibody response necessary for the location of antigen on FDCs.

5.2   Zoning in Germinal Centers

In the absence of antigen lymphocytes are highly polarized in the lymph node (see Figure 5-1) and move faster than other cell types. The prevailing random-walk pattern of T and B-cells within their respective regions is inconsistent with what would be expected for chemotaxis. On the other hand, recent studies have clarified the role of chemokines in enhancing overall lymphocyte motility (chemokinesis). Chemokines were shown to trigger downstream changes in lymphocyte polarity and migration.

Cell aggregation in primary follicles   Primary lymphoid organs are considered to be a precursor state of germinal centers [Beyer 08]. The main constituents of primary

lymphoid follicles are naïve B-cells and follicular dendritic cells (FDCs). Primary follicles are the sites where antigen, presented by FDCs, and naïve B-cells make encounters, with specialized transport systems that carry antigens from peripheral sites of entry into each secondary lymphoid organ.

In the last years, details have begun to emerge on the cues that guide cell movements inside lymphoid organs, and the central role for the chemokine family of molecules has been uncovered [Cyster 99]. In the most simple way, chemotactic cues lead to the formation of aggregates using homeostatic chemokines such as CCL19, CCL21 and CXCL13. These chemokines guide lymphocytes to their compartments, *i.e.* the dark and the light zone. Besides, specific interactions of T-cells with APCs (Antigen Presenting Cells) lead to the multicellular aggregation and formation of stable cell clusters observed both in vitro [Underhill 99] and in vivo [Ingulli 97]. It has also been shown that the interaction of TCRs with plate-bound cognate MHC molecules induced migratory arrest in T-cells provided by LFA-1/ICAM-1-mediated adhesion [Dustin 97].

Kesmir et al. [Kemir 03] proposed a novel mechanism where centrocytes are sorted on FDCs according to their affinity. The results obtained with a spatial model suggest that this adhesion-based selection mechanism is the most likely to generate the affinity maturation observed in vivo. Recently, Beyer et al. [Beyer 07] focused on the role of speed-based sorting of cells in GCs. An agent-based model was designed, where cell movement is guided by specific chemoattractants diffusing slower than cells are migrating considering the specificity of lymphocytes being rather fast cells in comparison to other cell types. Experimental data on cell speed distributions were reproduced. In addition, tissue homeostasis was not achieved by the balance of growth and death but by a flow equilibrium of cells migrating in and out the tissue under consideration.

Three models for B-cell migration in the GC Affinity maturation of B-cells occurs within germinal centers. During this process, a specific spatial cell sorting is observed within the two main compartments, *i.e.* the light and the dark zone. Intravital two-photon microscopy provides data of cell shape, motility and contact as a function of time. Experimentalists [Depoil 05, Allen 07b, Schwickert 07] and theoreticians [Figge 08] agree on the interpretation that B-cell motility follows a random walk with a directional persistence time. It is also observed from two-photon data, that B-cells migrate from one zone to another. However, there is no agreement on a unique

GC migration model of B-cells. Three different models were therefore proposed. The *cyclic re-entry model* assumes that a functional dependence exists between the light and the dark zone. B-cells proliferate and mutate in the dark zone then follow a gradient provided by the chemokine CXCL13 to the light zone. The migration back to the dark zone is made through an upregulation of the chemokine CXCL12 [MacLennan 94]. The *intra-zonal model* views the light and the dark zone as functionally independent zones. B-cells circulate only within one of the two zones. The exchange between both zones occurs only rarely [Hauser 07]. The *one-way migration model* suggests that cells perform a persistent random walk and re-entry of selected B-cells to the dark zone is neither necessary for reproliferation nor are these cells actively moving towards the dark zone. As a consequence B-cells proliferate also in the dark zone, and migration between zones occurs only by chance as a result of random migration [MacLennan 91]. Recently, Figge et al. [Figge 08] developed a model resulting in the conclusion that the intra-zonal circulation model is unlikely and that the data support a compromise between the one-way and the cyclic re-entry model. There was also an agreement in all three two-photon microscopy studies that the B-cell motility in GCs can be interpreted as a random walk with persistence time. Simulations showed that chemotaxis and desensitization mechanisms have a prominent impact on the GC organization and guarantee the existence of distinguishable zones without getting into conflict with the two-photon motility data that rather support a random walk. This implies that the morphology of the GC requires an additional mechanism that conducts freshly differentiated centrocytes from the dark zone to the light zone and recycled B-cells back to the dark zone. Natural candidates for such a random walk with a drift are the chemokines CXCL12 and CXCL13.

5.2.1 Summary of the Germinal Center dynamics

In the classical model, the GC dark zone is populated by large centroblasts that proliferate. The light zone is occupied by non proliferating centrocytes that compete for binding antigens on follicular dendritic cells. Competition for antigen is dependent on the affinity between BCRs (B-Cell Receptors) and the antigen presented in a form of ICs. In GCs, B-cells move from the light zone to the dark zone, this migration is performed with the help of CXCR4 chemokine provided that the CXCR4 and its ligand CXCL12 are much more abundant in the dark zone. The movement of GC B-cells in the other direc-

tion, *i.e* towards the light zone, requires the chemokine CXCR5 and its ligand CXCL13. Most of GC B-cells die after or do not make it through the process of competition for antigens. Dead B-cells are cleared by tingible body macrophages. The few GC B-cells that remain alive present the processed antigen to helper T-cells in the light zone which might promote their differentiation into memory B-cells or long-lived anti-body secreting plasma cells.

Two-photon live imaging provided insights that confute the classical view of germinal centers. Centroblasts and centrocytes were shown to be morphologically similar unlike what the two different terms might suggest. Proliferation occurs in both zones, and GC B-cells compete for T-cell help as well as for antigen. One of the major new findings, is that GC B-cells are highly motile and exhibit a dendritic morphology. Surprisingly, the speed and morphology of GC B-cells were similar in the dark and light zones. Cells transit between dark and light zones in both directions. The movement from the dark to the light zone, is due to the downregulation of the CXCR4 on GC B-cell surface. The movement from the light zone to the dark zone, seems to be achieved by an upregulation of CXCR4 [Allen 07a].

A new model for the GC organization was proposed by Cahalan et al. [Cahalan 08]. GC B-cells accumulate in the dark zone after undergoing mitosis and are constantly in cycle. However, the cellular growth during the early G1 phase (see Figure 5-7) occurs preferentially in the dark zone to leave space in the light zone for cells undergoing selection. Somatic mutation might also occur during this phase. Several hours after G1 phase (see Figure 5-7), CXCR4 is downregulated such that cells are not anymore retained in the dark zone and can migrate to the light zone in response to CXCL13. In the light zone, GC B-cells move rapidly around FDCs where they can bind to antigen. High affinity cells, may capture more antigens from FDCs than low affinity ones [Meyer-Hermann 06]. They might even pick up antigens from low affinity cells in a direct cell-cell competition. GC B-cells also compete with GC B-cell blebs, and with other GC B-cells for T-cell help in the light zone. Because T-cells must polarize in a fashion that only allows interaction with one antigen presenting cell at a time, a single GC T-cell is suggested to form a stable interaction with the GC B-cell that presents the highest number of antigen peptide-MHC class II complexes compared with neighboring cells [Meyer-Hermann 06, Depoil 05]. The time window in the light zone is tightly regulated, such that all GC B-cells must undergo apoptosis, exit the GC or return to the dark zone within few hours of entering the

light zone. Cells exiting the GC rapidly change to long-lived plasma cells or memory B-cells. The two zones do not have big state differences. However, there is may be further diversification in the Ig level by somatic hypermutation, and cell division in the light zone. Selection by antigen recognition and T-cell help might be followed by an asymmetric cell division, where GC B-cell is dividing to a GC B-cell and a plasma cell or a precursor memory-cell. Finally, selection might as well frequently occur in both zones but may be more efficient in the light zone.

---

[1]www.britannica.com.
[2]www.virginia.edu.
[3]Molecule of the Month by www.pdb.org.
[4]www.dnarp.com.
[5]Nature Reviews/Immunology.

6 An agent-based model of cellular aggregation

6.1 Mechanisms of aggregation

Cell aggregation involves intercellular communication and cellular migration, and is widely observed in different normal and pathological situations. This phenomena was proven to be mediated by chemotaxis to specific molecules secreted by aggregation centers, *i.e.* other cells or by phototaxis towards a light signal, observed in many works to be emitted by cells themselves. The aggregation process (see Figure 6-1) involves cellular adhesion achieved by the use of surface proteins with binding capacities either to other proteins on other cell surfaces or to the extracellular matrix, these proteins are often referred to as adhesion molecules such as Integrins. Cell adhesion is modulated by very precise mechanisms and interactions that lead to morphological or structural changes of tissues. In the immune system, B-cells provide one of the most striking examples of cellular adhesion and sorting at the adult stage. During the process of affinity maturation B-lymphocytes perform numerous intercellular contacts with FDCs [Kemir 03], and T-cells with antigen presenting cells (APCs). T-cells deliver adhesive and cytokine signals to the B-cells, leading to B-cell activation and differentiation either into B-memory or plasma cells.

In the model we developed Ref. (Section 6.2), we restrict our description of aggregate formation to the multicellular scale, by investigating the role of chemotaxis and phototaxis in inducing cell movement and aggregation and focusing on the properties of emergent patterns formed after receiving one of the two different signals. Cell transport is mediated by chemotaxis, phototaxis and/or diffusive motion. A parameter γ regulates detachment of single cells from already formed aggregates. For the model purpose we make the assumption that intercellular adhesion by signal is stronger than adhesion caused by a diffusive motion.
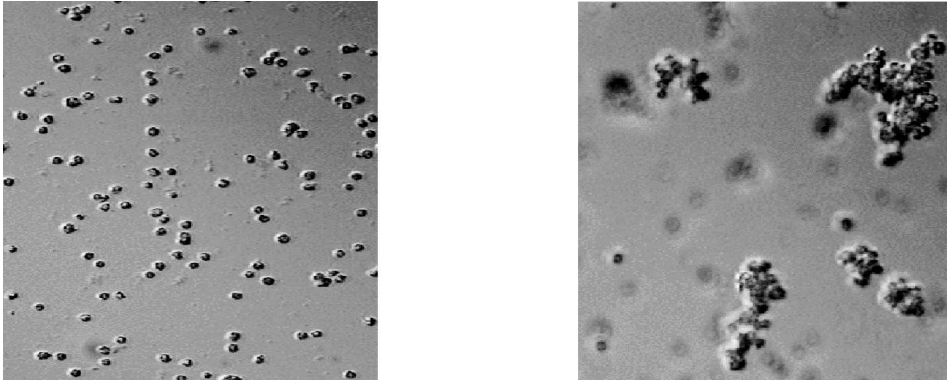
Figure 6-1: *Drosophila cells before and after aggregation.*[1]

6.2   An ABM for cellular interaction and aggregation

6.2.1   Mathematical modeling

The application of mathematical models to explain the dynamics of biological morphogenesis started with the work of D'Arcy Thompson who showed that mathematics can not only describe static forms but also the change of forms [Deutsch 04]. Models of biological pattern formation are dynamical systems in which concepts of space, time and interaction are combined. Pattern formation arises from the interplay of directed and random cell motion with short-or long-range mechano-chemical interactions of cells and/or molecules [Deutsch 04]. Traditional methods of mathematical modeling can handle systems with either few degrees of freedom that interact strongly, or very many degrees of freedom all of which interact weakly. However, complex systems occupy the intermediary regime, where local and global phenomena interact in complicated, often nonlinear ways.

The fact that complex systems are nevertheless organized systems, makes them accessible for mathematical modeling. Mainstream modeling of cell culture systems to date has followed two distinct approaches: Cell-population modeling and single-cell modeling. The former aims to capture increasing heterogeneity between cells, while the latter attempts to faithfully capture intracellular processes.

Models dealing with chemotaxis can also be separated in the above cited classes. The consideration of cell population models like the Keller-Segel's model (first model of chemotaxis built in 1971 [Keller 71]) and various modifications of it are not suitable to

the purpose of agent-based modeling. Mostly because these models usually introduce partial differential equations [Horstmann 02].

ABMs for cellular communication   Cells are able to sense other cells in their neighborhood and to communicate through chemokine release and detection. This communication plays an essential role, *e.g.* in tissue formation and function. It is well known that cells migrate towards each other, form aggregates as shown in Figure 6-1, and then move on collectively [Albrecht-Buehler 05, Miura 00]. Interestingly, it has been observed that cell migration and aggregation may also be mediated by light irradiation [Harris 01, Swartz 07, Kahn 64, Hong 80, Stavis 73]. Cells were also seen to emit biophotons [VanWijk 88] that carry information translatable to signals captured by the neighboring cells and that lead to a change in their functions or behavior inducing aggregation as observed in 3T3 cells by Albrecht-Buehler et al. [Albrecht-Buehler 05].

Mathematical models of cellular migration and aggregation are often focused on chemotaxis [Painter 00], whereas models of cellular aggregation induced by phototaxis are still rare [Levy 08]. A generic agent-based model is presented here to describe the dynamics of cellular aggregation to address the question: How can chemotaxis and phototaxis be distinguished on a phenomenological level? A two-dimensional ABM was developed for simulating cellular response to chemotaxis and light excitation where each cell is represented as a single node on a lattice (see Figure 6-2). Cellular aggregation was simulated using established modeling techniques [Deutsch 04], where cells are treated as discrete agents that migrate and communicate by intercellular signaling. Motivated by recent experiments [Albrecht-Buehler 05], the migration of cells is restricted to a quasi-one-dimensional stripe. The stripe-structured substrate is represented by a two-dimensional lattice of rectangular shape as shown in Figure 6-2 and the total number of lattice sites is given by:

$$N = N_x N_y, \tag{6.1}$$

where N_x and N_y refer to the x- and y-direction, respectively, with the consideration of the case:

$$N_y \ll N_x. \tag{6.2}$$

The lattice constant a is set to one cell diameter and each lattice site is occupied by at most one cell at a time. While the total cell number, N_{cell}, is a constant in time, both

the number of single cells N_{single} and the number of aggregates N_{agg} are functions of time. The update is asynchronously performed and cells are not allowed to exit the grid. Besides, cells can perform only one move per time step and are not allowed to move diagonally.

6.2.2   Modeling chemotaxis with an ABM

Models for chemotaxis mostly focus on the internal signaling requirement to sense spatial gradients. Global inhibition and local excitation assumptions usually provide a good estimate of the underlying mechanisms for the gradient sensing in eucaryotic cells [Levchenko 02]. In this work we focus on developing a model that offers an estimate for the maximum communication distances over which a single cell can meaningfully propagate a soluble signal received by another cell and that yield its movement. The signal distribution as a function of this distance will be used in the ABM.

The general diffusion equation reads as follows:

$$\frac{\partial c}{\partial t} = D \overrightarrow{\nabla}^2 c, \tag{6.3}$$

where c is the density of the diffusing cyto/chemokine and D is the diffusion coefficient. To describe the time dependent mass transport in the case of chemical signal propagation from a spherical source [Francis 97], the diffusion equation in the spherical coordinates reads:

$$\frac{\partial c}{\partial t} = D \frac{1}{r^2} \frac{\partial}{\partial r} \left[r^2 \frac{\partial c}{\partial r} \right]. \tag{6.4}$$

Solving the equation (Eq. 6.4) under the stationary boundary conditions of a constant flux at the cell surface and a complete dilution very far from the cell as shown in Figure 6-3 and mathematically stated as:

$$-D \frac{\partial c}{\partial r} = F_0 \text{ at } r = \rho \text{ and } c \to 0 \text{ as } r \to \infty, \tag{6.5}$$

leads to the solution [Francis 97]:

$$c(r, t) = \frac{F_0 \rho}{2Dr}, \tag{6.6}$$

here F_0 is the cyto/chemokine production rate (molecules/area.time) and ρ is the cell radius [Francis 97]. Thus, the signal distribution scales with the inverse distance from the cellular source. This result will be implemented in the ABM to model chemotaxis.

6.2.3   Modeling phototaxis with an ABM

In 2008, Levy et al. [Levy 08] proposed a model for phototaxis of Cyanobacterium. Communication between bacteria via cellular excitation levels was assumed. Cells propagated their excitation level to neighboring cells, including a memory effect facilitating the motion of cells to previously visited locations. Cells also tend to move faster on such regions while diffusing slowly and communicating between each other.

Cells sense the light intensity, as a function of the distance from the constant light source. The light source may be represented by cells themselves [VanWijk 88, Popp 02]. Light intensity scales with the inverse square of the distance from the light source. This scaling behavior is illustrated by the diagram in Figure 6-4, which shows the apparent light intensity of a fixed source with an intensity L_0 at distances r, $2r$, $3r$, etc. As the distance increases, the light spreads over a larger area in three dimensions. The intensity decrease scales with r^2 because the area over which the light spreads is proportional to the distance squared.

6.2.4   General description of the system

At the origin of aggregation is the attractive interaction between cells that migrate in response to signals released and detected by themselves. The following model differs in two aspects from previous models [Levy 08]. Firstly, the differences in the characteristic scaling behavior of the signal distribution for chemotaxis and phototaxis are explicitly taken into account. Secondly, The migration of aggregates was modeled as a whole to be suppressed by a factor that depends on the actual aggregate volume. During a time step of the simulation, the ith selected cell will either stay at its lattice site $\vec{r}_i$ or migrate to a nearest-neighbor site as the result of the following processes:

■ Intercellular signaling,
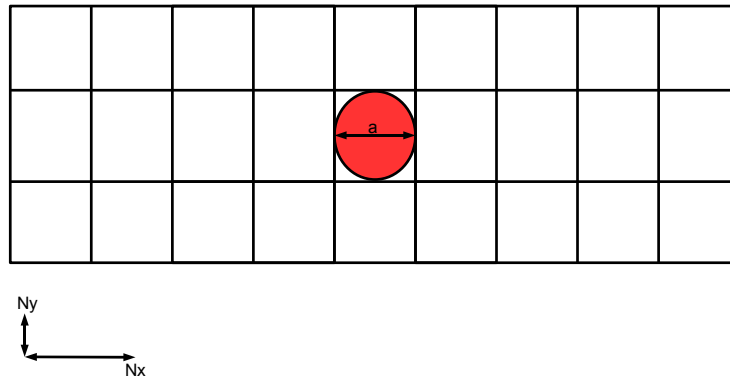■ Diffusive motion,
■ Cellular adhesion.

Figure 6-2: *Sketch of the used lattice. In red a cell/node of diameter a is represented.*
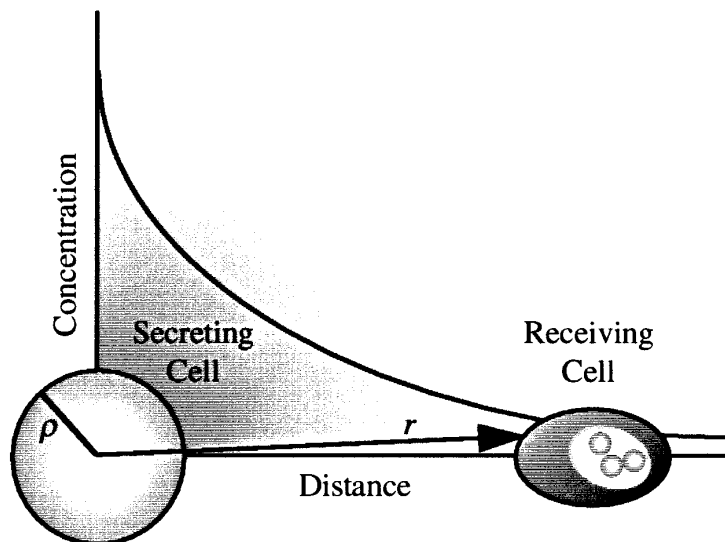

Figure 6-3: *Illustration of a solitary cell secreting a soluble cyto/chemokine and the concentration gradient that results from the secretion [Francis 97].*
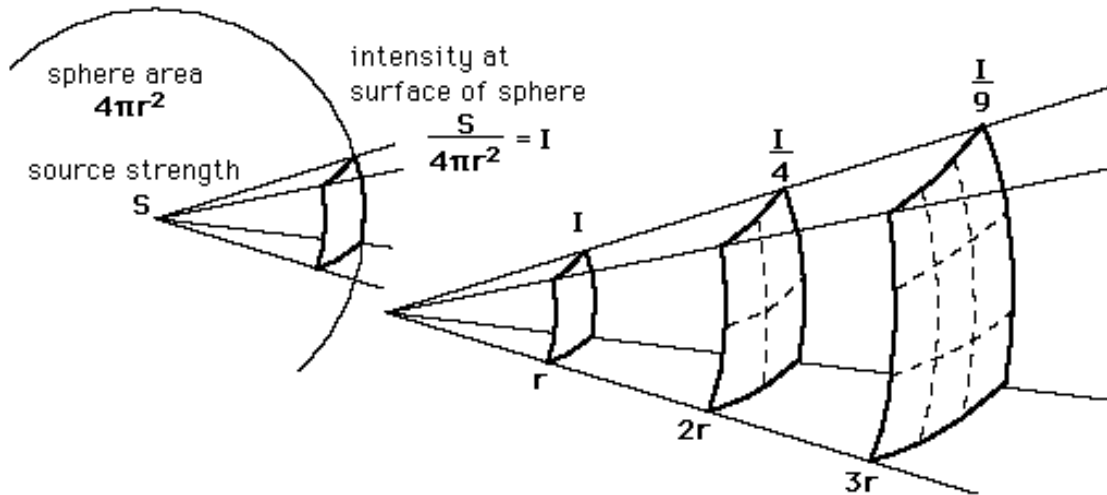
Figure 6-4: *Relationship between light intensity and distance from the source.*[2]

Response to signals   The movement of biological cells alternates between a random walk like behavior and that of a directed walk in presence of a signal. Relative to cellular diffusion, a cell is responding to signals with probability $p_{\text{cell sig}}$, where we consider the range:

$$0 \leq p_{\text{cell sig}} \leq 1. \tag{6.7}$$

The probability that aggregates respond to signals as a whole is reduced by the factor: $\frac{1}{N_{\text{agg cells}}}$, representing frictional forces acting on the aggregate:

$$p_{\text{agg sig}} = \frac{p_{\text{cell sig}}}{N_{\text{agg cells}}}. \tag{6.8}$$

Importantly, beside these processes for single cells, the agent-based model recognizes evolving cellular aggregates of two or more cells. These move and interact as a whole following the digram shown in Figure 6-5. Single cells can also move within an aggregate or detach from it.

Aggregate definition   We define an aggregate as a group of cells with direct contacts made of two cells or more. A script using a recursive function was developed to recognize aggregates, and store them with the list of cells composing each aggregate at each time

step. A randomly chosen cell is picked from the list of cells evolving in the system, and a procedure of neighborhood check is started. Cell positions are also stored at each time step, this information is used to define the aggregates. We consider two cells belonging to the same aggregate in the case where the two cells share the same position on the x-axis or the same position on the y-axis with at least one cell belonging to an aggregate.

Each process is associated with a time, τ_{process} and the corresponding realization probability of this process reads:

$$p_{\mathrm{process}} = \frac{\tau}{\tau_{\mathrm{process}}}, \tag{6.9}$$

with the simulation time step:

$$\tau \leq \tau_{\mathrm{process}}. \tag{6.10}$$

The simulation time step is determined by the fastest of all processes with:

$$p_{\mathrm{process}} = 1. \tag{6.11}$$

■ **Intercellular signaling**   Cells feel gradients and migrate in response to chemotaxis or phototaxis. The signals are considered to be sustained by the cells themselves. We assume that autochemotaxis does not give rise to the self-localization of cells [Grima 05] and we model signaling processes in the presence of diffusive cell motion as outlined above. The signal distribution $S_{ij,\alpha}$ for two interacting cells that are located at sites $\vec{r}_i$ and $\vec{r}_j$ is a function of their distance:

$$|\vec{r}_{ij}| = |\vec{r}_j - \vec{r}_i|. \tag{6.12}$$

It obeys the scaling law:

$$S_{ij,\alpha} = \frac{S_\alpha a^\alpha}{|\vec{r}_{ij}|^\alpha}, \tag{6.13}$$

where S_α represents the dimensionless signal strength and the exponent α is different for chemotaxis and phototaxis. In the case of chemotaxis, the signal is mediated by the concentration of chemokines that are permanently released from the cells with constant flux. Solving the corresponding three-dimensional diffusion equation (Eq. 6.6) for the spatio-
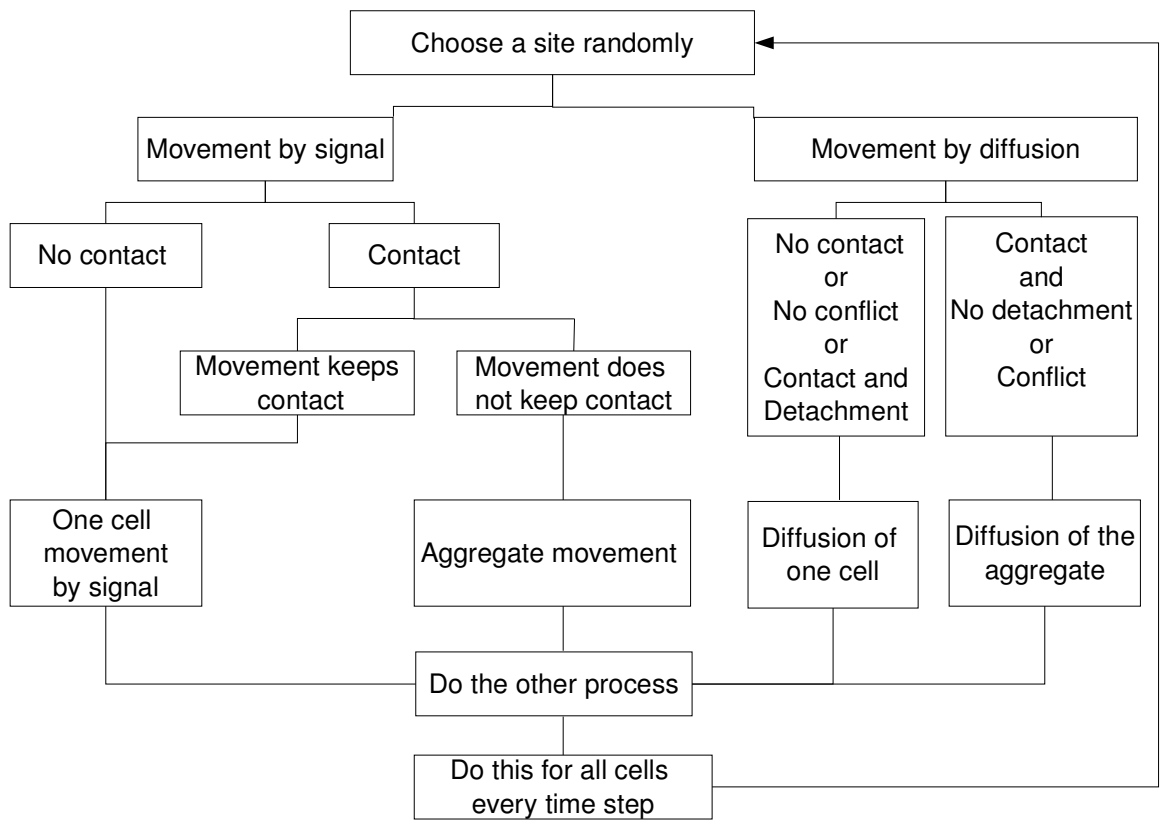
Figure 6-5: *Flowchart of the designed Agent-Based Model*

temporal chemokine concentration yields $\alpha = 1$ in the stationary limit [Francis 97]. In the case of phototaxis, the role of the mediating signal is taken over by the light intensity [Albrecht-Buehler 05]. A scaling argument reveals that the light intensity decreases in three dimensions with the square of the distance between emitting and receiving cells, thus, $\alpha = 2$ in this case. We stress that, while cell migration takes place on a surface, the three-dimensional nature of the cellular interaction is taken into account.

Since cells measure the gradient of signal distributions, we calculate the direction of cell migration by differentiation. For two cells i and j we obtain:

$$\vec{G}_{ij,\alpha} = -\vec{\nabla} S_{ij,\alpha}. \tag{6.14}$$

The additive impact of all cells on the ith cell is given by the superimposed gradient between all pairs of cells:

$$\vec{G}_{i,\alpha} = \sum_{j}' \vec{G}_{ij,\alpha}, \tag{6.15}$$

where the prime at the sum indicates the summation over all $j \neq i$.

In the spirit of modeling chemotaxis rather than chemokinesis, the direction of migration is obtained from the normalized vector $\vec{G}_{i,\alpha}/|\vec{G}_{i,\alpha}|$, whereas the speed of the cell does not depend on the value of $|\vec{G}_{i,\alpha}|$. However, we impose the biologically motivated condition that cell migration is only induced if the signal gradient is above a certain threshold T_α, *i.e.* expressed:

$$|\vec{G}_{i,\alpha}| > T_\alpha. \tag{6.16}$$

Thus, below this threshold value no migration of the cell is induced by the signal.

The concept of a signal gradient threshold can be expressed in terms of a maximal communication distance between two cells up to which these cells can still sense each other. This distance for a pair of cells depends on the underlying signaling mechanism and, in units of the cell diameter a, is given by:

$$R = \left(\frac{\alpha S_\alpha}{a T_\alpha} \right)^{1/(\alpha+1)}. \tag{6.17}$$

Thus, cells have the same sensitivity to chemo- and phototaxis signals, $T_1 = T_2$, if both signals exhibit a maximal interaction range of two cell diameters, $R = 2$. For $R > 2$

the sensitivity to phototaxis signals is larger than the sensitivity to chemotaxis signals, $T_1 > T_2$, whereas $T_1 < T_2$ for $R < 2$. Cells move alone if they appear to have no direct contact with other cells. In case of *conflict* with an other cell, this is to say that the future position of the calculated cell is occupied, the aggregate is recognized and all cells within the same aggregate move. However, if the cell can move alone without detaching from the aggregate, it is allowed to move which leads to the aggregate rearrangement. Note that the aggregates are also not allowed to move beyond the imposed lattice dimensions.

There is a restriction of the aggregates moving by signal, regarding their volume, and the medium they are evolving in by using the following expression and comparing it to a randomly generated number from a uniform distribution between 0 and 1:

$$P_1 \leq \frac{1}{N_{\mathrm{agg\,cells}}}, \tag{6.18}$$

where $P_1 \in [0, 1]$, and $N_{\mathrm{agg\,cells}}$ is the number of cells within the calculated aggregate.

■ **Cellular diffusion and adhesion**   Our model account for cellular diffusion. Each time step a random direction is picked for each move. Cells that randomly migrate within an aggregate are constantly reshaping it, whereas detachment of cells from an aggregate by diffusion may eventually result into its dissolution. However, adhesion between neighboring cells hampers their detachment from the aggregate and stabilizes the aggregate.

The probability of detachment by diffusion is measured relative to free cell diffusion:

$$p_{\mathrm{cell\,detach}} = \frac{p_{\mathrm{cell\,diff}}\gamma}{N_{\mathrm{nn}}}. \tag{6.19}$$

This is done by comparing a randomly generated number between 0 and 1 to:

$$P_2 \leq \frac{\gamma}{N_{\mathrm{nn}}}, \tag{6.20}$$

and is inversely proportional to the number of nearest-neighbor cells in the same aggregate N_{nn}, with $1 \leq N_{\mathrm{nn}} \leq 3$ and $P_2 \in [0, 1]$. The dimensionless parameter γ is considered in the range $0 \leq \gamma \leq 1$ and controls the relative impact of detachment.

Two approaches for looking at this problem were considered with the aim of comparing both. The first one considers cells to move without diffusive motion, where signals are the only initiators of cell movement. The second approach, includes a diffusive motion, and enables time consideration unlike the movement without diffusive motion.

Random migration of agents on a lattice mimics active cell migration into randomly chosen directions with a diffusion constant D:

$$D = \frac{a^2}{2d\tau_{\text{cell diff}}}, \tag{6.21}$$

where d denotes the spatial dimension and D the diffusion constant. For a given diffusion constant and a cell diameter the time step of the simulation can be gauged by:

$$\tau_{\text{cell diff}} = \frac{a^2}{2dD}, \tag{6.22}$$

The corresponding probability for cellular diffusion is given by:

$$p_{\text{cell diff}} = \frac{\tau}{\tau_{\text{cell diff}}}. \tag{6.23}$$

Similar to single cells, aggregates can perform random migration as a whole. However, this is realized with a reduced probability, since $N_{\text{agg cells}}$ cells that form the aggregate have to be moved collectively. The phenomenological ansatz is made:

$$p_{\text{agg diff}} = \frac{p_{\text{cell diff}}}{N_{\text{agg cells}}^2}, \tag{6.24}$$

which is the product of two equal contributions: *(i)* Diffusion of aggregates as a collective process of individual cells. *(ii)* Frictional forces in solution that hinder the free diffusion of aggregates.

Each contribution is considered to scale with the inverse aggregate volume, thus, enters the probability with a factor $\frac{1}{N_{\text{agg cells}}}$.

Two extreme limits are considered in this model.

□ **Cell diffusion is the fastest of all processes** This consideration seems closer to reality. In fact, two big processes are happening here, the cells move by signal and/or by diffusion.

$$p_{\text{cell diff}} = \frac{\tau}{\tau_{\text{cell diff}}} = 1. \tag{6.25}$$

One of these two processes is chosen by chance at the beginning. In addition, there is a probability of entering at all, each of these two processes that is decided by the values previously fixed between 0 and 1 of $p_{\text{cell diff}}$ or $p_{\text{cell sig}}$ and that are compared with a uniformly distributed random number.

□ **Cell diffusion is absent** Here we consider, that the cells are evolving in a very deterministic environment,

$$p_{\text{cell diff}} = 0, \tag{6.26}$$

where only the received signals with the previously set threshold are responsible of moving or not a cell. Since aggregate diffusion is absent no detachment of cells from aggregates occurs because cells are not allowed to detach by signal reception. Furthermore, the quantitative measure for τ is lost, therefore, the number of simulation steps is chosen sufficiently large in order to guarantee that the system configuration has reached equilibrium.

□ **Lattice artifacts** In the quasi-one-dimensional cell aggregation system, lattice artifacts become apparent in the limit of vanishing cell diffusion, $p_{\text{cell diff}} \to 0$. These artifacts are eliminated by randomizing the x- and y-direction of the signal-induced cell displacement with weights that are defined by the components of the total direction vector $\vec{G}_i / |\vec{G}_i|$. In the limit of fast cell diffusion, $p_{\text{cell diff}} \to 1$, such lattice artifacts are absent.

6.3   Results

Simulations are started from random initial configurations and performed with an asynchronous update, where at each time step each cell is randomly chosen and all processes are performed in random order.

6.3.1   Pattern formation

Typical cellular aggregation patterns in response to chemotaxis and phototaxis are shown in Figure 6-6, both in the absence and presence of diffusive motion. Simulations are performed where the two signaling mechanisms are compared for the same parameter values R and $S_1 = S_2 = S$. Since experimental values for S_α and T_α are generally not known, in all simulations we choose $S = 0.5$ and calculate the threshold value as a function of R the maximal communication distance:

$$T_\alpha = \frac{\alpha S}{a R^{\alpha+1}}. \tag{6.27}$$

The number of time steps are of the order 10^3 and 10^4 for $p_{\text{cell diff}} = 1$ and $p_{\text{cell diff}} = 0$, respectively. When measuring the degree of aggregation:

$$D_{\text{agg}} = \frac{1}{N_{\text{single}} + N_{\text{agg}}}, \tag{6.28}$$

we find in the case of chemotaxis, $D_{\text{agg}} = 13\%$ as shown in Figure 6-6 (b) and $D_{\text{agg}} = 100\%$ as shown in Figure 6-6 (c) in the absence and in the presence of diffusive motion, respectively. Similarly, for phototaxis we find $D_{\text{agg}} = 8\%$ (see Figure 6-6 (d)) and $D_{\text{agg}} = 25\%$ (see Figure 6-6 (e)), respectively.

6.3.2   Degree of aggregation

In the Figure 6-7, D_{agg} Ref. 6.28 is plotted as a function of R averaged over 100 simulations. We show the results for chemotaxis and phototaxis, and both in the absence (10^4 time steps) and in the presence (10^3 time steps) of diffusive motion. Even though we impose the condition that chemotaxis and phototaxis are detectable up to the same maximal distance, R, the degree of aggregation for the two signaling mechanisms is similar
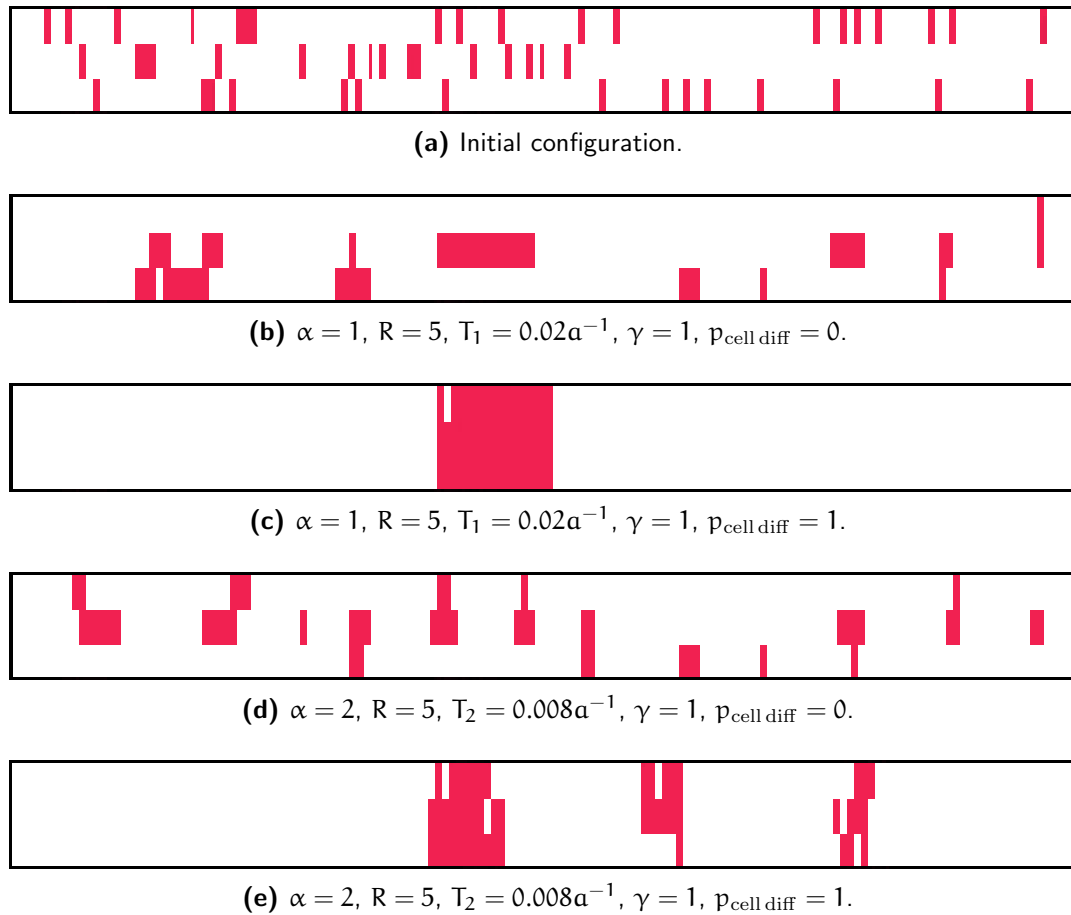
(a) Initial configuration.

(b) $\alpha = 1$, $R = 5$, $T_1 = 0.02a^{-1}$, $\gamma = 1$, $p_{\text{cell diff}} = 0$.

(c) $\alpha = 1$, $R = 5$, $T_1 = 0.02a^{-1}$, $\gamma = 1$, $p_{\text{cell diff}} = 1$.

(d) $\alpha = 2$, $R = 5$, $T_2 = 0.008a^{-1}$, $\gamma = 1$, $p_{\text{cell diff}} = 0$.

(e) $\alpha = 2$, $R = 5$, $T_2 = 0.008a^{-1}$, $\gamma = 1$, $p_{\text{cell diff}} = 1$.

Figure 6-6: *Typical cellular aggregation patterns as obtained from the same initial configuration (a) for chemotaxis ((b) without and (c) with diffusive motion) and for phototaxis ((d) without and (e) with diffusive motion). All patterns are obtained for parameter values $N_x = 150$, $N_y = 3$, $N_{\text{cell}} = 50$, $S = 0.5$, and $p_{\text{cell sig}} = 1$. Chemotaxis together with a diffusive motion produced full aggregation (c). Simulations without diffusive motion (b) and (d) lead to significantly smaller aggregates.*

only for R > 25, where the degree of aggregation attains the maximal value. Note that 25 cell diameters is still a realistic range of communication between two cells [Francis 97]. For smaller values of R, chemotaxis and phototaxis can be distinguished, with chemotaxis leading to a substantially higher degree of aggregation than phototaxis. This observation is made in the absence of diffusive motion (see Figure 6-7 (a)) as well as in the presence of diffusive motion (see Figure 6-7 (b)), however, the overall difference between both signaling processes becomes less significant for larger values of $p_{cell\,diff}$. In the presence of diffusive motion, the degree of aggregation increases faster for small R but does not reach $D_{agg} = 100\%$ since cells detach from aggregates.

6.3.3   Emerging communication distances

The average distance between neighboring aggregates, R_{agg}, is an emerging property of many interacting cells. This distance is measured from the center of mass of the aggregates and is calculated imposing periodic boundary conditions in the x-direction of the lattice. The result is presented in Figure 6-8 as a function of the two-cell interaction range R. Note the qualitative similarity between D_{agg} (see Figure 6-7) and R_{agg} (see Figure 6-8): As follows from Figure 6-7 (a), for the same degree of aggregation, *e.g.* around 60%, it is required that R = 10 for chemotaxis ($\alpha = 1$) and R = 20 for phototaxis ($\alpha = 2$). Extracting from Figure 6-8 (a) the corresponding value of the average distance between neighboring aggregates for chemotaxis (R = 10) and phototaxis (R = 20) we obtain $R_{agg} \approx 100$ for both signaling processes. It thus follows that the two aggregation patterns are comparable in regard to the number of aggregates and the average distance between them. On the level of interactions between two cells, this implies a clearly distinct value of R for the two mechanisms.

6.3.4   Influence of cellular adhesion

The impact of detachment on aggregation is studied by variation of γ. For chemotaxis ($\alpha = 1$) the result is shown in Figure 6-9, where a qualitative change in D_{agg} is observed when varying $p_{cell\,sig}$, *i.e.* the relative importance of movement by signaling versus diffusion. For small values of $p_{cell\,sig} < 0.3$ we observe that D_{agg} decreases for increasing γ, which reflects, as expected, the dissolution of aggregates by detachment. However, for large values $p_{cell\,sig} > 0.3$, aggregates do not dissolve but rather merge and give rise
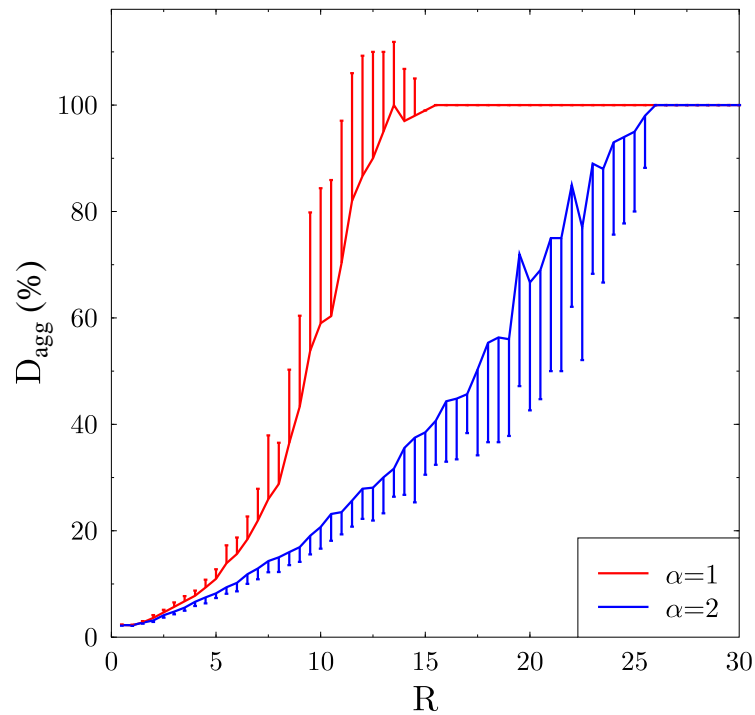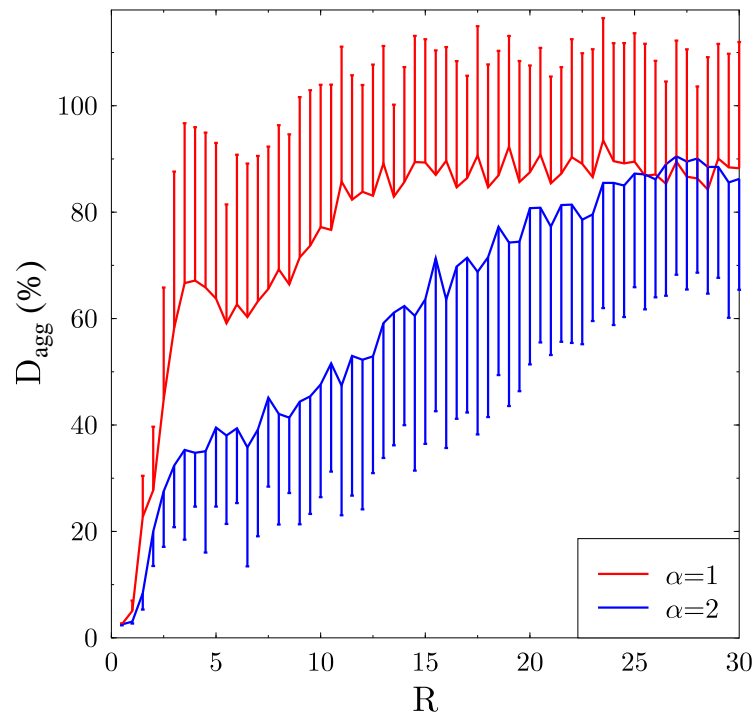
(a) $S = 0.5$, $\gamma = 1$, $p_{cell\,diff} = 0$.

(b) $S = 0.5$, $\gamma = 1$, $p_{cell\,diff} = 1$.

Figure 6-7: *Degree of aggregation, D_{agg}, as a function of the maximal two-cell inter-action distance R for the same parameter values as in Fig. 6-6. Error bars are plotted single-sided for reasons of clarity. In both cases, with and without diffusive motion, chemotaxis (red) experiments reach higher degrees of aggregation faster than photo-taxis (blue) experiments.*
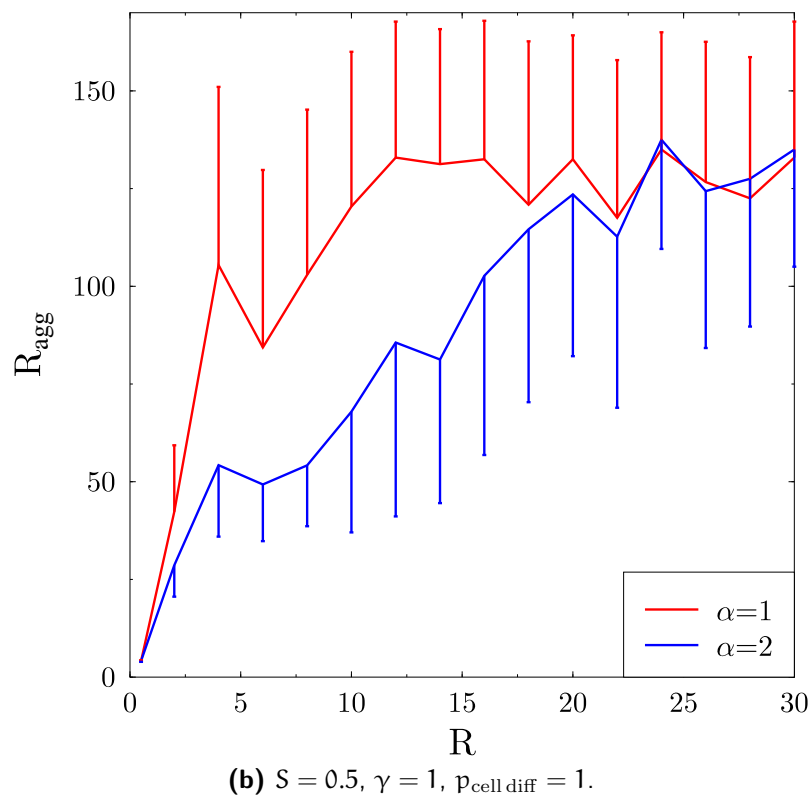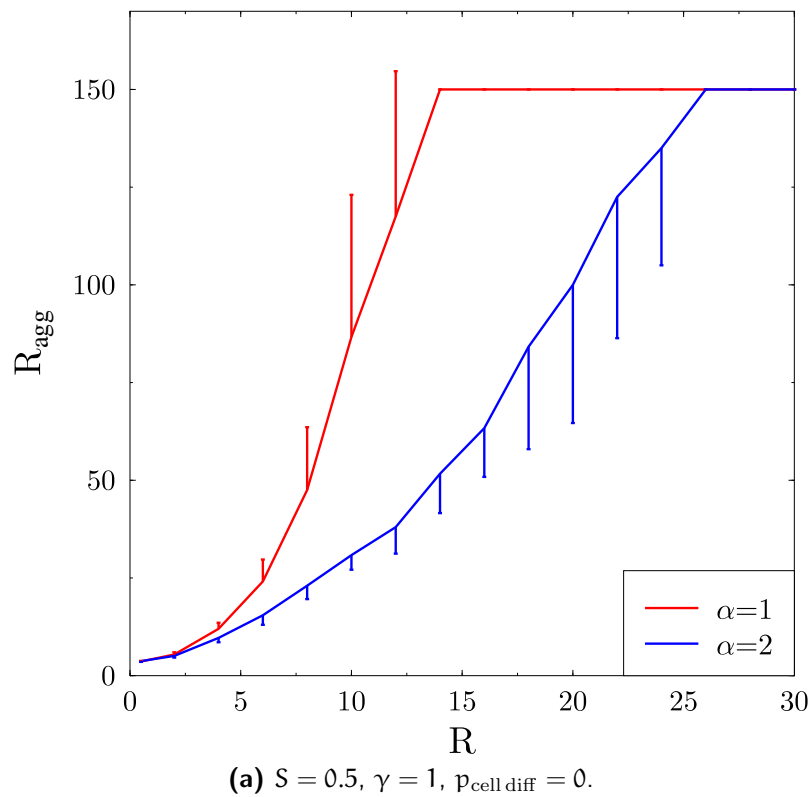
(a) $S = 0.5$, $\gamma = 1$, $p_{\text{cell diff}} = 0$.

(b) $S = 0.5$, $\gamma = 1$, $p_{\text{cell diff}} = 1$.

Figure 6-8: *Average effective distance between aggregates, R_{agg}, as a function of the maximal two-cell interaction distance R and for the same parameter values as in Figure 6-6. The emergent effective distances are bigger for chemotaxis experiments.*

to higher values of D_{agg}. The cellular rearrangement required in this process is found to be actually supported by increasing the detachment probability.

6.3.5 Importance of collective movement

We investigate the effect of the collective movement on the degree of aggregation, thus on patterns formed and the emerging communication distances. In this experiment aggregates were not allowed to move, and the model was run for the same parameters cited above (see Figure 6-7). We can seen from Figure 6-10, that the aggregate movement is essential for the emergence of patterns similar to what is observed in *in vitro* experiments. It is obvious, according to the obtained results, that the degree of aggregation D_{agg} hardly reaches 20% in both cases, with or without diffusive motion. This confirms that cells do not only move alone but also in groups of two and more to reach the range of communication distances observed experimentally. Besides, one also observes that in presence of a diffusive motion, the degree of aggregation is substantially bigger than in the absence of diffusive motion. Single cell diffusion supports aggregate formation.

6.3.6 Determination of aggregate size

The degree of aggregation D_{agg} presented above does not fully inform us about the exact size of aggregates. The way it is computed gives degrees of aggregations of for example 50% in the case of a final configuration of two aggregates, but it does not inform us about the size of the two aggregates. It could very well be that one is of 47 cells, and that the other one is of 3 cells only (all runs were performed with 50 cells). Of course, averaging over several runs gives reliable measurements that are valid for the interpretation of the general behavior of the system under study.

Still, the information concerning the number of cells constituting the aggregates is missing. A ratio for determining the aggregate size was then considered:

$$\text{Ratio of aggregates of size L} = \frac{1}{N_{exper}} \sum_{j=1}^{j=N_{exper}} \frac{N_{i=j}}{N_{i\neq j} + N_{i=j}}, \qquad (6.29)$$

where N_{exper} is the number of experiments that are run with the same parameters, $N_{i=j}$ is the number of aggregates of size i and $N_{i\neq j}$ the number of aggregates of different
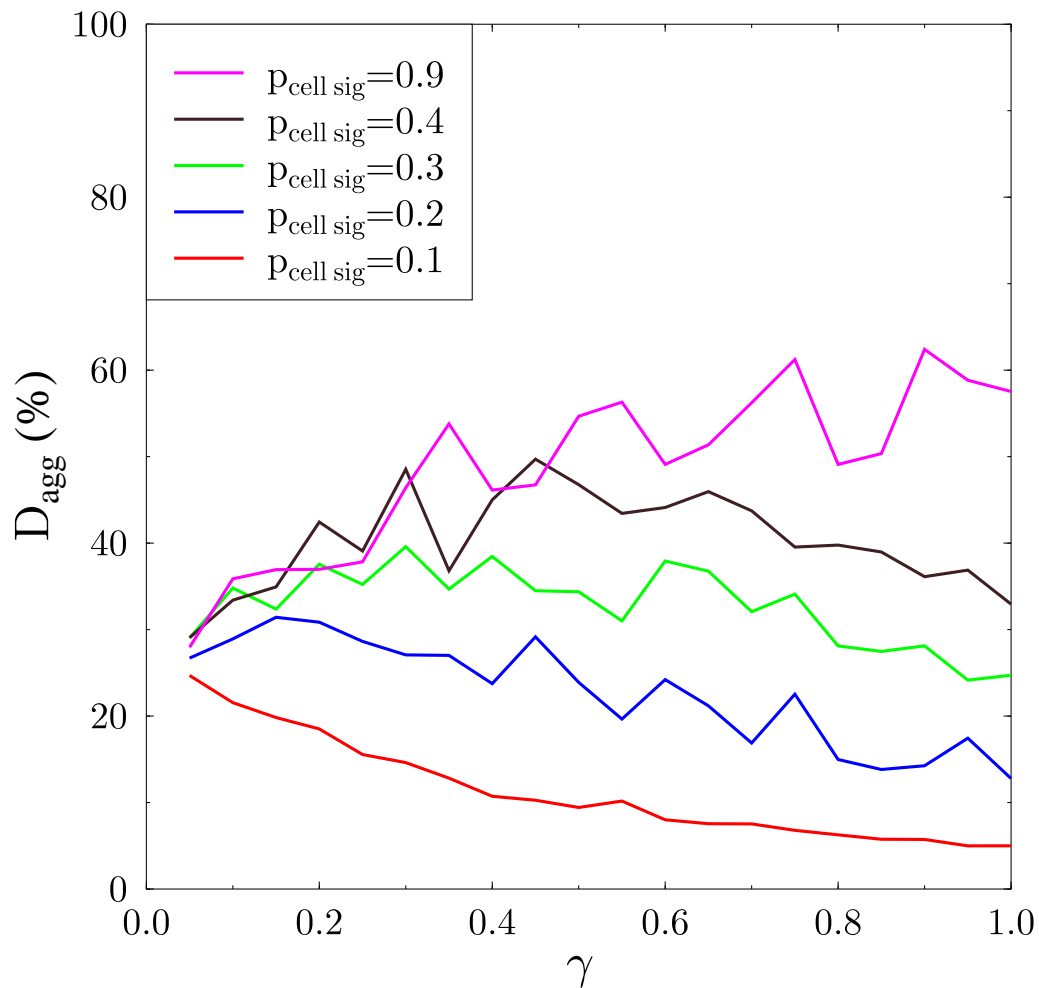
Figure 6-9: *Degree of aggregation as a function of γ for different values of $p_{cell\,sig}$ representing the impact of the signal distribution with $p_{cell\,diff} = 1$ and for the same parameter values as in Fig. 6-6 and with parameter values $N_x = 150$, $N_y = 3$, $N_{cell} = 50$, $\alpha = 1$, $R = 5$, $S = 0.5$, and $p_{cell\,diff} = 1$. Detachment lead to aggregate dissolution (smaller $D_a gg(\%)$) only in the case of weak signaling as shown for $p_{cell\,sig} = 0.1$, $p_{cell\,sig} = 0.2$ and $p_{cell\,sig} = 0.3$.*
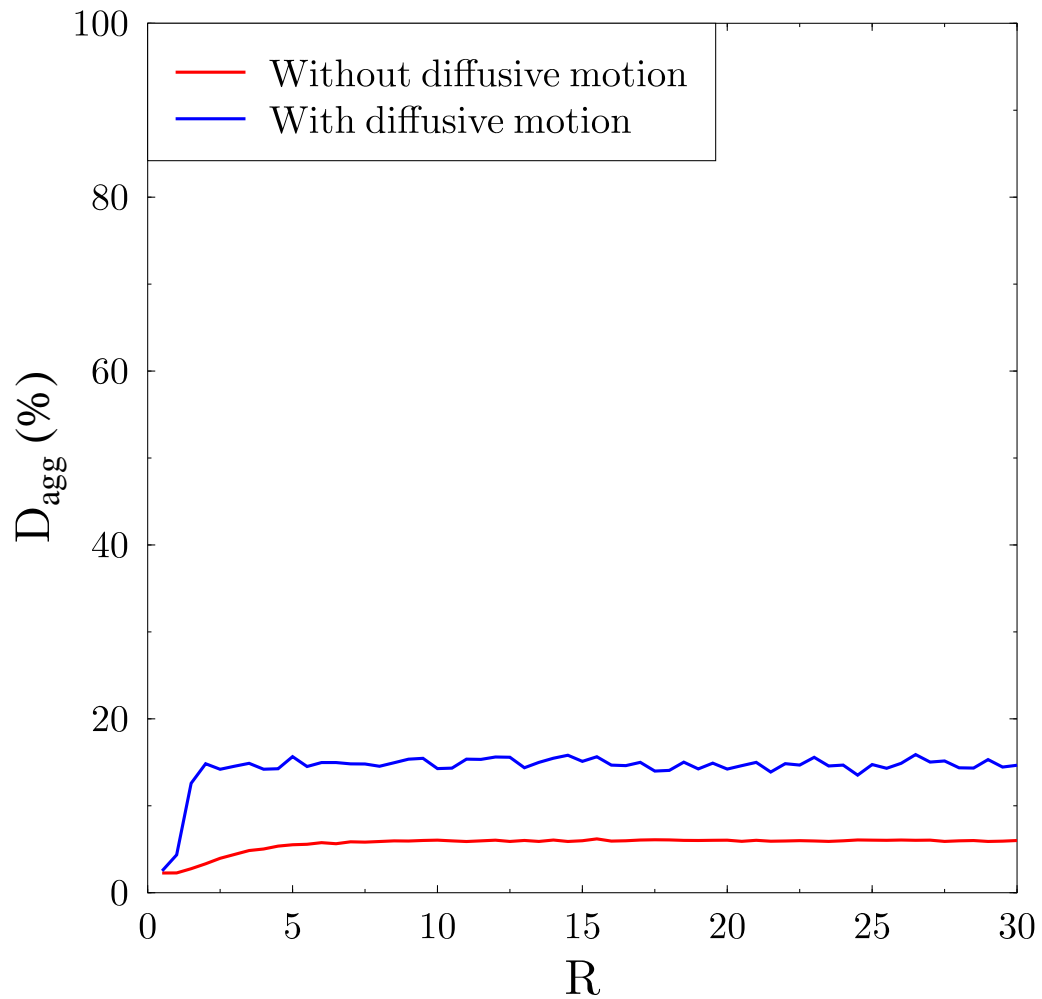
Figure 6-10: *Role of the collective movement on aggregate formation for values of* $p_{cell\,sig} = 1$, $p_{cell\,diff} = 1$, $\alpha = 1$, $R = 5$, $S = 0.5$, *and* $\gamma = 1$. *In both cases, with and without diffusive motion, the degree of aggregation remains lower then 20%, indicating the importance of the collective movement in reproducing the in vitro observations.*

size.   Each of Figures 6-11, 6-12, 6-13 and 6-14 shows a histogram of aggregates
of size L, where L varies between 2 and 50. These results also confirm the importance
of the diffusive motion and chemotaxis in comparison to phototaxis, with respect to
the formation of bigger aggregates for different maximal interaction distances R. If we
compare Figures 6-11 and 6-12, it is clear that for the same implemented values of R
and the same parameters, chemotaxis and phototaxis lead to different aggregate sizes.
A general conclusion would be that chemotaxis always leads to bigger aggregates than
phototaxis. This observation is still valid in the absence and presence of the diffusive
motion as shown in Figures 6-13 and 6-14.

6.3.7   Counting cellular moves

Cellular movements were recorded by the use of counters. These counters were incre-
mented every time a single cell, or an aggregate, moved due to a signaling process or
due to diffusive motion. This gives us an idea about the evolution of single cells and ag-
gregate movement with time and allows us to see whether the system reaches a dynamic
equilibrium.

Figure 6-15 shows a decreasing number of detachments with time. This is consistent
with aggregates getting bigger. Indeed, cells can only detach when they are on the
aggregate borders. The more aggregates we have the more detachments are seen, but
when aggregates get bigger because of merging with others the possibilities for a cell to
detach are smaller.

The same is observation holds when counting of signal-directed single cell move-
ments. The curve shows the expected behavior, single cells perform less movement
simply because they become part of aggregates, and perform aggregate movements.
The same observation is valid for the diffusion of single cells.

On the other hand, single cell movement within aggregates stays more or less of
the same order throughout the *in silico* experiment, due to an ongoing rearrangement
and reshaping of the aggregates. The restriction put on aggregate movements regarding
their size can also be seen from the counters, with less moves towards the end.
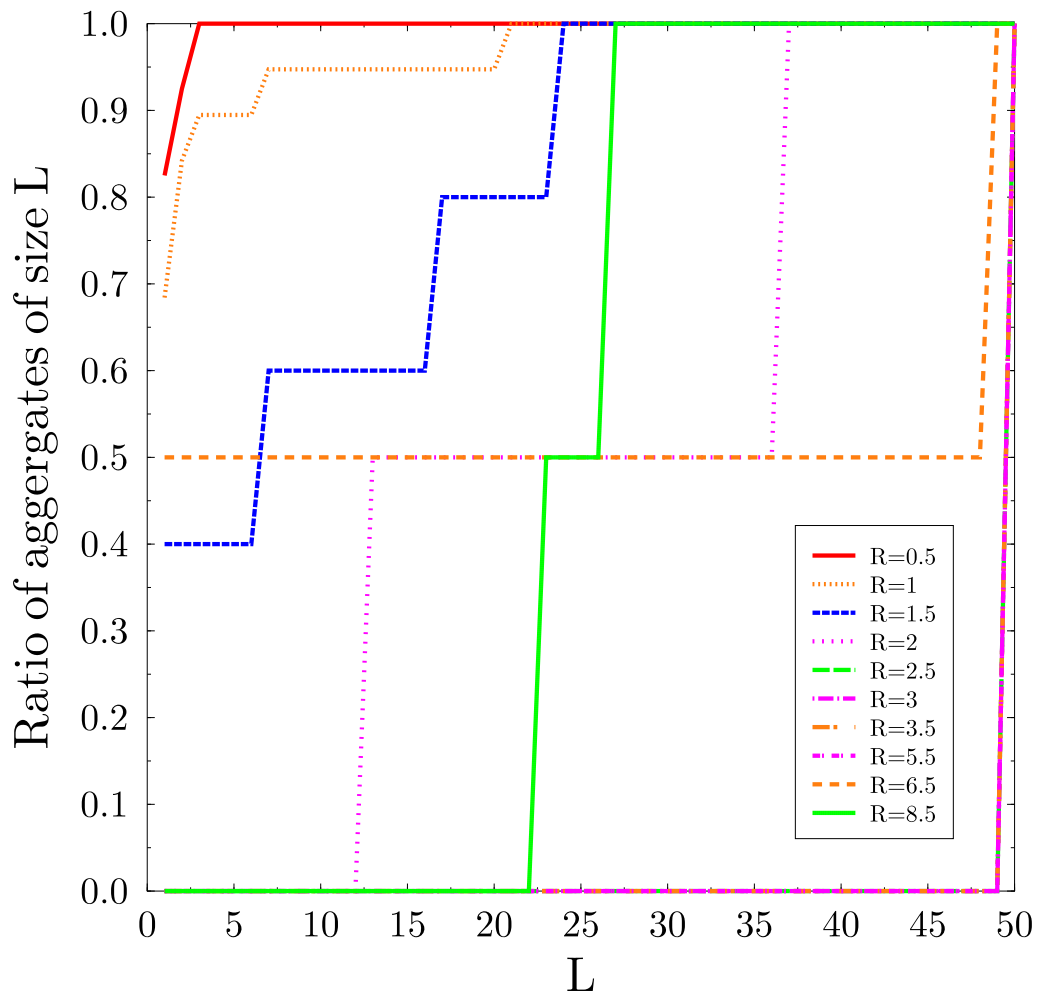
Figure 6-11: *Aggregate size in chemotaxis ($\alpha = 1$) simulations in the presence of diffusive motion. Aggregates are of bigger size for bigger R values, reaching one aggregate of fifty cells for R > 3.5.*
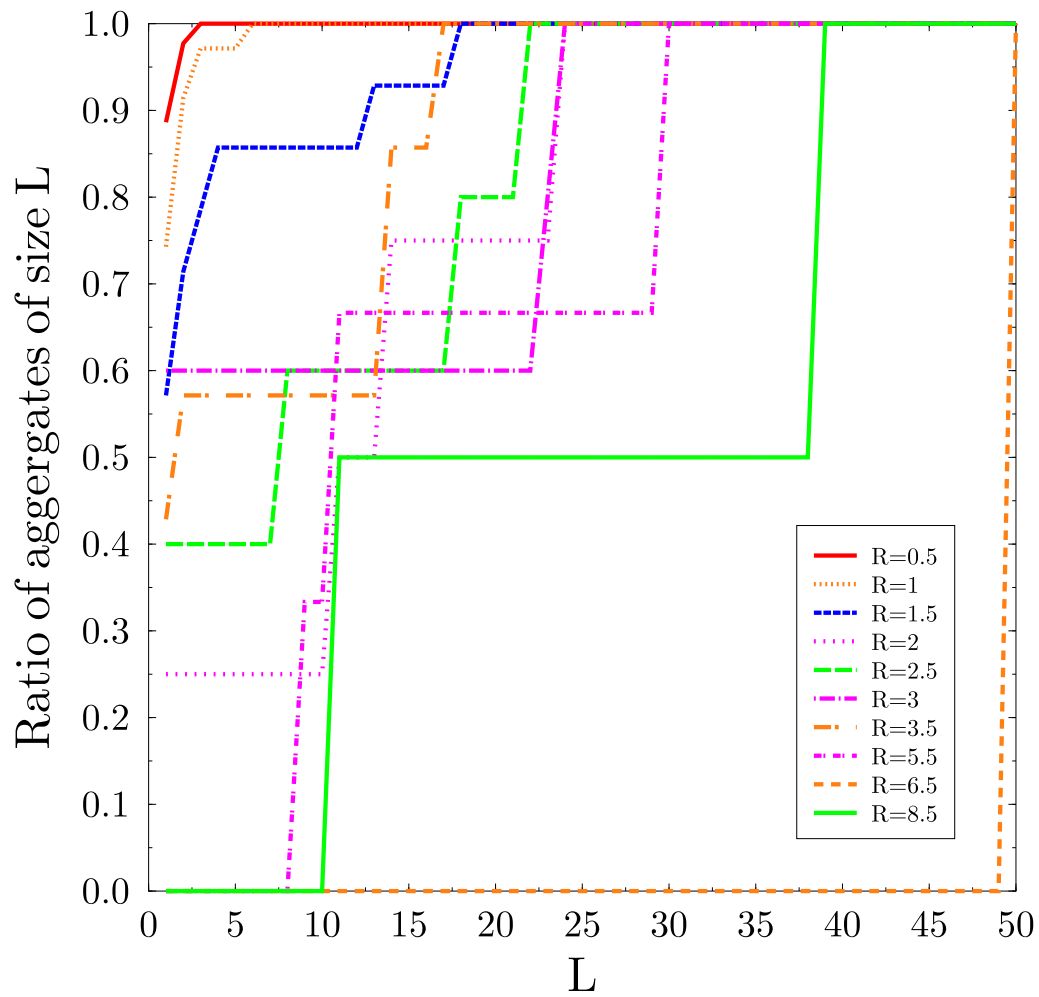
Figure 6-12: *Aggregate size in phototaxis ($\alpha = 2$) simulations in the presence of diffusive motion. Aggregates are of smaller size for the same R values as in Figure 6-11, reaching big aggregates of fifty cells only for R > 6.5.*
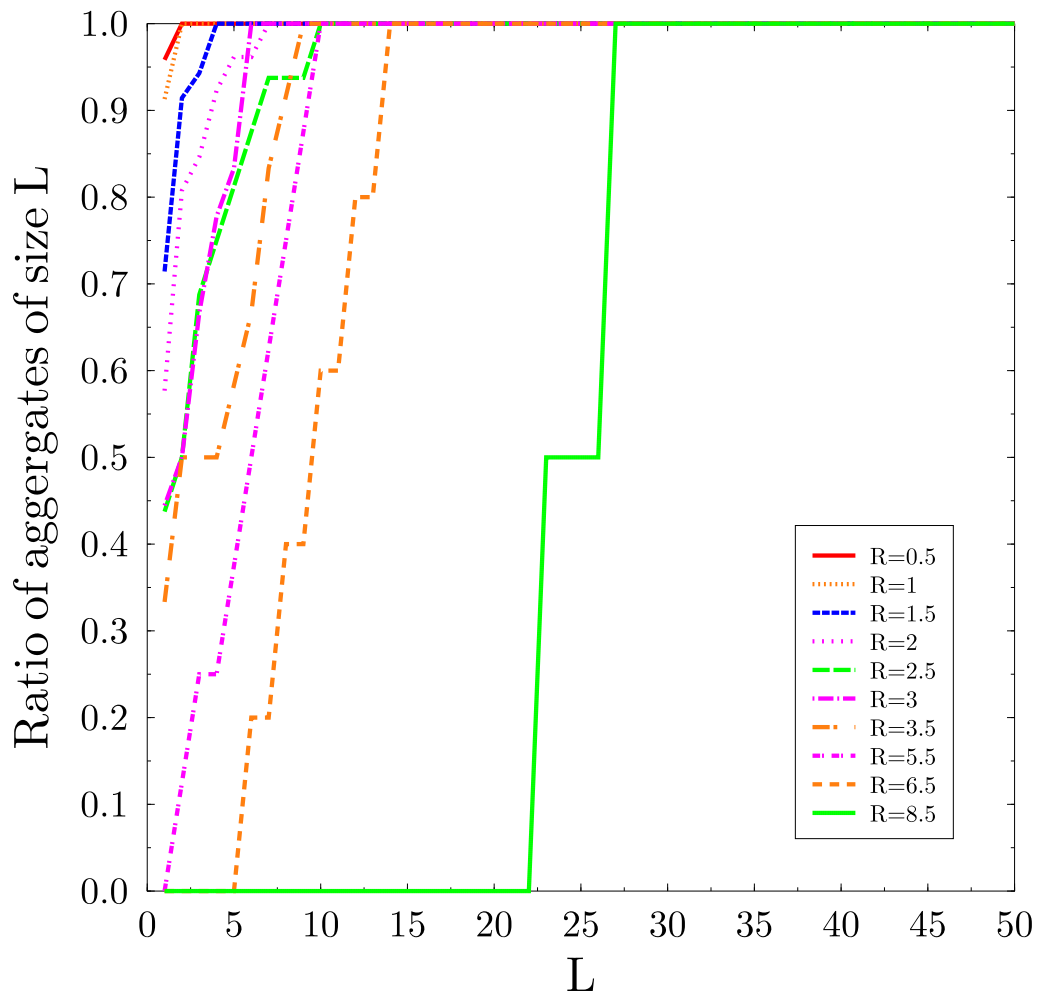
Figure 6-13: *Aggregate size in chemotaxis ($\alpha = 1$) simulations in the absence of diffusive motion. In this case full aggregation (one big aggregate of fifty cells) is not reached even for the biggest R values.*
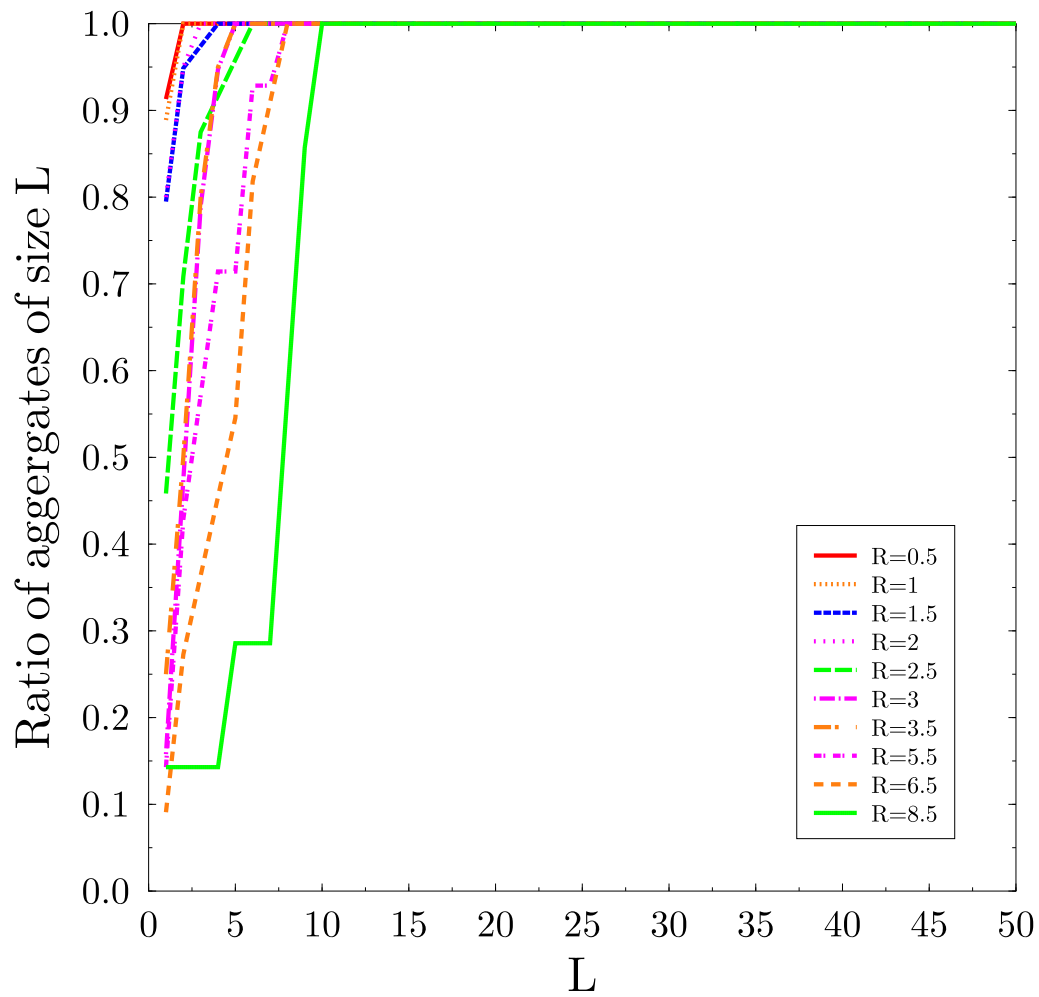
Figure 6-14: *Aggregate size in phototaxis ($\alpha = 2$) simulations in the absence of diffusive motion. The observations made for Figure 6-13 are also valid here, however, aggregates in this case are visibly smaller.*
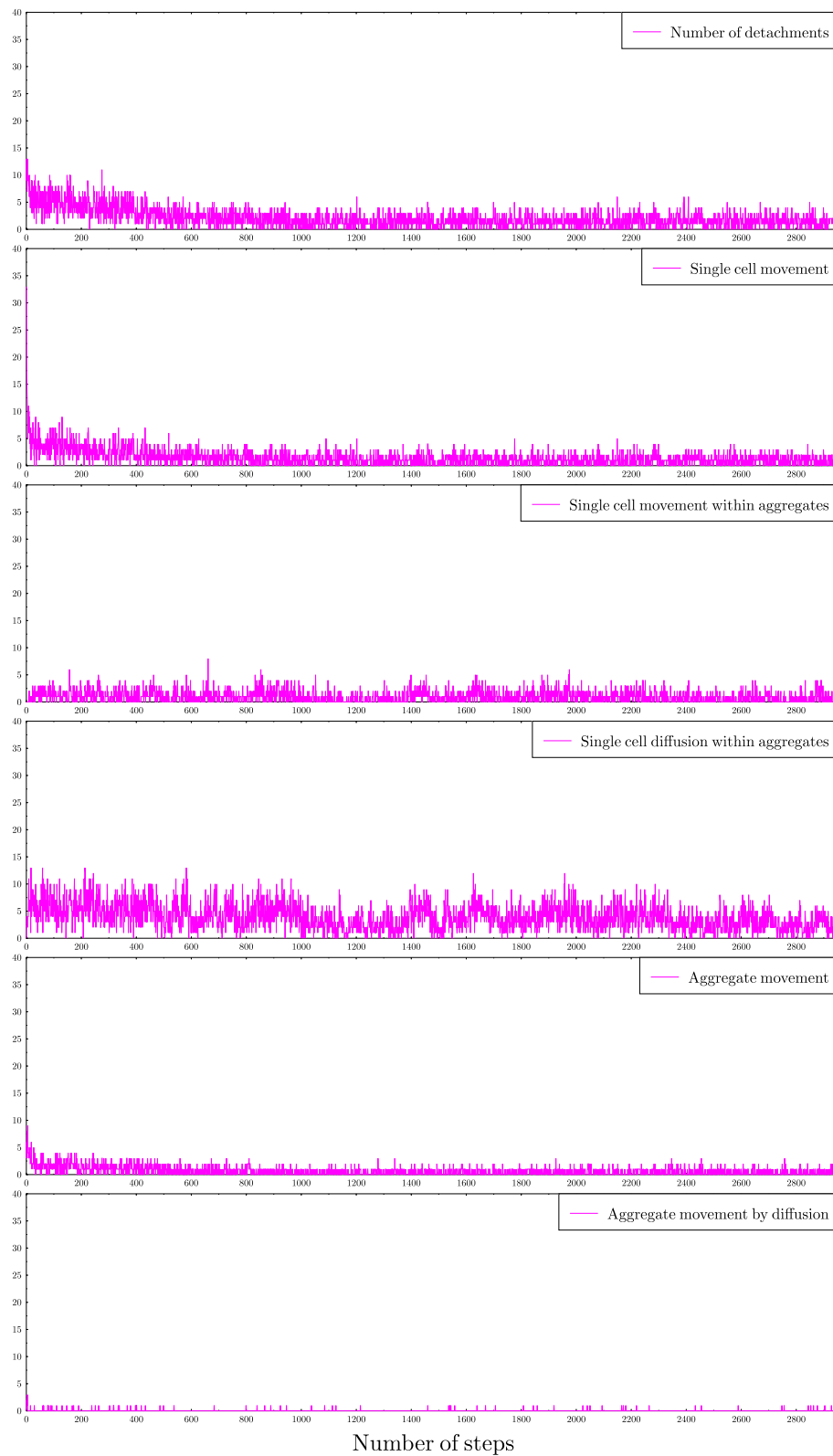
Figure 6-15: *Single cell as well as aggregate number of moves per time step using the following parameters:* $\alpha = 1$, $R = 5$, $S = 0.5$, $T_2 = 0.008a^{-1}$, $\gamma = 1$, $p_{cell\,diff} = 1$, $p_{cell\,sig} = 1$. *Single cell moves decrease with time as they become part of aggregates. Aggregate moves decrease with time as they become larger. However, single cell moves within aggregates stays steady all along the simulation time, indicating a continuous reshaping of aggregates.*

6.3.8   Aggregate dissolution

Specific simulations were run with the same initial configuration as in Figure 6-6, to investigate the effect of the ratio $\frac{p_{\text{cell sig}}}{p_{\text{cell diff}}}$ and γ on aggregation. The results show that using a small probability of movement by the emitted signal and a high diffusion coefficient increases the chances of aggregate dissolution. This is a consequence of detachment being only allowed during the diffusion process. For the same number of simulation steps, aggregates loose cells at their edges as shown in Figures 6-16(c) and 6-16(e). Increasing or reducing the detachment parameter γ has an effect only when $p_{\text{cell sig}}$ is small enough compared to $p_{\text{cell diff}}$. Figure 6-16(e) shows the result of a very small probability of moving $p_{\text{cell sig}}$ by signal combined with a big detachment value for instance $\gamma = 1$. If we compare this figure to Figure 6-16(d) where the ratio $\frac{p_{\text{cell sig}}}{p_{\text{cell diff}}}$ is very big, is become clear that ratio is also responsible for aggregate formation or dissolution. To summarize, we observe for the same values of the detachment parameter γ, that only when $p_{\text{cell sig}} = 0.1$, namely only when the signal is weak enough in comparison to diffusion, detachment is observed. It is also clear from the initial configuration of cells (see Figure 6-16(a)), that aggregates did form then dissolved during the simulation time. If the γ value is big, aggregates are smaller for the same values of $p_{\text{cell sig}}$ and $p_{\text{cell diff}}$, as shown in Figures 6-16(b) and (d). This is due to cells performing more detachment, however, the signal is so strong that it keeps them from detaching by forming smaller aggregates.

---

[1]web.neurobio.arizona.edu.
[2]imagine.gsfc.nasa.gov.

(a) Initial configuration

(b) $\alpha = 1$, $R = 5$, $S = 0.5$, $\gamma = 0.2$, $p_{\text{cell diff}} = 0.1$, $p_{\text{cell sig}} = 1$.

(c) $\alpha = 1$, $R = 5$, $S = 0.5$, $\gamma = 0.2$, $p_{\text{cell diff}} = 1$, $p_{\text{cell sig}} = 0.1$.

(d) $\alpha = 1$, $R = 5$, $S = 0.5$, $\gamma = 1$, $p_{\text{cell diff}} = 0.1$, $p_{\text{cell sig}} = 1$.

(e) $\alpha = 1$, $R = 5$, $S = 0.5$, $\gamma = 1$, $p_{\text{cell diff}} = 1$, $p_{\text{cell sig}} = 0.1$.
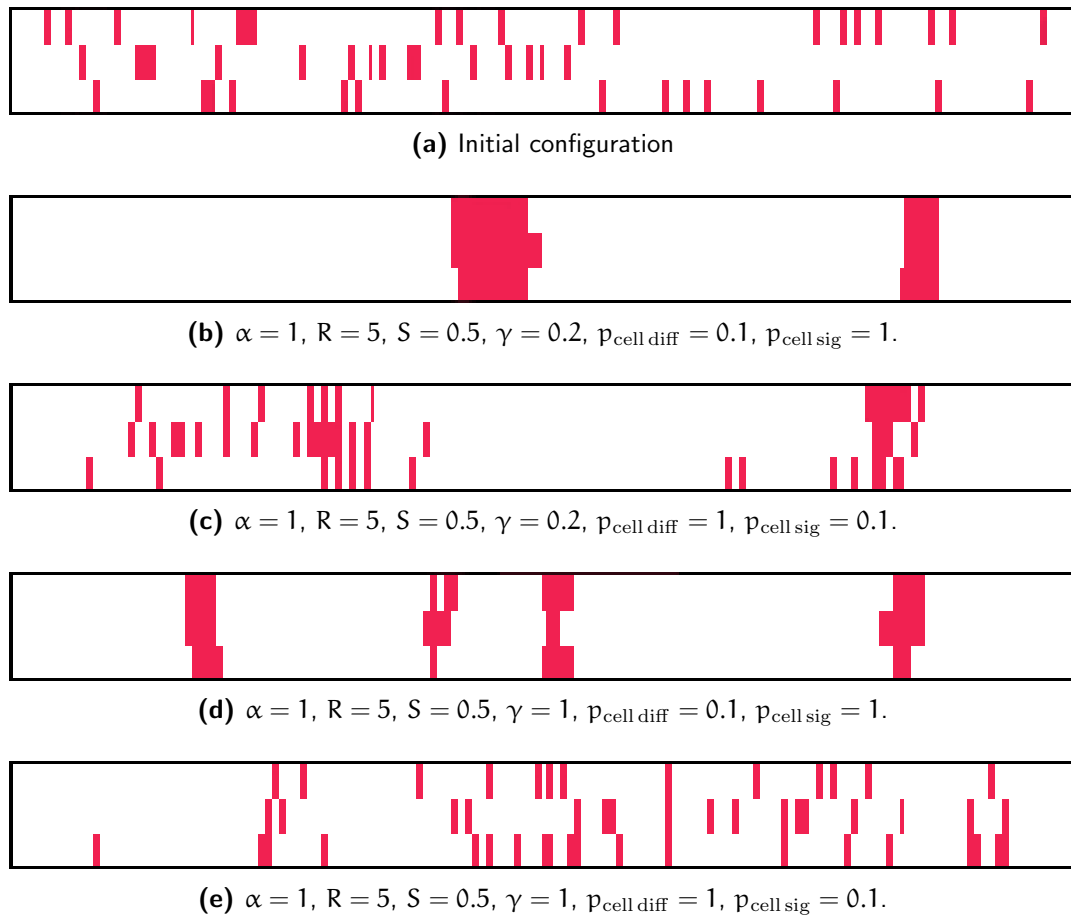
Figure 6-16: *The importance of a precise adjustment of the detachment parameter γ, the diffusive motion and the signal strength in aggregates formation or dissolution. To reach high aggregate dissolution, the response to signals has to be smaller than the diffusive motion with a maximal value of γ.*

7 Summary

The presented PhD work proposes a mathematical model to help distinguish between several cellular interactions by the study of the emergent patterns. Chemotaxis, photo-taxis and random diffusion were used as well identified interactions for the analysis of the emergent properties.

In the introduction of this thesis, communication between cells was shown to be of great importance in many processes with a focus on cell migration and aggregation. Different ways of cellular communication and signaling were introduced. We then concentrated our attention on the importance of pattern analysis in recognizing the underlying mechanisms behind a given behavior. Mathematical modeling could revealed chemotaxis presence despite experimental data supporting random walk. Cell migration data together with cell compartmentalization were shown to allow the determination of the underlying interaction modes.

It was also indicated that chemotaxis is necessary for actions performed during the immune response. Evidence using live two-photon imaging techniques together with mathematical modeling demonstrated the primordial role chemotaxis plays in inducing cellular migration and aggregation within germinal centers. These signaling pathways are essential for affinity maturation and therefore for a proper functioning of the immune response. In parallel, evidence for the existence of a light-based cellular communication and a light directed movement were presented. The role of phototaxis in different mechanisms like increasing bacteria's virulence and cellular aggregation were as well discussed. These two signals are used as a base for the construction of our model, for them being well known signals that present different scaling behaviors.

Later, we introduced the agent-based modeling technique as a reliable and relatively flexible tool for simulating biological systems. It enables the study of the evolution of many-cell systems in presence of different interactions. Its particular advantages over other modeling techniques were discussed as well, especially in the case of investigating pattern emergence which is the aim of the presented dissertation.

After what, we described our agent-based model that simulates chemotaxis and phototaxis as intrinsic processes of the cell. This is to say that cells emit and receive signals responsible of their actions. Our model also account for cellular diffusion or random walk. We also described the way our model is recognizing aggregates, including aggregate signaling and movement. Cellular adhesion is also incorporated in the model via a detachment parameter that regulates aggregate dissolution.

The results of our simulations showed that cellular aggregation is more subtle than might be thought on first sight. Yet, our simulations show that the same maximum communication distance R can lead to very different information held in and deducible from the aggregation patterns. The implemented distance R is a one-cell/one-cell range of detection. However, the resulting effective communication distance R_{eff} is not the same due to the collective effect of aggregates that accounts for broader signaling distances and that varies depending on the chosen signal. The signals used have two different scaling behaviors with the distance between two communicating cells. The general description reads $1/r^\alpha$, $\alpha = 1$ is representative of chemotaxis and $\alpha = 2$ of phototaxis. The resulting effective communication distance over which cells seem to feel each other is incontestably the key parameter for recognizing different signals. Within our model, chemotaxis always produced bigger R_{eff}.

Allowing the detachment of cells from an already formed aggregate may have the counterintuitive effect of ultimately increasing the degree of aggregation. Indeed, diffusion has usually an effect of making the aggregation process harder. However, under specific values of the detachment parameter, cells detached from small aggregates to reattach to bigger aggregates with stronger emitted signals. More detachment was recorded in the case of a bigger α, due to smaller resulting aggregates and therefore bigger chances to detach from them.

Recordings of cellular moves showed that aggregates incessantly oscillate around their centers of mass, as a result of the diffusion and rearrangement process. Hopping around the same position does not contradict the experimental observations. Cells that are moved within the aggregates by diffusion are brought back to a more stable position in dependence of the attractive strength of the signal.

The range of R-values for which chemotaxis and phototaxis can be distinguished was shown to be relevant to real cells. For example, hematopoietic CD34+ cells were seen to communicate across 14 cell diameters [Francis 97], this is in agreement with our model

results. Thus, our model can be used to uncover the unknown signaling process for an estimated threshold value T or signal strength S. Experimental determination of R from two-cell experiments and R_{eff} from the analysis of aggregate patterns will then be sufficient to distinguish between the different underlying signals.

The model aims to present a tool to define the signal behind a particular cellular behavior on a phenomenological level. It is a first attempt to compare patterns induced by different signals, for instance chemotaxis and phototaxis, while accounting for a collective movement of cells and providing the key parameters for this. For further applications specific types of the studied cells have to be considered which will obviously involve more parameters. Yet, the field is lacking experimental data relevant for the mathematical representation, caused by limitations either in designing new experiments or restrictions on their feasibility. We endeavor to point out the differences between two signaling mechanisms to propose a tool that will help experimentalists discern between different regimes given certain parameters. In addition, we believe that our model will facilitate the exploration of other parameters which can be used for studying larger systems with higher cell densities with the integration of new interactions and new rules. The next natural extension of this model would be the investigation of inter-dependencies between chemokine release, phototaxis, chemotaxis and cellular diffusion on pattern emergence.

List of Figures

List of Tables

Acknowledgments

I wish to thank Dr. Michael Meyer-Hermann, for allowing me to do my PhD within his group and for his influence on my work through very fruitful discussions and supportive leadership. He has been of great aid to me in designing the model this thesis was based on by raising new questions and sharing with me his scientific knowledge and experience as a theoretical biologist.

My PhD work would have not advanced without the help and experience of Dr. Tilo Beyer, especially in the programing and debugging part, and Dr. Marc Thilo Figge whom I would particularly like to thank for his patience, assistance, scientific advice and surely his time spent in correcting my thesis.

My work in FIAS has also profited from the incomparable environment offered to its PhD students in terms of scientific diversity and openness. As a mechanical Engineer, the daily exchange with physicists, chemists, and others was very enriching and stimulating. I learned a lot about other fields and had the chance to discover different scientific approaches. In addition, I would like to thank the FIAS directors, von der Malsburg and Horst Stöcker for their continuous effort in helping the micro-society of foreign students getting integrated.

My Frankfurter life would not have been as exciting without the encounter of some remarkable people. Met either in FIAS or elsewhere of whom I would like to cite Adilah Hussien, Emanuele Scifoni, Dominik Heide and many others. To whom I am grateful for their scientific advice, help in soft skills and friendship.

Finally, I would like to thank my family and friends for always supporting me in my decisions, and for their presence in tough moments.

Bibliography

[Albrecht-Buehler 05] G. Albrecht-Buehler. *A long-range attraction between aggregating 3T3 cells mediated by near-infrared light scattering.* PNAS, vol. 102, pages 5050–5055, April 2005.

[Allen 07a] Christopher D. C. Allen, T. Okada, HL. Tang & JG. Cyster. *Imaging of germinal center selection events during affinity maturation.* Science, vol. 315, pages 528–31, 2007.

[Allen 07b] Christopher D C Allen, Takaharu Okada & Jason G Cyster. *Germinal-center organization and cellular dynamics.* Immunity, vol. 27, no. 2, pages 190–202, Aug 2007.

[Asperti-Boursin 07] François Asperti-Boursin, Eliana Real, Georges Bismuth, Alain Trautmann & Emmanuel Donnadieu. *CCR7 ligands control basal T-cell motility within lymph node slices in a phosphoinositide 3-kinase-independent manner.* J Exp Med, vol. 204, no. 5, pages 1167–1179, May 2007.

[Aydar 03] Yüksel Aydar, Peter Balogh, John G .Tew & Andras K . Szakal. *Altered regulation of Fc gamma RII on aged follicular dendritic cells correlates with immunoreceptor tyrosine-based inhibition motif signaling in B-cells and reduced germinal center formation.* J Immunol, vol. 171, no. 11, pages 5975–5987, Dec 2003.

[Bajenoff 06] M. Bajenoff, JG. EGEN, Y. KOO Lily, JP. LAUGIER, F. BRAU, N. GLAICHENHAUS & RN. GERMAIN. *Stromal cell networks regulate lymphocyte entry, migration, and territoriality in lymph nodes.* Immunity, vol. 25, pages 989–1001, 2006.

[Bardi 01] G. Bardi, M. Lipp, M. Baggiolini & P. Loetscher. *The T-cell chemokine receptor CCR7 is internalized on stimulation with ELC, but not with SLC.* Eur J Immunol, vol. 31, no. 11, pages 3291–3297, Nov 2001.

[Beauchemin 07]   Catherine Beauchemin, Narendra M. Dixit & Alan S. Perelson. *Characterizing T cell movement within lymph nodes in the absence of antigen.* J Immunol, vol. 178, no. 9, pages 5505–5512, May 2007.

[Beltman 07a]   Joost B. Beltman, Athanasius F. M. Mare & Rob J. de Boer. *Spatial modelling of brief and long interactions between T cells and dendritic cells.* Immunol Cell Biol, vol. 85, no. 4, pages 306–314, Jun 2007.

[Beltman 07b]   Joost B Beltman, Athanasius F M Mare, Jennifer N Lynch, Mark J Miller & Rob J de Boer. *Lymph node topology dictates T cell migration behavior.* J Exp Med, vol. 204, no. 4, pages 771–780, Apr 2007.

[Benhamou 06]   Simon Benhamou. *Detecting an orientation component in animal paths when the preferred direction is individual-dependent.* Ecology, vol. 87, no. 2, pages 518–528, Feb 2006.

[Beyer 07]   Tilo Beyer & Michael Meyer-Hermann. *Modeling emergent tissue organization involving high-speed migrating cells in a flow equilibrium.* Phys Rev E Stat Nonlin Soft Matter Phys, vol. 76, no. 2 Pt 1, page 021929, Aug 2007.

[Beyer 08]   Tilo Beyer & Michael Meyer-Hermann. *Mechanisms of organogenesis of primary lymphoid follicles.* Int Immunol, vol. 20, no. 4, pages 615–623, Apr 2008.

[Beyer 09]   Tilo Beyer, Peter Lane & Michael Meyer-Hermann. *Chemokinesis determines B/T segregation in the spleen.* Submitted, 2009.

[Burriesci 08]   Matthew Burriesci & Devaki Bhaya. *Tracking phototactic responses and modeling motility of Synechocystis sp. strain PCC6803.* J Photochem Photobiol B, vol. 91, no. 2-3, pages 77–86, May 2008.

[Cahalan 08]   MD. Cahalan & I. Parker. *Choreography of cell motility and interaction dynamics imaged by two photon microscopy in lymphoid organs.* Annu. Rev. Immunol., vol. 26, pages 585–626, 2008.

[Chavali 08]   Arvind K. Chavali, Erwin P. Gianchandani, Kenneth S. Tung, Michael B. Lawrence, Shayn M. Peirce & Jason A. Papin. *Characterizing emergent properties of immunological systems with multi-cellular*

rule-based computational modeling. Trends Immunol, vol. 29, no. 12, pages 589–599, Dec 2008.

[Chowdhury 91]   D. Chowdhury, M. Sahimi & D. Stauffer. *A discrete model for immune surveillance, tumor immunity and cancer.* J Theor Biol, vol. 152, no. 2, pages 263–270, Sep 1991.

[Cyster 99]   J. G. Cyster. *Chemokines and cell migration in secondary lymphoid organs.* Science, vol. 286, no. 5447, pages 2098–2102, Dec 1999.

[Cyster 00]   J. G. Cyster, K. M. Ansel, K. Reif, E. H. Ekland, P. L. Hyman, H. L. Tang, S. A. Luther & V. N. Ngo. *Follicular stromal cells and lymphocyte homing to follicles.* Immunol Rev, vol. 176, pages 181–193, Aug 2000.

[Dallon 97]   J. C. Dallon & H. G. Othmer. *A discrete cell model with adaptive signalling for aggregation of Dictyostelium discoideum.* Philos Trans R Soc Lond B Biol Sci, vol. 352, no. 1351, pages 391–417, Mar 1997.

[Delon 02]   Jerôme Delon, Sabine Stoll & Ronald N Germain. *Imaging of T-cell interactions with antigen presenting cells in culture and in intact lymphoid tissue.* Immunol Rev, vol. 189, pages 51–63, Nov 2002.

[Depoil 05]   David Depoil, Rossana Zaru, Martine Guiraud, Anne Chauveau, Julie Harriague, Georges Bismuth, Clemens Utzny, Sabina Müller & Salvatore Valitutti. *Immunological synapses are versatile structures enabling selective T-cell polarization.* Immunity, vol. 22, no. 2, pages 185–194, Feb 2005.

[Deutsch 04]   Andreas Deutsch & Sabine Dormann. *Cellular Automaton Modeling of Biological Pattern Formation: Characterization, Applications, and Analysis.* Birkhäuser, 2004.

[Devreotes 03]   Peter Devreotes & Chris Janetopoulos. *Eukaryotic chemotaxis: distinctions between directional sensing and polarization.* J Biol Chem, vol. 278, no. 23, pages 20445–20448, Jun 2003.

[Dustin 97]   M. L. Dustin, S. K. Bromley, Z. Kan, D. A. Peterson & E. R. Unanue. *Antigen receptor engagement delivers a stop signal to migrating T lymphocytes.* Proc Natl Acad Sci U S A, vol. 94, no. 8, pages 3909–3913, Apr 1997.

[Figge 06]   M.T. Figge & M. Meyer-Hermann. *Geometrically repatterned immuno-logical synapses uncover formation mechanisms.* PLoS Comput Biol, vol. 2, no. 11, page e171, Nov 2006.

[Figge 08]   M.T. Figge, A . Garin, M. Gunzer, M. Kosco-Vilbois, K . Toellner & M. Meyer-Hermann. *Deriving a germinal center lymphocyte migration model from two-photon data.* JEM, 2008.

[Figge 09]   M.T. Figge & M. Meyer-Hermann. *Modeling receptor-ligand binding kinetics in immunological synapse formation.* European Physical Journal D 51, page 153160, 2009.

[Foxman 99]   E. F. Foxman, E. J. Kunkel & E. C. Butcher. *Integrating conflicting chemotactic signals. The role of memory in leukocyte navigation.* J Cell Biol, vol. 147, no. 3, pages 577–588, Nov 1999.

[Francis 97]   K. Francis & Bernhard O. Palsson. *Effective intercellular communication distances are determined by the relative time constants for cyto/chemokine secretion and diffusion.* PNAS, vol. 94, pages 12258–12262, August 1997.

[Grima 05]   R. Grima. *Strong-coupling dynamics of a multicellular chemotactic system.* Phys Rev Lett, vol. 95, no. 12, page 128103, Sep 2005.

[Häder 91]   D. P. Häder, S. M. Liu & K. Kreuzberg. *Orientation of the photosynthetic flagellate, Peridinium gatunense, in hypergravity.* Curr Microbiol, vol. 22, no. 3, pages 165–172, Mar 1991.

[Harris 01]   E. H. Harris. *Chlamydomonas as a model organism.* Annu. Plant Physiol. Plant Mol. Biol., vol. 52, pages 363–406, 2001.

[Hauser 07]   Anja E Hauser, Mark J Shlomchik & Ann M Haberman. *In vivo imaging studies shed light on germinal-centre development.* Nat Rev Immunol, vol. 7, no. 7, pages 499–504, Jul 2007.

[Heit 02]   Bryan Heit, Samantha Tavener, Eko Raharjo & Paul Kubes. *An intracellular signaling hierarchy determines direction of migration in opposing chemotactic gradients.* J Cell Biol, vol. 159, no. 1, pages 91–102, Oct 2002.

[Helmchen 05]   F. Helmchen & W. Denk. *Deep tissue two-photon microscopy.* Nature Methods, vol. 2, pages 932–940, 2005.

[Hoff 94]   W. D. Hoff, P. Dux, K. Hard, B. Devreese, I. M. Nugteren-Roodzant, W. Crielaard, R. Boelens, R. Kaptein, J. van Beeumen & K. J. Hellingwerf. *Thiol ester-linked p-coumaric acid as a new photoactive prosthetic group in a protein with rhodopsin-like photochemistry.* Biochemistry, vol. 33, no. 47, pages 13959–13962, Nov 1994.

[Hong 80]   Choo Bong Hong, Maria A. Haeder, Donat-P. Haeder & Kenneth L. Poff. *Phototaxis in Dictyostelium discoideum Amoebae.* Photochem. and Photobiol., vol. 33, pages 373–377, 1980.

[Horstmann 02]   Dirk Horstmann. *On the existence of radially symmetric blow-up solutions for the Keller-Segel model.* J Math Biol, vol. 44, no. 5, pages 463–478, May 2002.

[Huang 07]   Julie H. Huang, L. Isabel Cardenas-Navia, Charles C. Caldwell, Troy J. Plumb, Caius G. Radu, Paulo N. Rocha, Tuere Wilder, Jonathan S. Bromberg, Bruce N. Cronstein, Michail Sitkovsky, Mark W. Dewhirst & Michael L. Dustin. *Requirements for T lymphocyte migration in explanted lymph nodes.* J Immunol, vol. 178, no. 12, pages 7747–7755, Jun 2007.

[Iglesias 02]   Pablo A Iglesias & Andre Levchenko. *Modeling the cell's guidance system.* Sci STKE, vol. 2002, no. 148, page RE12, Sep 2002.

[Ingulli 97]   E. Ingulli, A. Mondino, A. Khoruts & M. K. Jenkins. *In vivo detection of dendritic cell antigen presentation to CD4(+) T cells.* J Exp Med, vol. 185, no. 12, pages 2133–2141, Jun 1997.

[Kahn 64]   Arnold J. Kahn. *The Influence of Light on Cell Aggregation in polysphondylium pallidum.* Biol. Bull., vol. 127, pages 85–95, 1964.

[Keller 71]   E. F. Keller & L. A. Segel. *Model for chemotaxis.* J Theor Biol, vol. 30, no. 2, pages 225–234, Feb 1971.

[Kemir 03]   Can Kemir & Rob J De Boer. *A spatial model of germinal center reactions: cellular adhesion based sorting of B cells results in efficient*

affinity maturation. J Theor Biol, vol. 222, no. 1, pages 9–22, May 2003.

[Kim 98] C. H. Kim, L. M. Pelus, J. R. White, E. Applebaum, K. Johanson & H. E. Broxmeyer. *CK beta-11/macrophage inflammatory protein-3 beta/EBI1-ligand chemokine is an efficacious chemoattractant for T and B-cells.* J Immunol, vol. 160, no. 5, pages 2418–2424, Mar 1998.

[Kohler 00] B. Kohler, R. Puzone, P. E. Seiden & F. Celada. *A systematic approach to vaccine complexity using an automaton model of the cellular and humoral immune system. I. Viral characteristics and polarized responses.* Vaccine, vol. 19, no. 7-8, pages 862–876, Nov 2000.

[Kosco-Vilbois 03] Marie H. Kosco-Vilbois. *Are follicular dendritic cells really good for nothing?* Nat Rev Immunol, vol. 3, no. 9, pages 764–769, Sep 2003.

[Lee 94] Y. Lee, L. V. McIntire & K. Zygourakis. *Analysis of endothelial cell locomotion: Differential effects of motility and contact inhibition.* Biotechnol Bioeng, vol. 43, no. 7, pages 622–634, Mar 1994.

[Levchenko 02] Andre Levchenko & Pablo A Iglesias. *Models of eukaryotic gradient sensing: application to chemotaxis of amoebae and neutrophils.* Biophys J, vol. 82, no. 1 Pt 1, pages 50–63, Jan 2002.

[Levy 08] Doron Levy & Tiago Requeijo. *Stochastic models for phototaxis.* Bull Math Biol, vol. 70, no. 6, pages 1684–1706, Aug 2008.

[Lui 91] Y.J. Lui, J. Zhang, P.J. Lane, E.Y. Chan & I.C. MacLennan. *Sites of specific B cell activation in primary and secondary responses to T cell-dependent and T cell-independent antigens.* Eur. J. Immunol., vol. 21, pages 2951–2962, 1991.

[MacLennan 91] I. C. MacLennan, G. D. Johnson, Y. J. Liu & J. Gordon. *The heterogeneity of follicular reactions.* Res Immunol, vol. 142, no. 3, pages 253–257, 1991.

[MacLennan 94] Ian C. M. MacLennan. *Germinal Centers.* Annu. Rev. Immunol., vol. 12, pages 117–39, 1994.

[Mallet 06]   D. G. Mallet & L. G. De Pillis. *A cellular automata model of tumor-immune system interactions.* J Theor Biol, vol. 239, no. 3, pages 334–350, Apr 2006.

[Mempel 04]   TR. Mempel, SE. Henrickson & UH. von Andrlan. *T-cell priming by dendritic cells in lymph nodes occurs in three distinct phases.* Nature, vol. 427, pages 154–59, 2004.

[Meyer-Hermann 05a]   ME. Meyer-Hermann & PK. Mainy. *Interpreting two-photon imaging data of lymphocyte motility.* PR E 71, vol. 296, pages 061912–1–12, 2005.

[Meyer-Hermann 05b]   Michael E Meyer-Hermann & Philip K Maini. *Cutting edge: Back to "one-way" germinal centers.* J Immunol, vol. 174, no. 5, pages 2489–2493, Mar 2005.

[Meyer-Hermann 06]   Michael E Meyer-Hermann, Philip K Maini & Dagmar Iber. *An analysis of B cell selection mechanisms in germinal centers.* Math Med Biol, vol. 23, no. 3, pages 255–277, Sep 2006.

[Miller 02]   MJ. Miller, SH. Wei, I. Parker & MD. Cahalan. *Two-photon imaging of lymphocyte motility and antigen response in intact lymph node.* Science, vol. 296, pages 1869–73, 2002.

[Miller 03]   Mark J. Miller, Sindy H. Wei, Michael D. Cahalan & Ian Parker. *Autonomous T cell trafficking examined in vivo with intravital two-photon microscopy.* Proc Natl Acad Sci U S A, vol. 100, no. 5, pages 2604–2609, Mar 2003.

[Miller 04]   Mark J Miller, Olga Safrina, Ian Parker & Michael D Cahalan. *Imaging the single cell dynamics of CD4+ T-cell activation by dendritic cells in lymph nodes.* J Exp Med, vol. 200, no. 7, pages 847–856, Oct 2004.

[Miura 00]   K. Miura & F. Siegert. *Light affects cAMP signalling and cell movement activity in Dictyostelium discoideum.* PNAS, vol. 97, pages 2111–2116, February 2000.

[Möbest 02]   D. Möbest, S. Ries, R. Mertelsmann & R. Henschler. New developments and new applications in animal cell technology. Springer Netherlands, 2002.

[Monk 89]   P. B. Monk & H. G. Othmer. *Cyclic AMP oscillations in suspensions of Dictyostelium discoideum.* Philos Trans R Soc Lond B Biol Sci, vol. 323, no. 1215, pages 185–224, Mar 1989.

[Moser 04]   Bernhard Moser, Marlene Wolf, Alfred Walz & Pius Loetscher. *Chemokines: Multiple levels of leukocyte migration control.* Trends Immunol, vol. 25, no. 2, pages 75–84, Feb 2004.

[NIH 03]   NIH. *The immune system.* Rapport technique 035423, NIH Publication, 2003.

[Okada 05]   Takaharu Okada, Mark J. Miller, Ian Parker, Matthew F. Krummel, Margaret Neighbors, Suzanne B. Hartley, Anne O'Garra, Michael D. Cahalan & Jason G. Cyster. *Antigen-engaged B-cells undergo chemotaxis toward the T zone and form motile conjugates with helper T-cells.* PLoS Biol, vol. 3, no. 6, page e150, Jun 2005.

[Okada 07]   Takaharu Okada & Jason G Cyster. *CC chemokine receptor 7 contributes to Gi-dependent T-cell motility in the lymph node.* J Immunol, vol. 178, no. 5, pages 2973–2978, Mar 2007.

[Okubo 80]   A. Okubo & S. A. Levin. Diffusion and ecological problems. Springer, 1980.

[Painter 00]   K. J. Painter, P. K. Maini & H. G. Othmer. *Development and applications of a model for cellular response to multiple chemotactic cues.* J Math Biol, vol. 41, no. 4, pages 285–314, Oct 2000.

[Petty 07]   HR. Petty. *Fluorescence microscopy: Established and emerging methods, experimental strategies, and applications in immunology.* Microsc. Res. Tech., vol. 70, pages 687–709, 2007.

[Popp 88]   F.A. Popp, K. H. Li, W. P. Mei, m. Galle & R. Neurohr. *Physical aspects of biophotons.* Experientia, Birkhäuser Verlag, pages 576–585, 1988.

[Popp 02]   F.A Popp, J.J. Chang, A. Herzog, Z. Yan & Y. Yan. *Evidence of non-classical light in biological systems.* Phys. Lett. A, vol. 293, pages 98–102, 2002.

[Schwickert 07]   Tanja A Schwickert, Randall L Lindquist, Guy Shakhar, Geulah Livshits, Dimitris Skokos, Marie H Kosco-Vilbois, Michael L Dustin & Michel C Nussenzweig. *In vivo imaging of germinal centres reveals a dynamic open structure.* Nature, vol. 446, no. 7131, pages 83–87, Mar 2007.

[Shlomchik 03]   M. J. Shlomchik, C. W. Euler & et al. *Activation of rheumatoid factor (RF) B cells and somatic hypermutation outside of germinal centers in autoimmune-prone MRL/lpr mice.* Ann N Y Acad Sci, vol. 987, pages 38–50, 2003.

[Stachowiak 06]   Agnieszka N Stachowiak, Yana Wang, Yen-Chen Huang & Darrell J Irvine. *Homeostatic lymphoid chemokines synergize with adhesion ligands to trigger T and B lymphocyte chemokinesis.* J Immunol, vol. 177, no. 4, pages 2340–2348, Aug 2006.

[Stavis 73]   Robert L. Stavis & Rona Hirschberg. *Phototaxis in Chlamydomonas Reinhardtii.* J. Cell Bio., vol. 59, pages 367–377, 1973.

[Swartz 07]   T. E. Swartz, Tong-Seung Tseng, Marcus A. Frederickson, Gastón Paris, Diego J. Comerci, Gireesh Rajashekara, Jung-Gun Kim, Mary Beth Mudgett, Gary A. Splitter, Rodolfo A. Ugalde, Fernando A. Goldbaum, Winslow R. Briggs & Roberto A. Bogomolni. *Blue-light-activated histidine kinases: Two-component sensors in bacteria.* Science, vol. 317, pages 1090–1093, August 2007.

[Tomhave 94]   E. D. Tomhave, R. M. Richardson, J. R. Didsbury, L. Menard, R. Snyderman & H. Ali. *Cross-desensitization of receptors for peptide chemoattractants. Characterization of a new form of leukocyte regulation.* J Immunol, vol. 153, no. 7, pages 3267–3275, Oct 1994.

[Trush 78]   M. A. Trush, M. E. Wilson & Van Dyke K. *The generation of chemiluminescence (CL) by phagocytic cells.* Meth. Enzymol, vol. 62, page 462494, 1978.

[Underhill 99]   D. M. Underhill, M. Bassetti, A. Rudensky & A. Aderem. *Dynamic interactions of macrophages with T cells during antigen presentation.* J Exp Med, vol. 190, no. 12, pages 1909–1914, Dec 1999.

[Uttieri 07]   Marco Uttieri, Daniela Cianelli, J. Rudi Strickler & Enrico Zambianchi. *On the relationship between fractal dimension and encounters in three-dimensional trajectories.* J Theor Biol, vol. 247, no. 3, pages 480–491, Aug 2007.

[VanWijk 88]   R. VanWijk & D. H. J. Schambart. *Regulatory aspects of low intensity photon emission.* Experimentia, Birkhäuser Verlag, vol. 44, pages 586–593, 1988.

[Wang 05]   Y. Wang & R.H. Carter. *CD19 regulates B-cell maturation, proliferation, and positie selection in the FDC zone of murine splenic germinal centers.* Immunity., vol. 22, pages 749–761, 2005.

[Willimann 98]   K. Willimann, D. F. Legler, M. Loetscher, R. S. Roos, M. B. Delgado, I. Clark-Lewis, M. Baggiolini & B. Moser. *The chemokine SLC is expressed in T-cell areas of lymph nodes and mucosal lymphoid tissues and attracts activated T-cells via CCR7.* Eur J Immunol, vol. 28, no. 6, pages 2025–2034, Jun 1998.

[Woolf 07]   Eilon Woolf, Irina Grigorova, Adi Sagiv, Valentin Grabovsky, Sara W Feigelson, Ziv Shulman, Tanja Hartmann, Michael Sixt, Jason G Cyster & Ronen Alon. *Lymph node chemokines promote sustained T lymphocyte motility without triggering stable integrin adhesiveness in the absence of shear forces.* Nat Immunol, vol. 8, no. 10, pages 1076–1085, Oct 2007.

[Worbs 07]   Tim Worbs, Thorsten R Mempel, Jasmin Bölter, Ulrich H von Andrian & Reinhold Förster. *CCR7 ligands stimulate the intranodal motility of T lymphocytes in vivo.* J Exp Med, vol. 204, no. 3, pages 489–495, Mar 2007.

[Yoshida 98]   R. Yoshida, M. Nagira, M. Kitaura, N. Imagawa, T. Imai & O. Yoshie. *Secondary lymphoid-tissue chemokine is a functional ligand for the CC chemokine receptor CCR7.* J Biol Chem, vol. 273, no. 12, pages 7118–7122, Mar 1998.

Publications

H. Fatehi, M.T. Figge and M. Meyer-Hermann.
Modelling cellular aggregation induced by chemotaxis and phototaxis.
(Submitted to Mathematical Medecine and Biology in March 2009)

Curriculum Vitae

PERSONAL INFORMATION

Address	Hasnaa FATEHI, Habsburgerallee 22, 60385, Frankfurt am Main.
E-mail	fatehi@fias.uni-frankfurt.de
Birth	19.01.1980 in Casablanca, Morocco.
Marital	Single

EDUCATION

Since 10/2005	PhD student of the Goethe Universität at the Frankfurt Institute for Advanced Studies, Frankfurt am Main, Germany.
2004-2005	Msc. in Engineering for health and drugs, specializing in the spatio-temporal approach of the living at the Medical Faculty of Grenoble, France.
2003-2004	Maîtrise in Mechanical Eng. at the University of Sherbrooke, Canada, within the CREPUQ program.
2002-2003	Licence in Mechanical Eng. at the University Joseph Fourier, Grenoble, France.
1999-2002	DEUG in Physics at the University of Joseph Fourier, Grenoble, France.
1997-1998	Baccalaureat in Experimental Sciences, Wallada High-school, Casablanca, Morocco.

INTERNSHIPS

01-06/2005	TIMC-DynaCell laboratory: Inverse problem in coronarian elastography.
04-06/2004	BIOMEC laboratory: SEM-VP characterization of morphological changes in a biomedical cement used for vertebroplasty.
05-07/2003	Laboratoire de RHEOLOGIE: Flow effects on tumor cells extravasation through a vascular wall.